



MID-AMERICA TRANSPORTATION CENTER

Report # MATC-KU: 363

Final Report



Performance of Geogrid Reinforced Ballast under Dynamic Loading

Robert Parsons, Ph.D., P.E.

Professor

Department of Civil, Environmental, and Architectural Engineering
University of Kansas

Milad Jowkar

Graduate Research Assistant

Jie Han, Ph.D., P.E.

Professor



2012

**A Cooperative Research Project sponsored by the
U.S. Department of Transportation Research and
Innovative Technology Administration**

The contents of this report reflect the views of the authors, who are responsible for the facts and the accuracy of the information presented herein. This document is disseminated under the sponsorship of the U.S. Department of Transportation's University Transportation Centers Program, in the interest of information exchange. The U.S. Government assumes no liability for the contents or use thereof.

MATC

Performance of Geogrid Reinforced Ballast under Dynamic Loading

Robert Parsons, Ph.D., P.E.
Professor
Civil, Environmental, & Architectural Engineering
University of Kansas

Milad Jowkar
Graduate Research Assistant
Civil, Environmental, & Architectural Engineering
University of Kansas

Jie Han, Ph.D., P.E.
Professor
Civil, Environmental, & Architectural Engineering
University of Kansas

A Report on Research Sponsored by

Mid-America Transportation Center
University of Nebraska-Lincoln

July 2012

Technical Report Documentation Page

1. Report No. 25-1121-0001-363	2. Government Accession No.	3. Recipient's Catalog No.	
4. Title and Subtitle Performance of Geogrid Reinforced Ballast under Dynamic Loading		5. Report Date July 2012	
		6. Performing Organization Code	
7. Author(s) Robert Parsons, Milad Jowkar, and Jie Han		8. Performing Organization Report No. 25-1121-0001-363	
9. Performing Organization Name and Address Mid-America Transportation Center 2200 Vine St. PO Box 830851 Lincoln, NE 68583-0851		10. Work Unit No. (TRAIS)	
		11. Contract or Grant No.	
12. Sponsoring Agency Name and Address Research and Innovative Technology Administration 1200 New Jersey Ave., SE Washington, D.C. 20590		13. Type of Report and Period Covered July 2009-December 2011	
		14. Sponsoring Agency Code MATC TRB RiP No. 24487	
15. Supplementary Notes			
16. Abstract Railroad ballast consists of open graded crushed stone used as a bed for railroad track to provide stability. Over time, ballast degrades and loses its strength. Fouling of ballast with fines has been a major issue of railway engineering. In this experimental study, a full-scale railroad section 5 ft in length was constructed with and without geogrid reinforcement. A full-scale trapezoidal cross-section of a railroad was built. The subgrade was covered with 2 ft of ballast 9 ft wide at the top and sloped down on both sides on a 2:1 slope. The track panel ties were embedded in the ballast to a depth of 7 in. The reinforced test section that had geogrid placed 7 in. below the tie performed better than the unreinforced test section in regards to settlement and fouling of ballast. Settlement of the reinforced test section between the ties and geogrid was reduced by 37 to 65 percent compared with the settlement of the same portion of the unreinforced test section. The percentage of rock dust and small diameter particles generated by ballast breakdown beneath the ties was less for the reinforced test section than for the unreinforced test section.			
17. Key Words Ballast, geogrid, railroad, fouling		18. Distribution Statement	
19. Security Classif. (of this report) Unclassified	20. Security Classif. (of this page) Unclassified	21. No. of Pages 119	22. Price

Table of Contents

Acknowledgements.....	xi
Disclaimer.....	xi
Abstract.....	xiii
Chapter 1 Introduction.....	1
Chapter 2 Literature Review.....	5
2.1 Fouling Ballast.....	5
2.2 Stiffness of Geocell Material.....	6
2.3 Load Carrying Capacity.....	6
2.4 Improving Poor Track Formations using Geosynthetics.....	7
2.5 Stabilizations of Ballasted Rail Tracks.....	9
2.6 Use of Geosynthetics in Railways Including Geocomposites and Vertical Drains.....	10
Chapter 3 Research Scope.....	12
3.1 Test Section Design.....	12
3.1.1 Loading Frame.....	14
3.1.2 Wooden Frames.....	16
3.2 Subgrade.....	17
3.3 Instrumentation.....	21
3.3.1 Tell-Tales.....	21
3.3.2 Pressure Cells.....	23
3.3.3 Displacement Transducers.....	24
3.3.4 String Pots.....	25
3.4 Ballast.....	26
3.5 Track.....	31
3.6 Geogrid.....	32
3.7 Quality Control Tests.....	32
3.7.1 Light Weight Deflectometer Test (LWD).....	33
3.7.2 Density Testing by Drive Tube.....	34
3.7.3 DCP /9Dynamic Cone Penetrometer).....	35
Chapter 4 Test Results.....	36
4.1 Unreinforced Test Section.....	38
4.1.1 East String Pot.....	39
4.1.2 East String Pot versus Dynamic Loading at 1100 psi (9 psi tie bearing pressure).....	39
4.1.3 East String Pot versus Dynamic Loading at 2500 psi (21 psi Tie Bearing Pressure).....	40
4.1.4 East String Pot versus Dynamic Loading at 3500 psi (31 psi Tie Bearing Pressure).....	42

4.1.5 East String Pot versus Dynamic Loading at 4500 psi (38 psi Tie Bearing Pressure).....	43
4.1.6 East String Pot versus Dynamic Loading at 4500 psi (Soaked) (40 psi Tie Bearing Pressure).....	45
4.1.7 West String Pot	47
4.1.8 Unreinforced Test (Displacement Transducers).....	53
4.1.9 Displacement Transducers at 1100 psi (Southeast) (9 psi Tie Bearing Pressure).....	54
4.1.10 Displacement Transducers at 4500 psi Dry (Southeast).....	58
4.1.11 Displacement Transducers at 4500 psi Soaked (40 psi Tie Bearing Pressure).....	62
4.1.12 Pressure Cell Results for Unreinforced Test.....	67
4.2 Reinforced Test Section.....	70
4.2.1 East String Pot (Reinforced Test).....	71
4.2.2 East String Pot versus Dynamic Loading at 1100 psi - Reinforced (9 psi Tie Bearing Pressure).....	71
4.2.3 East String Pot versus Dynamic Loading at 2500 psi - Reinforced (21 psi Tie Bearing Pressure).....	73
4.2.4 East String Pot versus Dynamic Loading at 3500 psi - Reinforced (29 psi Tie Bearing Pressure).....	73
4.2.5 East String Pot versus Dynamic Loading at 4500 psi - Reinforced (Not Soaked, 39 psi Tie Bearing Pressure).....	74
4.2.6 East String Pot versus Dynamic Loading at 4500 psi - Reinforced (Soaked, 39 psi Tie Bearing Pressure).....	77
4.2.7 West String Pot (Reinforced Test).....	79
4.2.8 Reinforced Test (Displacement Transducers).....	85
4.2.9 Displacement Transducers (DT) at 1100 psi (Southeast, 9 psi Bearing Pressure).....	86
4.2.10 Pressure Cells Results for Reinforced Test.....	90
4.2.11 Pressure Cells Results at Subgrade Level.....	91
4.3 Unreinforced vs. Reinforced: Settlement Comparison.....	93
4.3.1 Reinforced vs. Unreinforced (East String Pot).....	97
4.3.2 Number of Cycles versus Settlement (West String Pot).....	100
4.3.3 Number of Cycles versus Settlement (East String Pot).....	101
4.3.4 Actual Pressure vs. Settlement.....	101
4.4 Additional Testing such as LWD, CBR, Sieve Analysis, and Tell-Tale Readings.....	105
4.4.1 LWD.....	105
4.4.2 CBR.....	106
4.4.3 Tell-Tales and Sources of Settlement.....	107

4.4.4 Generation of Fouling Material	109
4.5 General Observations	115
Chapter 5 Conclusions and Recommendations	116
5.1 Conclusions	116
5.2 Recommendations for Future Study	116
References	118

List of Figures

Figure 1.1 Placing geocell in the field.....	3
Figure 1.2 Filling geocell.....	3
Figure 1.3 Placement of geogrid under railroad track.....	4
Figure 2.1 Critical ballast fouling and illustration of loss of aggregate to aggregate contact.....	6
Figure 2.2 Measured vertical stresses on subgrade, unreinforced sand (1) and geocell “typ1” reinforced sand (r).....	7
Figure 2.3 Placing geotextiles sheet.....	8
Figure 2.4 Placing geocell.....	8
Figure 2.5 Placement of soil in geocell.....	8
Figure 2.6 Placement of soil in geocell.....	8
Figure 2.7 Stress reduction.....	9
Figure 2.8 Effect of geosynthetics on the settlement of ballast.....	10
Figure 2.9 Vertical deformation of the ballast layer.....	11
Figure 2.10 Section of ballasted track bed with geocomposite layer.....	11
Figure 3.1 Schematic of the rail road cross-section unreinforced (not to scale).....	12
Figure 3.2 3-D view of the test section (not to scale).....	13
Figure 3.3 Schematic of the rail road cross-section reinforced (not to scale).....	13
Figure 3.4 Loading frame.....	14
Figure 3.5 Loading cylinder.....	15
Figure 3.6 Wooden frames.....	16
Figure 3.7 Grain size distributions for subgrade.....	17
Figure 3.8 Standard proctor compaction curve of the subgrade.....	18
Figure 3.9 Standard Atterberg limit test curve of the subgrade.....	19
Figure 3.10 Unconfined compression test curves.....	20
Figure 3.11 Placing subgrade and compaction.....	21
Figure 3.12 Tell-tale.....	22
Figure 3.13 Location of tell-tales.....	23
Figure 3.14 Model 3515 circular earth pressure cells during placement.....	24
Figure 3.15 Pressure cell locations (not to scale).....	24
Figure 3.16 Displacement transducer placement.....	25
Figure 3.17 String pot.....	26
Figure 3.18 Recycled ballast after sieve.....	27
Figure 3.19 Washed rock.....	28
Figure 3.20 Sieve analysis for ballast.....	29
Figure 3.21 Sieve shaker for ballast.....	30
Figure 3.22 A wooden tie track panel.....	31
Figure 3.23 Triaxial geogrid used in reinforced test.....	32

Figure 3.24 Light weight deflectometer.....	33
Figure 3.25 Drive tube and sampler driver.....	34
Figure 4.1 Unreinforced test section.....	36
Figure 4.2 Geogrid after replacement in the reinforced test.....	37
Figure 4.3 Test during dynamic loading.....	37
Figure 4.4 Dynamic loading vs. deformation (east string pot).....	39
Figure 4.5 East string pot deformations versus dynamic loading at 1100 psi.....	40
Figure 4.6 East string pot versus dynamic loading at 2500 psi.....	41
Figure 4.7 East string pot versus dynamic loading at 3500 psi.....	42
Figure 4.8 East string pot versus dynamic loading at 4500 psi (not soaked).....	44
Figure 4.9 East string pot reading versus dynamic loading at 4500 psi soaked.....	46
Figure 4.10 Dynamic loading vs. deformation (west string pot).....	47
Figure 4.11 West string pot versus dynamic loading at 1100 psi.....	48
Figure 4.12 West string pot versus dynamic loading at 2500 psi.....	49
Figure 4.13 West string pot versus dynamic loading at 3500 psi.....	50
Figure 4.14 West string pot versus dynamic loading at 4500 psi (not soaked).....	51
Figure 4.15 West string pot versus dynamic loading at 4500 psi (soaked).....	52
Figure 4.16 Displacement transducers.....	53
Figure 4.17 Displacement transducer reading at 1100 psi (southeast).....	54
Figure 4.18 Displacement transducer reading at 1100 psi (northeast).....	55
Figure 4.19 Displacement transducer reading at 1100 psi (northwest).....	56
Figure 4.20 Displacement transducer reading at 1100 psi (southwest).....	57
Figure 4.21 Displacement transducer reading at 4500 psi not soaked (southeast).....	58
Figure 4.22 Displacement transducer reading at 4500 psi not soaked (northeast).....	59
Figure 4.23 Displacement transducer reading at 4500 psi not soaked (northwest).....	60
Figure 4.24 Displacement transducer reading at 4500 psi not soaked (southwest).....	61
Figure 4.25 Displacement transducer reading at 4500 psi soaked (southeast).....	63
Figure 4.26 Displacement transducer reading at 4500 psi soaked (northeast).....	64
Figure 4.27 Displacement transducer reading at 4500 psi soaked (northwest).....	65
Figure 4.28 Displacement transducer reading at 4500 psi soaked (southwest).....	66
Figure 4.29 Pressure cells.....	67
Figure 4.30 Pressure cells vs. pump pressure at subgrade level.....	68
Figure 4.31 Pressure cells vs. tie bearing pressure on ballast.....	69
Figure 4.32 Dynamic loading vs. deformation (reinforced test).....	71
Figure 4.33 East string pot deformations versus dynamic loading at 1100 psi.....	72
Figure 4.34 East string pot deformations versus dynamic loading at 2500 psi.....	73
Figure 4.35 East string pot deformations versus dynamic loading at 3500 psi.....	74
Figure 4.36 East string pot versus dynamic loading at 4500 psi (not soaked).....	76
Figure 4.37 East string pot versus dynamic loading at 4500 psi (soaked).....	78
Figure 4.38 Dynamic loading vs. deformation. (reinforced test).....	79

Figure 4.39 West string pot versus dynamic loading at 1100 psi	80
Figure 4.40 West string pot versus dynamic loading at 2500 psi	81
Figure 4.41 West string pot versus dynamic loading at 3500 psi	82
Figure 4.42 West string pot versus dynamic loading at 4500 psi (not soaked)	83
Figure 4.43 West string pot versus dynamic loading at 4500 psi (soaked)	84
Figure 4.44 Displacement transducers	85
Figure 4.45 Displacement transducer readings at 1100 psi (southeast)	87
Figure 4.46 Displacement transducer readings at 1100 psi (northwest)	88
Figure 4.47 Displacement transducer readings at 1100 psi (southwest)	89
Figure 4.48 Pressure cells	90
Figure 4.49 Pressure cells vs. pump pressure at subgrade level	91
Figure 4.50 Pressure cells vs. tie bearing pressure	92
Figure 4.51 West string pot result comparison	94
Figure 4.52 West string pot result comparison (after adjusting for load differences)	96
Figure 4.53 East string pot result comparison	97
Figure 4.54 East string pot result comparison (after adjusting for load differences)	99
Figure 4.55 Number of cycles vs. settlement (west string pot)	100
Figure 4.56 Number of cycles vs. settlement (east string pot)	101
Figure 4.57 Deformation vs. actual tie bearing pressure at early cycles (west)	102
Figure 4.58 Deformation vs. actual tie bearing pressure at middle cycles (west)	102
Figure 4.59 Deformation vs. actual tie bearing pressure at later cycles (west)	103
Figure 4.60 Deformation vs. actual tie bearing pressure at early cycles (east)	103
Figure 4.61 Deformation vs. actual tie bearing pressure at middle cycles (east)	104
Figure 4.62 Deformation vs. actual tie bearing pressure at later cycles (east)	104
Figure 4.63 LWD reading locations	105
Figure 4.64 CBR vs. depth	106
Figure 4.65 Tell-Tales locations (not to scale)	107
Figure 4.66 Settlements and strains within sections	109
Figure 4.67 Condition of ballast after unreinforced test	110
Figure 4.68 Condition of ballast at top of subgrade after unreinforced test	111
Figure 4.69 Condition of ballast at top of geogrid after reinforced test	112
Figure 4.70 Condition of ballast at top of subgrade after reinforced test	113
Figure 4.71 Grain size distribution of ballast	114

List of Tables

Table 3.1 ASTM standards.....	17
Table 3.2 Atterberg limits data.....	18
Table 3.3 Unconfined compression tests on subgrade.....	20
Table 3.4 BNSF specification limits (class 1).....	27
Table 3.5 Sieve analysis for ballast.....	30
Table 4.1 Loading information for unreinforced test.....	38
Table 4.2 Pressure cells vs. pump pressure at subgrade level (unreinforced test).....	69
Table 4.3 Pressure cells vs. tie bearing pressure (unreinforced).....	70
Table 4.4 Loading information for reinforced test.....	70
Table 4.5 Pressure cells vs. pump at subgrade level.....	92
Table 4.6 Pressure cells vs. tie bearing pressure (reinforced).....	93
Table 4.7 Comparison between unreinforced and reinforced test for unit weight and number of cycles.....	93
Table 4.8 Comparison of settlement between the reinforced test and unreinforced test (west string pot).....	95
Table 4.9 Reinforced loading vs. unreinforced loading.....	96
Table 4.10 Comparison of settlement between reinforced test and unreinforced test (East string pot).....	98
Table 4.11 LWD results.....	105
Table 4.12 Tell-tale readings.....	107

List of Abbreviations

California Bearing Ratio (CBR)
Dynamic Cone Penetrometer (DCP)
Fat Clay (CH)
High-Density Polyethylene (HDPE)
High-Speed Rail (HSR)
Light Weight Deflectometer Test (LWD)
University of Kansas (KU)

Acknowledgements

The authors thank the Mid-America Transportation Center (MATC) for providing financial support for the research described in this report, and Mr. Hank Lees of BNSF and Mr. Mark Wayne of Tensar International Corporation for providing material and technical support for this research. We also thank the many individuals who contributed to the completion of this research, including Mr. Danny Syml, Mr. AJ Rahman, Mr. Jitendra Thakur, Mr. Kahle Loveless, Mr. Baghaban Acharya, Mr. Deep Khatri, Mr. Cheng Lin, Mr. Raju Acharya, and especially Mr. Jim Weaver and Mr. Matthew Maksimowicz for their help with the physical testing.

Disclaimer

The contents of this report reflect the views of the authors, who are responsible for the facts and the accuracy of the information presented herein. This document is disseminated under the sponsorship of the Department of Transportation University Transportation Centers Program, in the interest of information exchange. The U.S. Government assumes no liability for the contents or use thereof.

Abstract

Railroad ballast consists of open graded crushed stone used as a bed for railroad track to provide stability. It plays a significant role in providing support for the track base and distributing the load to the weaker subgrade below. Ballast also helps with drainage, which is an important factor for any type of transportation structure, including railroads. This issue has become more acute as heavier car loads place more demand on track structure than before.

Over time, ballast degrades and loses its strength. Fouling of ballast with fines has been a major issue of railway engineering. Fouling could be caused by breakdown of ballast itself or intrusion of fines from below or from the environment.

In this experimental study, a full-scale railroad section 5 ft in length was constructed with and without geogrid reinforcement. A full-scale trapezoidal cross-section of a railroad was built. The subgrade was covered with 2 ft of ballast 9 ft wide at the top and sloped down on both sides on a 2:1 slope. The track panel ties were embedded in the ballast to a depth of 7 in.

The reinforced test section that had geogrid placed 7 in. below the tie performed better than the unreinforced test section in regards to settlement and fouling of ballast. Settlement of the reinforced test section between the ties and geogrid was 37 to 65 percent less than settlement of the same portion of the unreinforced test section. The percentage of rock dust and small diameter particles generated by ballast breakdown beneath the ties was less for the reinforced test section than for the unreinforced test section.

Chapter 1 Introduction

Railroad ballast consists of open graded crushed stone used as a bed for railroad track to provide stability. It plays a significant role in providing vertical and lateral support for the track base and distributing the load to the weaker subgrade below. Ballast also helps with drainage, which is an important factor for any type of transportation structure, including railroads. This issue has become more acute as heavier car loads place more demand on track structure than they did in the past.

Over time ballast degrades and loses its strength. Fouling of ballast with fines has been a major issue of railway engineering. Fouling can be caused by breaking down or by contamination or upwards migration from the subgrade.

Five sources of fouling have been identified: ballast breakdown; infiltration from the ballast surface; sleeper (tie) wear; infiltration from underlying granular layers; and subgrade infiltration (Selig and Waters 1994). Major causes of ballast fouling include tamping and undercutting procedures, repetitive loading and vibration from trains, and contamination from both above and below the ballast level.

The specific area of research addressed in this thesis is extension of the life of ballast by limiting fouling of the ballast and improving performance. Development of an effective method for extending the ballast life cycle would have significant value. The research in this thesis focused on how to reinforce ballast using geogrids to reduce fouling. Having a stable reinforced section would help reduce the number of maintenance actions required to keep the railroad in good repair.

Track maintenance operations are very time consuming and costly. Track maintenance can cost between \$26- and \$80,000 per mile of track (Zarembski and Cikota 2008). In addition, trains

have become much heavier and faster than in the past, while the majority of the track condition has not been substantially improved.

An increase of high-speed rail (HSR) in the United States would most likely increase track maintenance costs. Therefore, research that would help in the reduction of maintenance costs would be beneficial to HSR economics. This includes research on reducing the amount of fouling in the ballast.

Geosynthetics are very durable polymeric products being used in various civil engineering applications in order to provide strength, stability, and durability. Use of geosynthetic materials has become more and more common in the past 40 years for a number of applications, and they have the potential to reduce the cost of maintenance by increasing design life. Geosynthetics can be categorized into eight different products, as follows: geotextiles, geogrids, geonets, geomembranes, geosynthetic clay liners, geofoam, and geocells.

Geocells are a three-dimensional, honeycomb-shaped product made of high-density polyethylene (HDPE). The United States Army Corps of Engineers used geocells for providing lateral confinement to the granular material during the 1970s (Webster 1979). Examples of geocells are shown figures 1.1 and 1.2.



Figure 1.1 Placing geocell in the field



Figure 1.2 Filling geocell

Geogrids are a flexible polymeric product, consisting of sets of parallel tensile ribs used in civil engineering for five major functions: separation, reinforcement, filtration, drainage, and containment (Koerner 1998).

The main potential advantage of geogrids is extension of the maintenance cycle and life of the ballast through reinforcement of the ballast. Geogrids can also be used to reinforce the sub-ballast, which increases the bearing capacity of soft subgrade.

While both geocells and geogrids have the potential to extend the life of ballast and the time between maintenance cycles, geogrid has the additional advantage of being less expensive and easier to install during a maintenance action, as shown in figure 1.3. For these reasons geogrid was selected as the reinforcement product to be used in this study.



Figure 1.3 Placement of geogrid under railroad track (Tensar International 2012)

Chapter 2 Literature Review

Degradation of ballast in railway engineering has long been an issue because it can lead to misalignment of the rails. Several factors, such as number of load cycles, gradation of aggregates, track confining pressure, and angularity and fracture of individual grains of ballast, can cause ballast degradation and deformation.

Some studies have been published regarding reinforcement of ballast with geogrid, which is a geosynthetic. A summary of selected previous research is provided in this chapter.

2.1 Fouling of Ballast

Tutumluer et al. (2008). Fouling of ballast in the railroad industry occurs as the voids within the ballast are filled with finer particles. Accumulation of coal dust in ballast is a primary concern for railroad engineers. In this paper, several tests, such as Atterberg limits, specific gravity, moisture-density relationships (Proctor), and shear strength, were conducted to determine coal dust's mechanical and physical properties. After mixing ballast with coal dust at a series of different moisture contents and coal dust weight percentages, it was found that it takes about 25% coal dust by weight to fill up all the voids in ballast, given a void ratio for the ballast of 43%. Also, when the ballast was fully fouled with coal dust with 35% moisture content, it was determined that the friction angle of ballast was approximately the same as the friction angle of coal dust. The study found that under this condition the ballast particles will be separated by coal fines, as shown in figure 2.1, which can result in track misalignment.

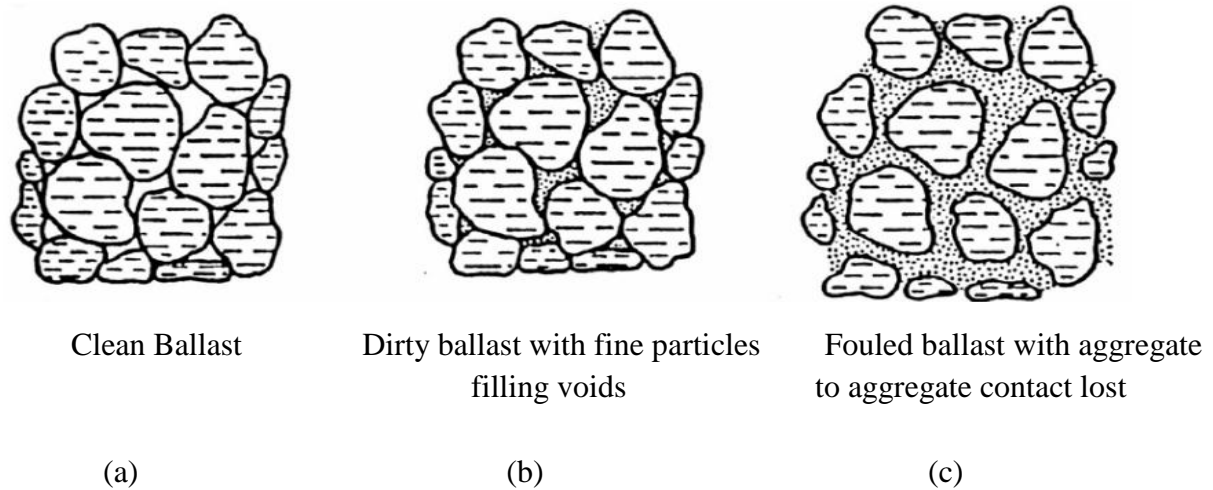


Figure 2.1 Critical ballast fouling and illustration of loss of aggregate to aggregate contact (Tutumluer et al 2008)

2.2 Stiffness of Geocell Material

Mengelt et al. (2006) focused on the resilient modulus of coarse-grained soil (gravel, sand) and fine-grained soil (silt, clay). An increase in resilient modulus was found using single geocell reinforcement for both soil types; however, only the improvement of resilient modulus for the case of fine-grained soil was significant. Resilient modulus increased by only 1.4–3.2% when the infill was coarse-grained, but increased by 16.5–17.9% when the infill was fine-grained.

As the subgrade stiffness increased, the ultimate bearing capacity of reinforced sand was observed to increase. Reinforcement provided very good improvement of resistance to repeated loads.

2.3 Load Carrying Capacity

Emersleben and Meyer (2005) investigated the vertical stress distribution on an artificial mixed soil called “Glyben” used to simulate soft subgrade material. Three different vertical loads (200 kN/m³, 300 kN/m³ and 400 kN/m³) were applied to the base. The vertical stress on glyben subgrade, unreinforced sand, and geocell reinforced sand were measured. The reinforced soil had

higher stiffness, and the stress on subgrade was reduced between 30%-36%, depending on the applied load. The test results also showed that for the unreinforced case, stresses were concentrated more directly beneath the load plate, while for the reinforced case, stresses were distributed over a larger area, as shown in figure 2.3. This result indicates that a geocell layer acts like a stiff mat, distributing the footing load over a larger area, thus reducing the vertical stresses directly beneath the load plate (Emersleben and Meyer 2005).

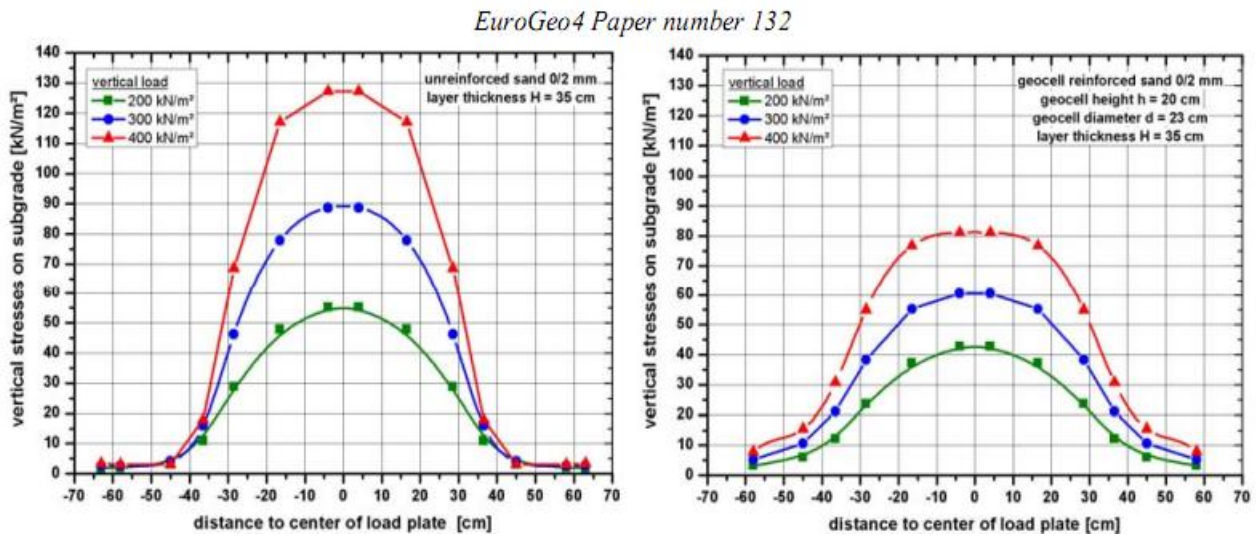


Figure 2.2 Measured vertical stresses on subgrade, unreinforced sand (1) and geocell “typ1” reinforced sand (r)

2.4 Improving Poor Track Formations using Geosynthetics

Kea et al. (2007) showed that shrinkage and swelling of a clay subgrade would result in both upward and downward movement of the rail profile. Geocell reinforcement provides tensile strength as well as shear strength. It also has a major effect on increasing the bearing capacity of the subgrade. Geotextiles were also used to prevent migration of fine particles into ballast. Figures 2.3 through 2.6 show the construction process:



Figure 2.3 Placing geotextile sheet



Figure 2.4 Placing geocell



Figure 2.5 Placement of soil in geocell



Figure 2.6 Placement of soil in geocell

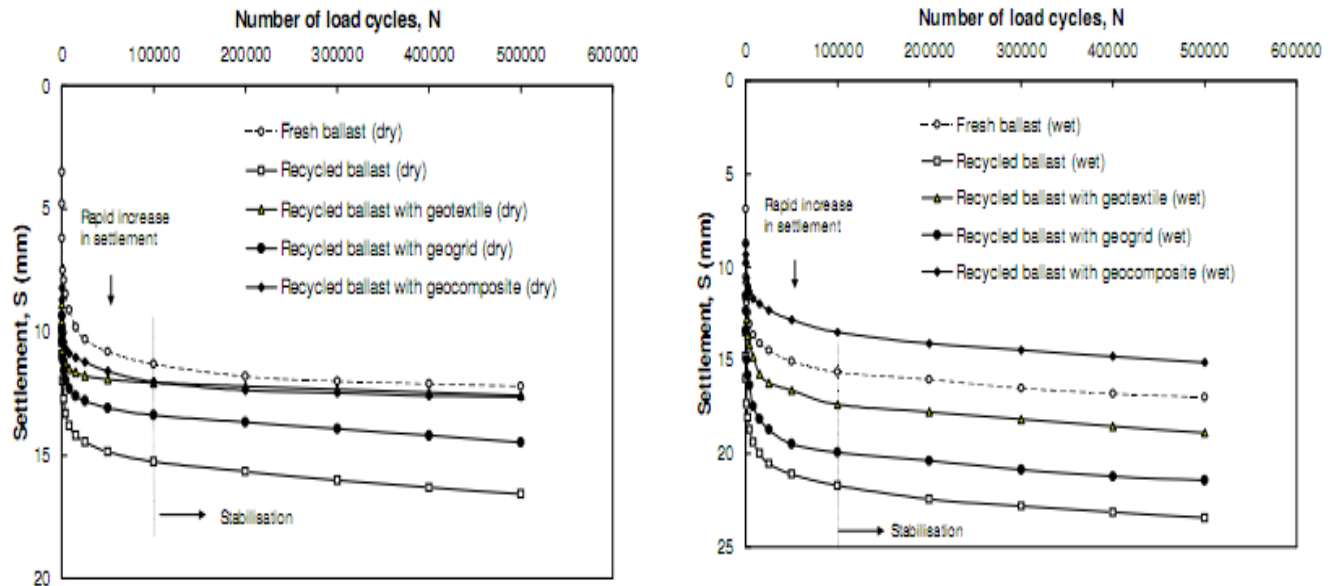
Laboratory work shows a significant stress reduction on the subgrade for different depths to the top of treatment (Hannes and Grabe 2010). Stress reductions observed for series of products are shown in figure 2.7.

Products	Depth mm		
	200	400	600
Geotextiles			
GT1	51%	61%	87%
GT2	22%	52%	83%
Geogrids			
GG1	54%	34%	66%
Geocells			
GC1	24%	5%	24%
Gc2	25%	5%	85%
GC3	1%	16%	96%
GC4	34%	53%	93%

Figure 2.7 Stress reduction (reproduced from Grabe 2010)

2.5 Stabilizations of Ballasted Rail Tracks

Indraratna et al. (2006) conducted a series of tests to measure the settlement, vertical strain, and lateral strain of reinforced (geogrid-geotextile) recycled ballast in wet and dry conditions. The usage of geogrid-geotextile showed an increase in the bearing capacity and resilient modulus of recycled ballast (fig. 2.8). The results also indicated a decrease in degradation and lateral movement of ballast. A finite element analysis was conducted to determine the optimum depth at which the geosynthetic was the most effective. It was found that optimum depth for geosynthetics was in the range of 150-200 mm beneath the ties.



(a) Dry samples

(b) Wet samples

Figure 2.8 Effect of geosynthetics on the settlement of ballast (Indraratna et al. 2006)

2.6 Use of Geosynthetics in Railways Including Geocomposites and Vertical Drains

Indraratna et al. (2011) conducted series of tests using fresh ballast, recycled ballast, fresh ballast with geocomposite, and recycled ballast with geocomposite. The geocomposite was used between the sub-ballast and ballast interface. Figures 2.9 and 2.10 show a reduction in average vertical deformations of recycled ballast at a large number of cycles when reinforcement is used.

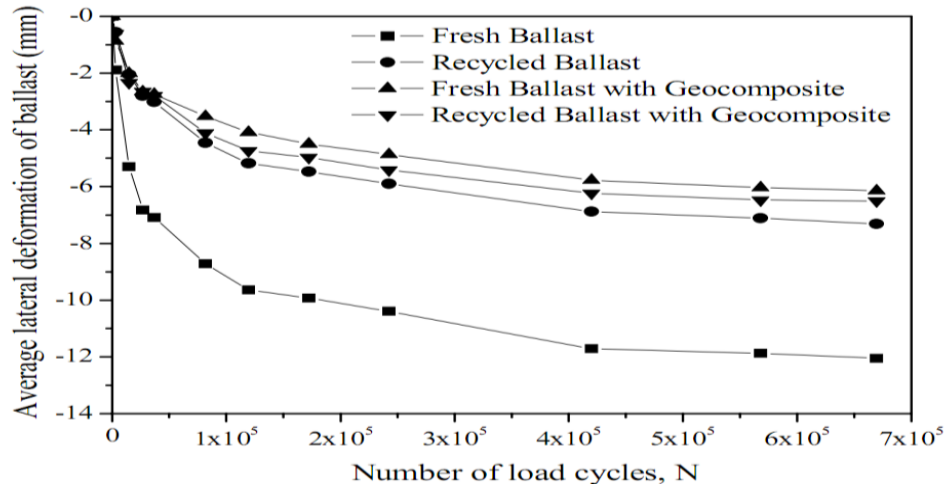


Figure 2.9 Vertical deformation of the ballast layer (Indraratna et al. 2011)

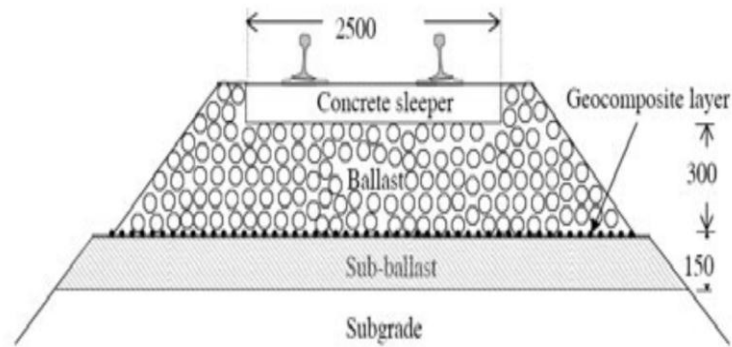


Figure 2.10 Section of ballasted track bed with geocomposite layer (modified from Indraratna et al. [2011])

Chapter 3 Research Scope

This chapter contains summaries of the test setup, instrumentation, and scope of material testing of subgrade and ballast.

3.1 Test Section Design

A full-scale railroad section 5 ft in length was constructed with and without geogrid reinforcement. Figures 3.1 and 3.2 illustrate how the lab test sections were constructed. A full-scale trapezoidal cross-section of a railroad was built, which consisted of a 2 ft deep subgrade that was 4.5 ft wide from centerline of the trapezoid on each side at the top and sloped down on a 2:1 slope. The subgrade was covered with 2 ft of ballast 9 ft wide at the top and sloped down on both sides on a 2:1 slope. Additional sub-ballast was added at a 1.5:1 slope to prevent sieving a large amount of ballast on the sides, as shown in figures 3.1, 3.2, and 3.3.

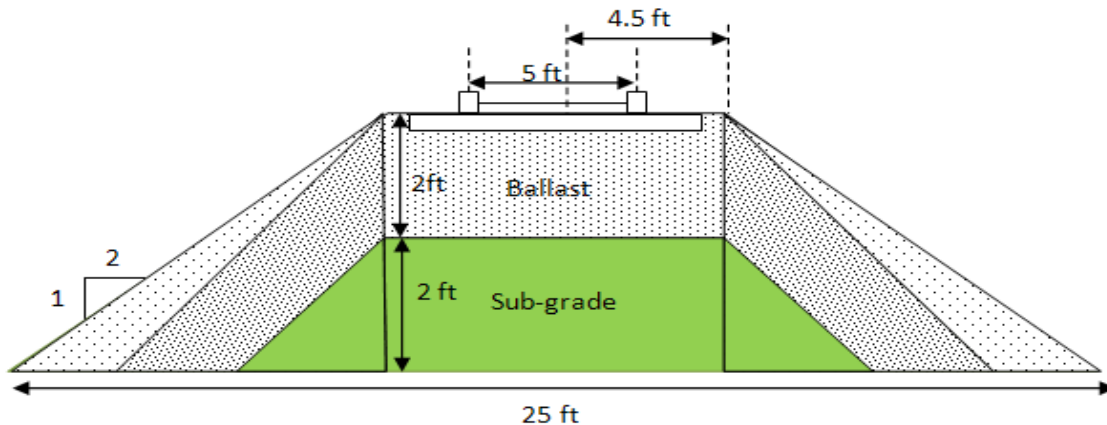


Figure 3.1 Schematic of the unreinforced railroad cross-section (not to scale)

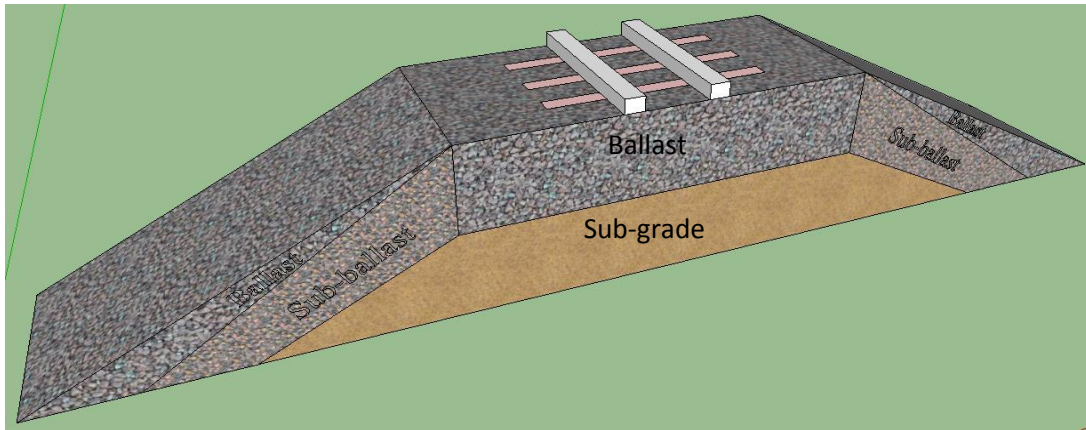


Figure 3.2 3-D view of the test section (not to scale)

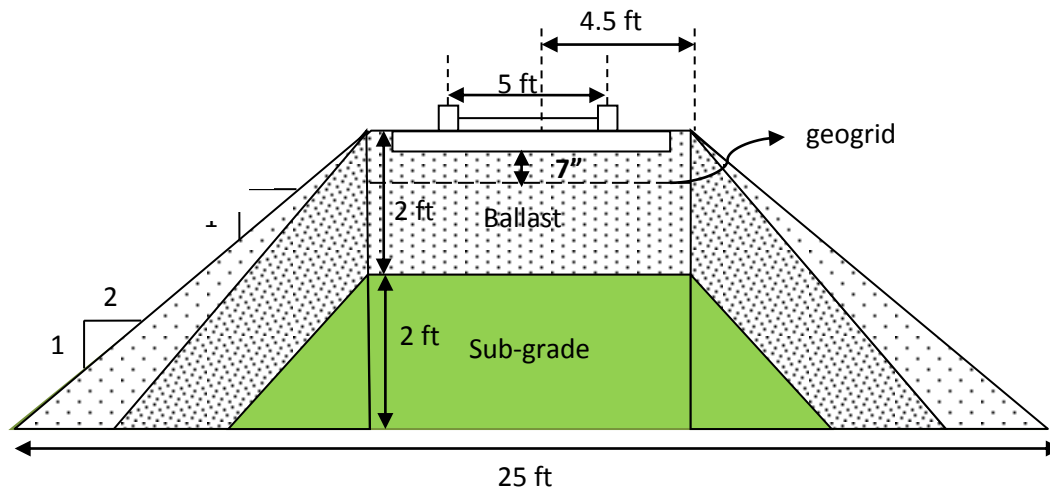


Figure 3.3 Schematic of the railroad cross-section (not to scale)

3.1.1 Loading Frame

A self-reacting loading frame with a 100,000 lb capacity was constructed and is shown in figure 3.4. The inside column spacing is 9.5 ft, and the clearance between the bottom of the overhead beam and slab is 13 ft. Three reinforced 3 ft by 5 ft concrete slabs were built and post-tensioned together to construct the self-reacting loading frame. Figure 3.5 shows the loading cylinder with maximum capacity of 104,000 lb.

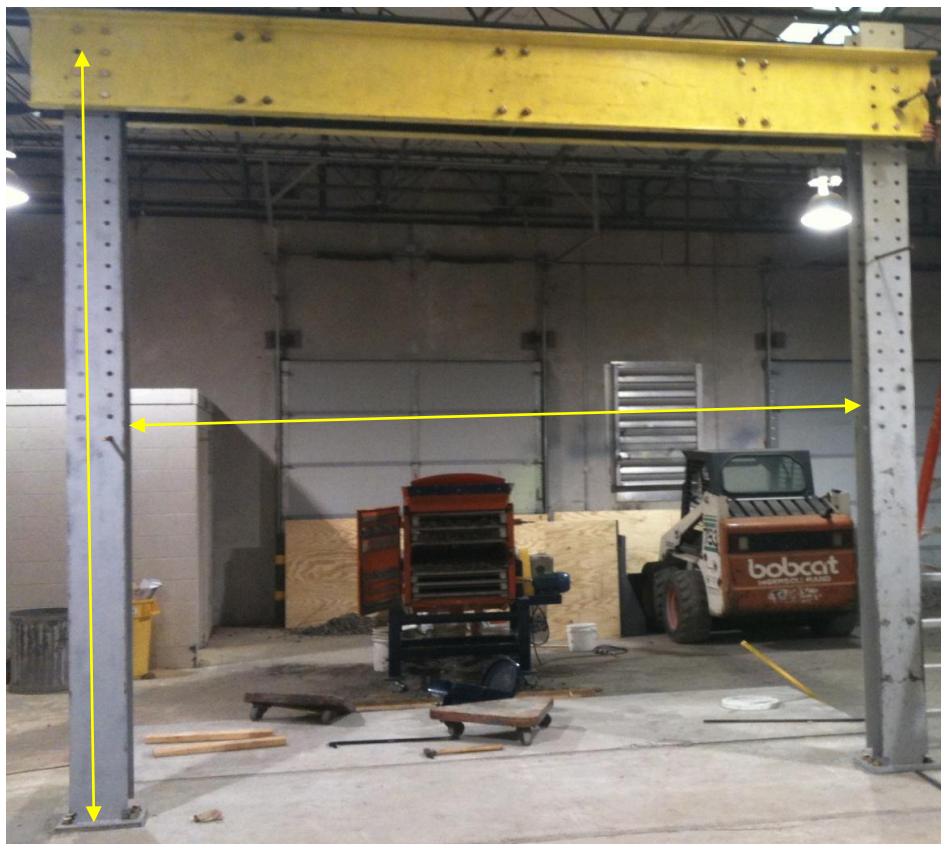


Figure 3.4 Loading frame



Figure 3.5 Loading cylinder

3.1.2 Wooden Frames

Two 28 ft long (14 ft from center line) wooden frames were added, as shown in figure 3.6, to restrain deformation in the longitudinal direction.

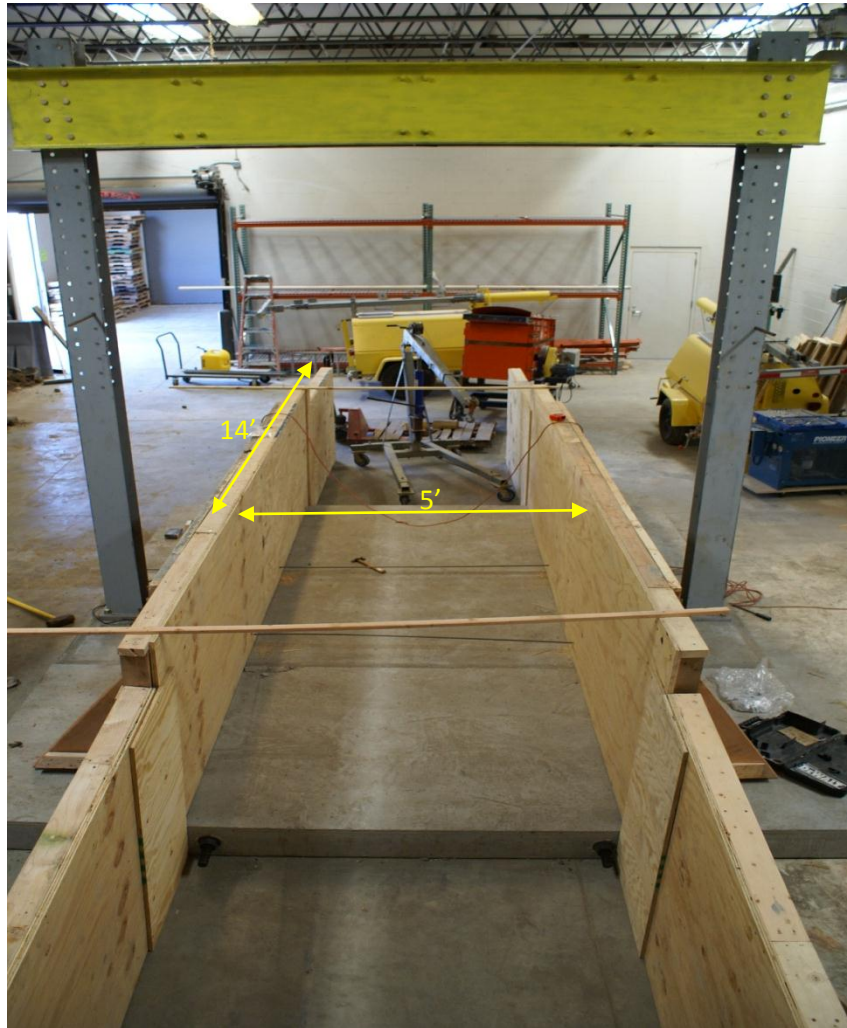


Figure 3.6 Wooden frames

3.2 Subgrade

The source of the subgrade was the yard in front of Learned Hall on the main campus of KU. The soil was characterized in accordance with the tests listed in table 3.1. The grain size distribution of the subgrade soil is shown in figure 3.7.

Table 3.1 ASTM standards

ASTM Standards	Lab Tests
D422.2703-1	Hydrometer Analysis
D2166.14900-1	Unconfined Compression
D3080.2626-1	Direct Shear
D4318.3420-1	Atterberg Limits
D2216-267-1	Moisture Content
D698.23713-1	Proctor Test
D6951/D6951M	DCP Test

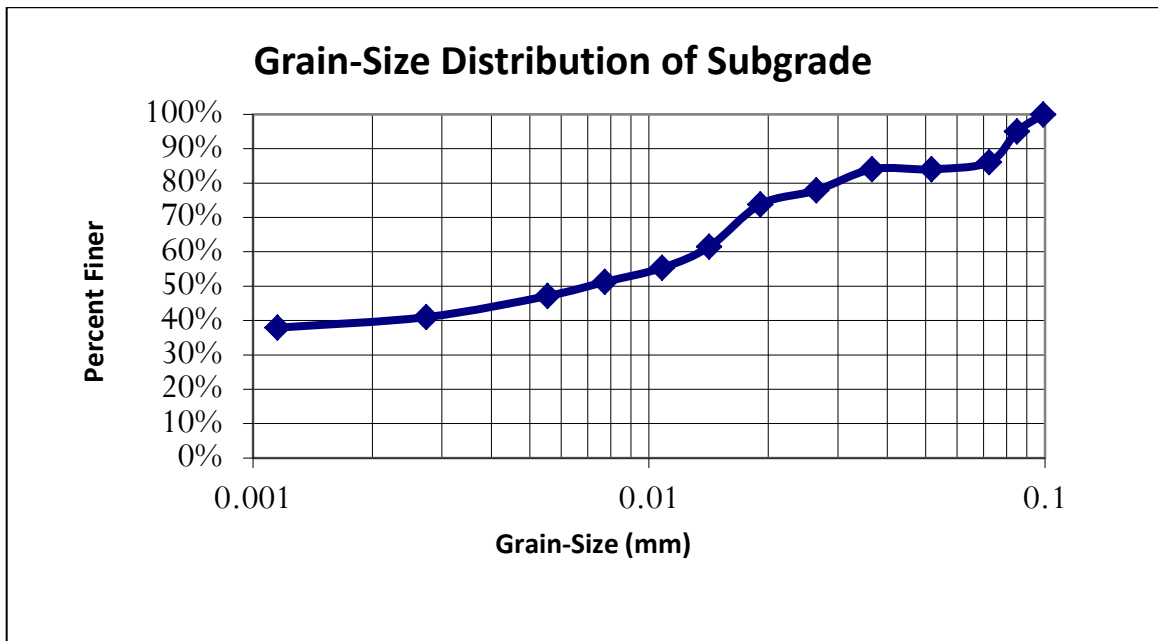


Figure 3.7 Grain size distribution for subgrade

The sub-grade had an optimum moisture content of 23% and maximum dry density of 99.5 lb/ft³. Figure 3.8 shows the compaction test curve. Results of Atterberg limits testing are shown in figure 3.9 and table 3.2. Based on the Atterberg limits and grain size distribution the soil was classified as fat clay (CH).

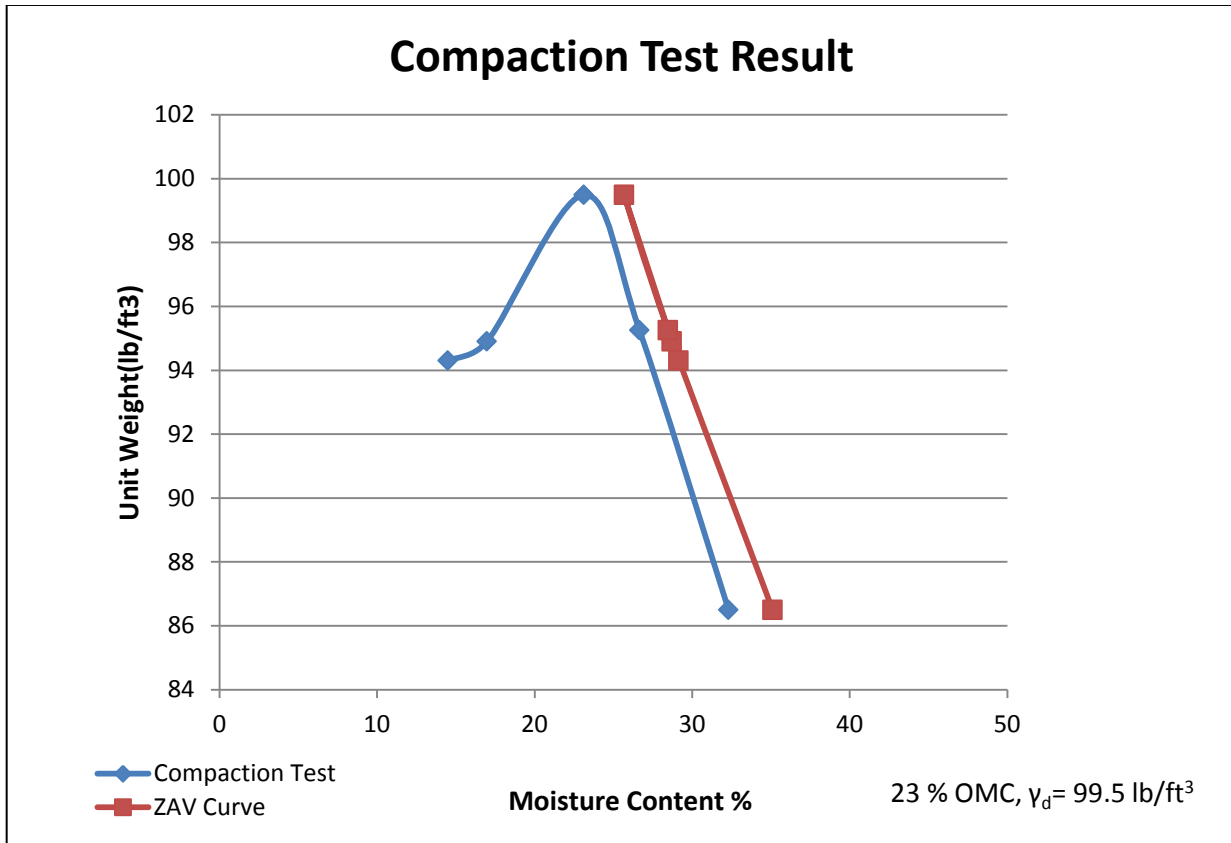


Figure 3.8 Standard proctor compaction curve of the subgrade

Table 3.2 Atterberg limits data

PL=	21
LL=	52
PI=	31

High Plasticity Clay

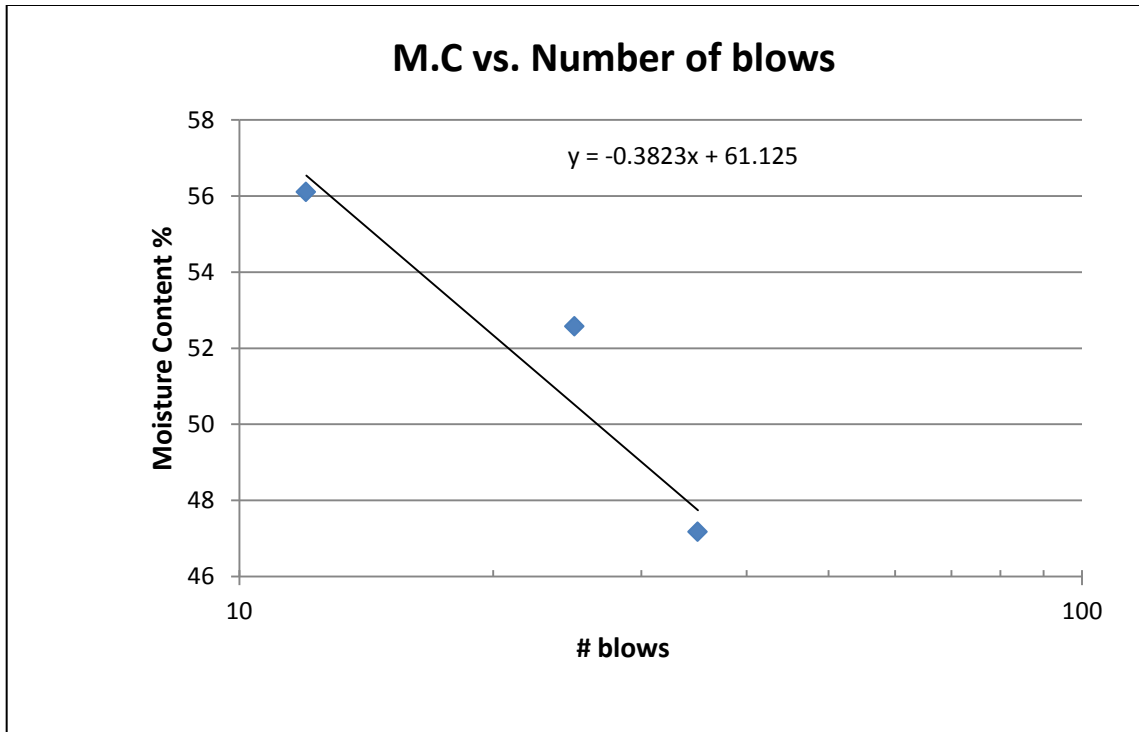


Figure 3.9 Standard Atterberg limit test curve of the subgrade

Unconfined compression tests were conducted to determine the undrained shear strength (S_u) of the subgrade. The results are presented in figure 3.10.

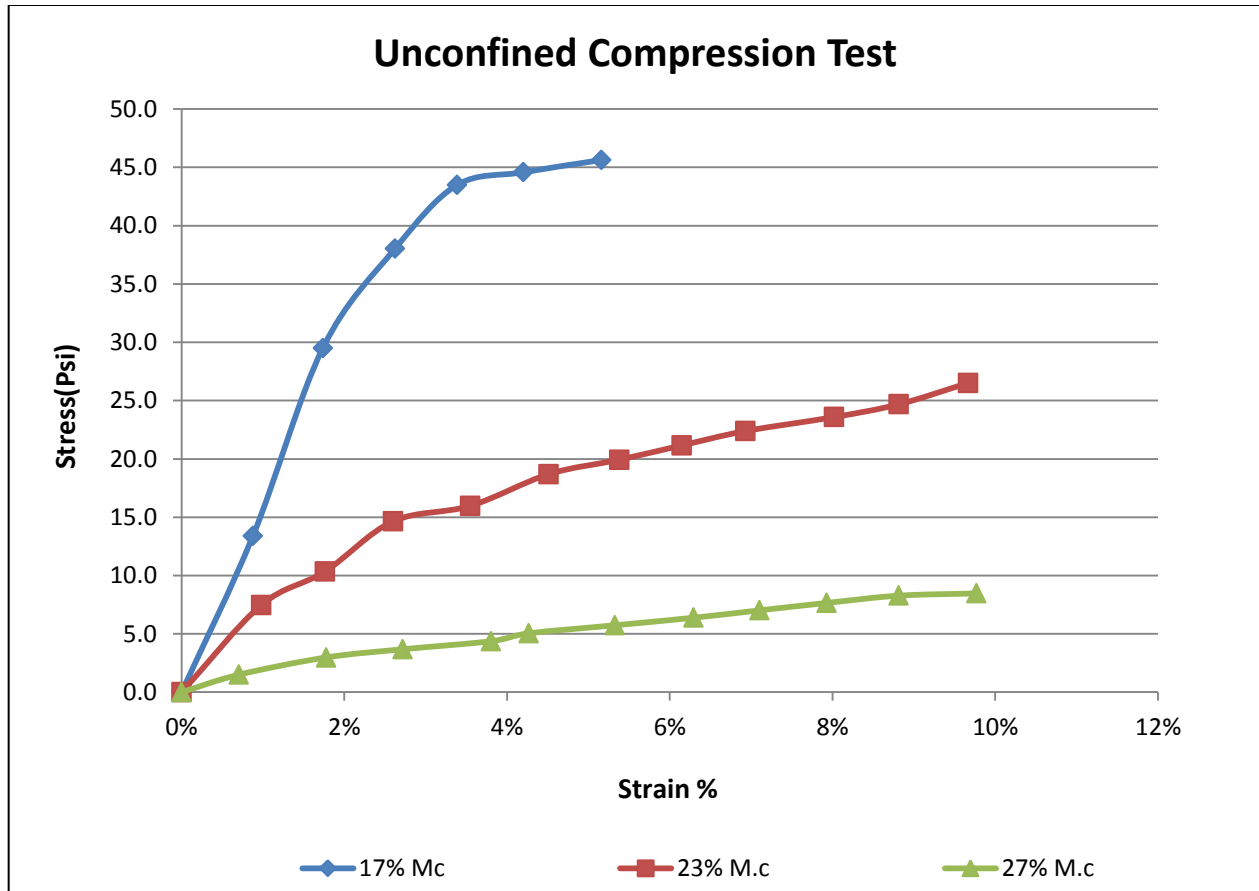


Figure 3.10 Unconfined compression test curves

Table 3.3 Unconfined compression tests on subgrade

Length (in)	Area (in ²)	Mass (lb)	Moisture (%)	q _u (psi)	S _u = q _u /2 (psi)	S _u =q _u /2 (psf)
2.79	1.343	0.255	19.15	45.45	22.73	3272
2.813	1.341	0.275	22.7	26.93	13.47	1939
2.714	1.335	0.25	28.5	8.78	4.39	632

As shown in figure 3.11, the subgrade was placed with a skid loader in 6 in. lifts. Each lift was compacted with a vibratory plate compactor, as shown in figure 3.11. Unreinforced and reinforced sections were compacted at 26% moisture content and densities of 91.5 lb/ft³ dry density and 93 lb/ft³ dry density, respectively.



Figure 3.11 Placing subgrade and compaction

3.3 Instrumentation

3.3.1 Tell-Tales

Tell-tales are used to measure vertical deformation in soil profiles at selected depths. As the load is applied to the section, the base plate and the interior pipe move with the soil at the base plate elevation.



Figure 3.12 Tell-tale

The exterior pipe minimizes interference from the soil or ballast above the base plate. Two tell-tales were set at the subgrade interface with ballast and the other two were set 7 in. below the ties in the unreinforced and reinforced tests. Locations of tell-tales are shown in figure 3.14.

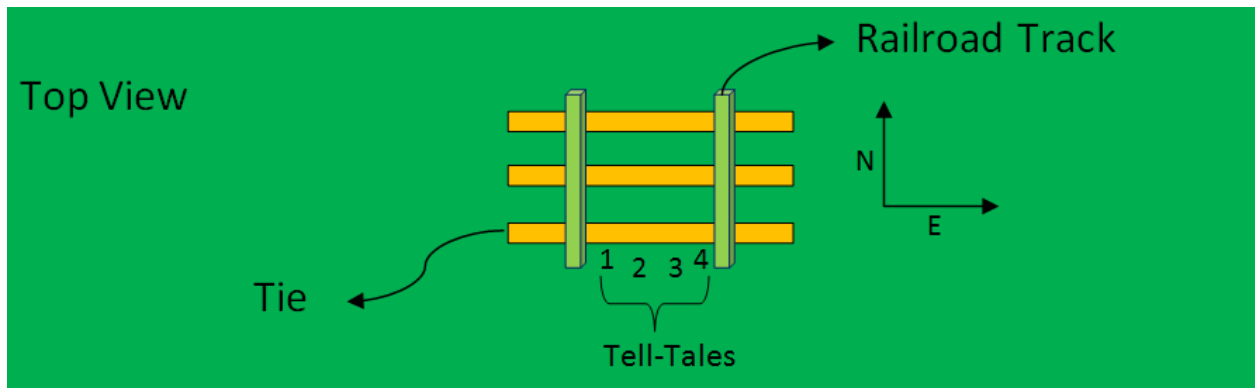


Figure 3.13 Locations of tell-tales

3.3.2 Pressure Cells

Model 3515 Geokon pressures cells are heavy duty cells and are recommended for railroad applications. Five pressure cells were placed between the subgrade and ballast directly beneath the railroad ties as shown in figures 3.14 and 3.15. These earth pressure cells have a diameter of 9 in. and a capacity of 58 psi.



Figure 3.14 Model 3515 circular earth pressure cells during placement

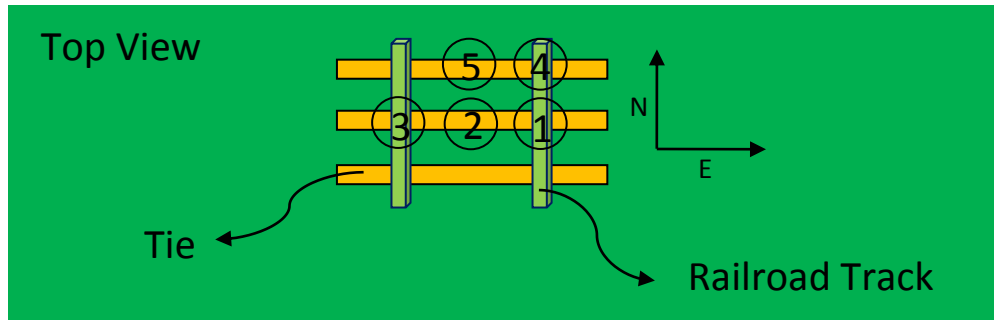


Figure 3.15 Pressure cell locations (not to scale)

3.3.3 Displacement Transducers

A total of four displacement transducers were used to instrument the corners of the track panel, as shown in figure 3.17. The displacement transducers were manufactured by Tokyo Sokki Kenkyujo, Co., Ltd., Japan. Two types of displacement transducers, the CDP-100 (100 mm capacity) and CDP-50 (50 mm capacity), were used to measure the surface displacement of railroad track.

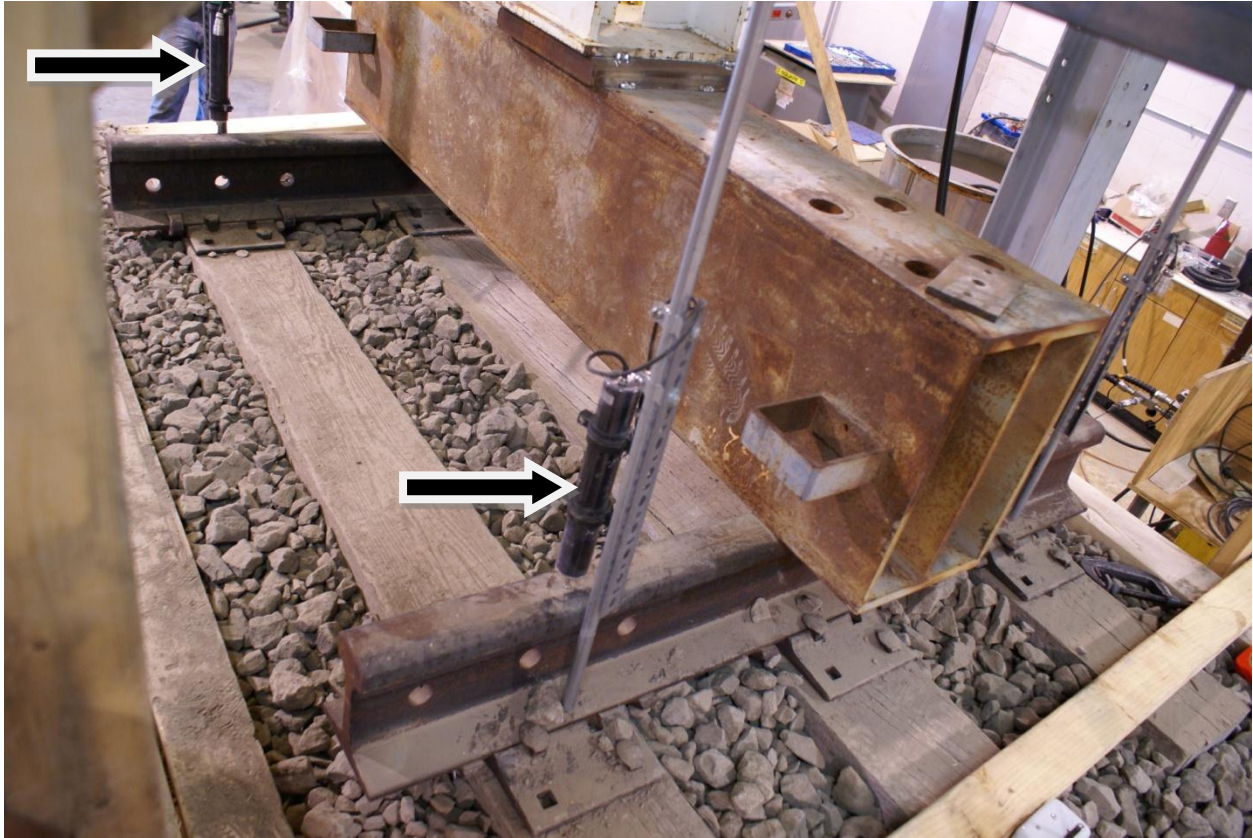


Figure 3.16 Displacement transducer placement

3.3.4 String Pots

Two string potentiometers (string pots) with a maximum range of 20 in. were used to measure the displacement of center ties in the railroad section, as shown in figure 3.18.



Figure 3.17 String pot

3.4 Ballast

Recycled ballast was provided by BNSF and came from track undergoing maintenance in Gardner, Kansas. It was sieved to remove fouling material and to meet the gradation size of BNSF specification limits (class 1), reported in table 3.4. A picture of the sieved material is shown in figure 3.19. This ballast is composed of heterogeneous igneous rock. Samples of the washed rock are shown in figure 3.20. The grain size distribution is shown in figure 3.21, and table 3.5 contains the sieve analysis data. The recycled ballast was sieved with a sieve shaker provided by BNSF, as shown in figure 3.22.

Table 3.4 BNSF specification limits (class 1)

Sieve Analysis (ASTM C 136)	
Sieve Size	BNSF Specification Limits (class 1)
2.5 "	100
2"	90-100
1.5"	50-80
1"	10-35
0.75"	0-10
0.5"	0-5



Figure 3.18 Recycled ballast after sieve



Figure 3.19 Washed rock

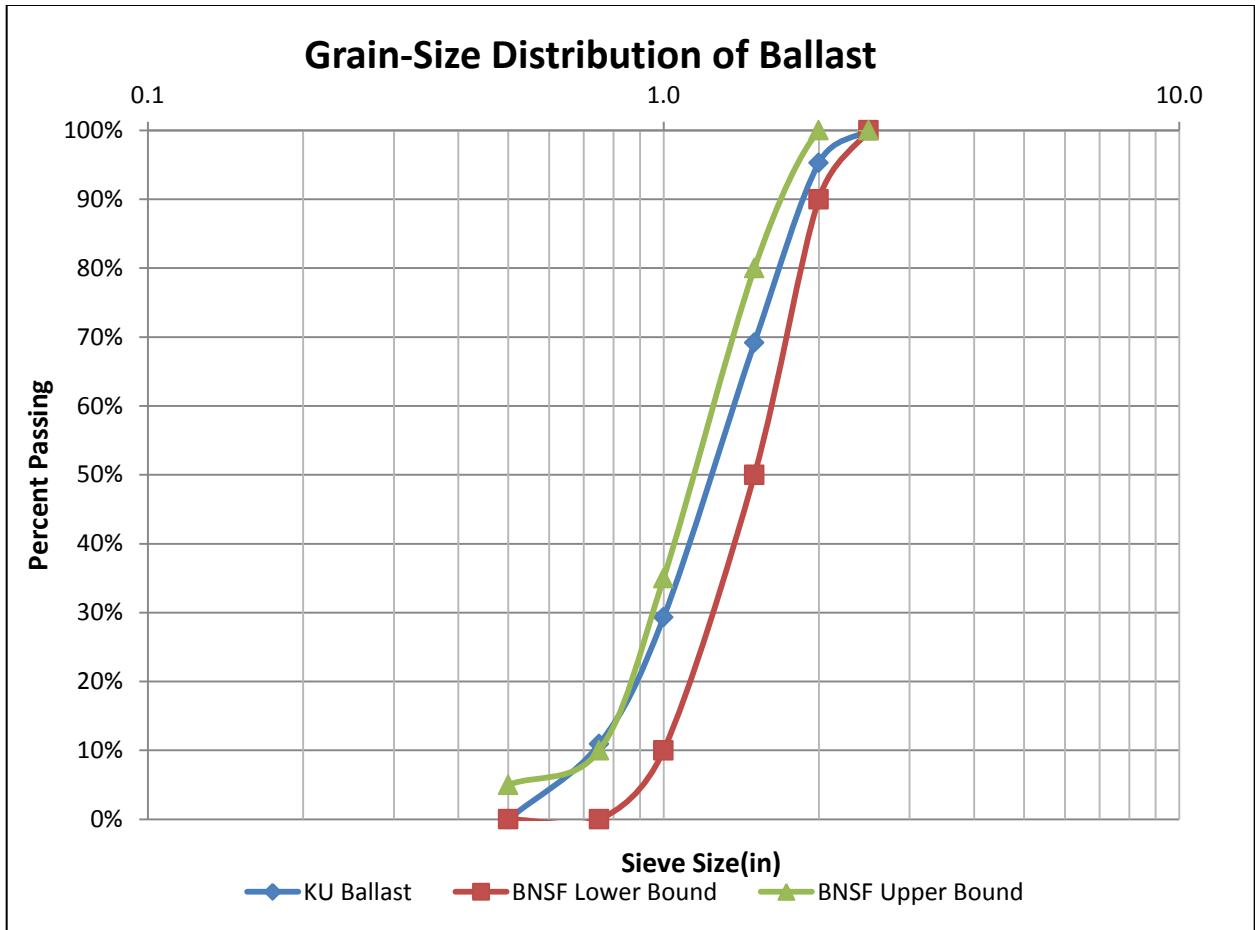


Figure 3.20 Sieve analysis for ballast

Table 3.5 Sieve analysis for ballast

Sieve Opening	Mass Clean Sieve	Mass Sieve and Soil	Mass Retained	% Mass Retained	Cumulative % Retained	% Passing
2.50	22.38	22.38	0	0.0%	0.0%	100.0%
2.00	17.54	20.38	2.84	4.7%	4.7%	95.3%
1.50	21.14	36.84	15.7	26.1%	30.8%	69.2%
1.00	18.3	42.26	23.96	39.9%	70.7%	29.3%
0.75	21.3	32.36	11.06	18.4%	89.1%	10.9%
0.50	22.38	28.94	6.56	10.9%	100.0%	0.0%



Figure 3.21 Sieve shaker for ballast

All sizes were within the range gradation sizes recommended by BNSF except for the 0.75 in. material, which exceeded the limit by 1%. After review, it was the judgment of KU and BNSF that the sieved ballast was essentially consistent with their specifications and would be accepted for use.

3.5 Track

A track panel 5 ft in length and with wooden ties (7" x 9" x 8.5') was in the test setup, as shown in figure 3.23.

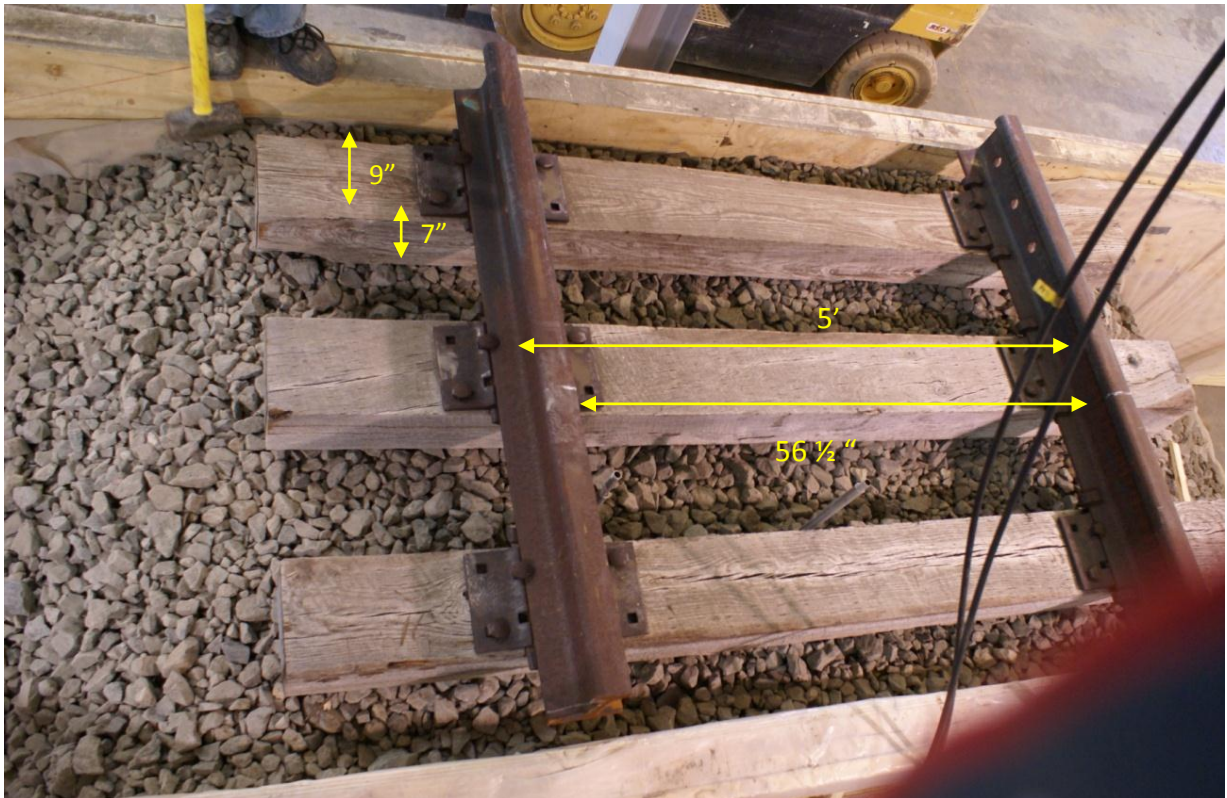


Figure 3.22 A wooden tie track panel

3.6 Geogrid

Triaxial geogrid (TX190L) provided by Tensar Int. Corporation was used to reinforce the ballast section in the reinforced test.

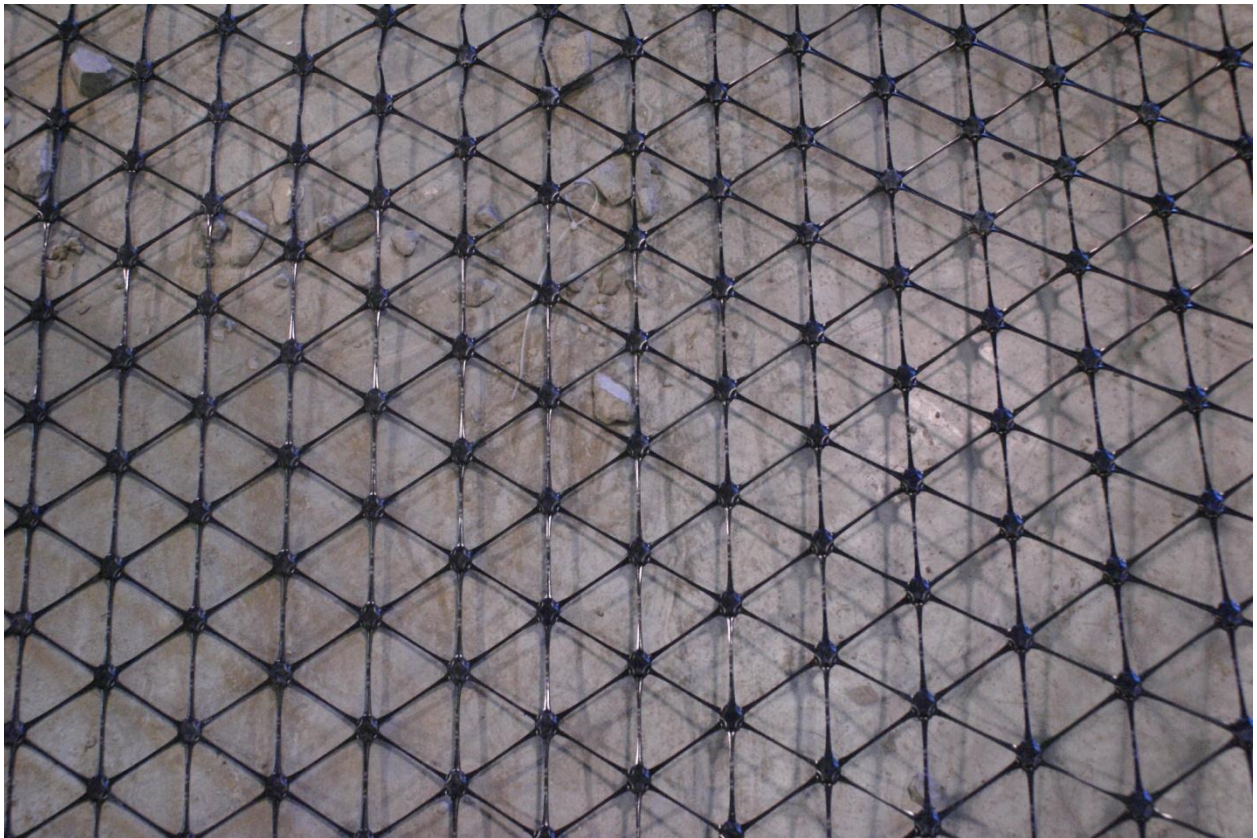


Figure 3.23 Triaxial geogrid used in reinforced test

3.7 Quality Control Tests

Three sets of quality control tests were performed before and after each test in order to verify the compaction quality, modulus, and CBR (DCP Index) of the subgrade.

3.7.1 Light Weight Deflectometer Test (LWD)

LWD is a test method for measuring deflection and compaction quality control during construction. There is an acceleration sensor on the loading plate. LWD also measures the degree of compressibility and average settlement of the section. The LWD tests were carried out on the subgrade with the 30 cm plate, since this plate is suitable for fine soil. This device has a 10 kg drop hammer with a drop height of 1 meter. In LWD, the device hammer is released, which hits the plate. Acceleration is measured with time, and a modulus is calculated based on the force required to generate a given deflection for that soil type. Figure 3.25 shows the LWD.



Figure 3.24 Light weight deflectometer

3.7.2 Density Testing by Drive Tube

Drive tubes were used to determine the level of compaction of the subgrade, as shown in figure 3.18. The average dry unit weight for the subgrade based on an average of four samples was 91.5 lb/ft³ for the unreinforced test (92% of Proctor) and 93lb/ft³ for reinforced case (93% of Proctor).



Figure 3.25 Drive tube and sampler driver

3.7.3 DCP (*Dynamic Cone Penetrometer*)

The DCP was used to measure the in-situ strength of subgrade before and after each test. Results from DCP were then converted to CBR (California bearing ratio) values using the following correlation:

$$\text{CBR}\% = 292/(\text{DPI}) \quad (3.1)$$

where,

DPI units = mm/blow.

Chapter 4 Test Results

Two dynamic loading tests were conducted on full scale railroad sections to investigate the effects of triaxial geogrid on reducing settlement and ballast degradation. The first test was conducted on an unreinforced control section. The second test was conducted with reinforcement using triaxial geogrid. Figure 4.1 shows the unreinforced section prior to placement of the track panel, and figure 4.2 shows the reinforced section with geogrid in place. Figure 4.3 shows the test setup with loading frame.



Figure 4.1 Unreinforced test section



Figure 4.2 Geogrid after replacement in the reinforced test



Figure 4.3 Test during dynamic loading

4.1 Unreinforced Test Section

For this test, dynamic loading was conducted in five steps, as shown in table 4.1. Values in terms of tie bearing pressure are also given; for this research the bearing pressure was calculated assuming the entire area of the tie transmitted the same pressure to the ballast rather than a portion of the tie.

Table 4.1 Loading information for the unreinforced test

Load Step	Cycles	Loading Rate (Sec/Cycle)	Target Supply Pressure (psi)	Actual Average Total Load (lb)	Tie Bearing Pressure (psi)
1	79	5.5	1100	22000	8
2	116	7	2500	50500	18
3	52	19	3500	75600	27
4	100	21	4500 (dry)	92300	34
5	100	22	4500 (soaked)	92100	33

4.1.1 East String Pot

Figure 4.4 shows the deformation with dynamic loading on the east side of the middle tie.

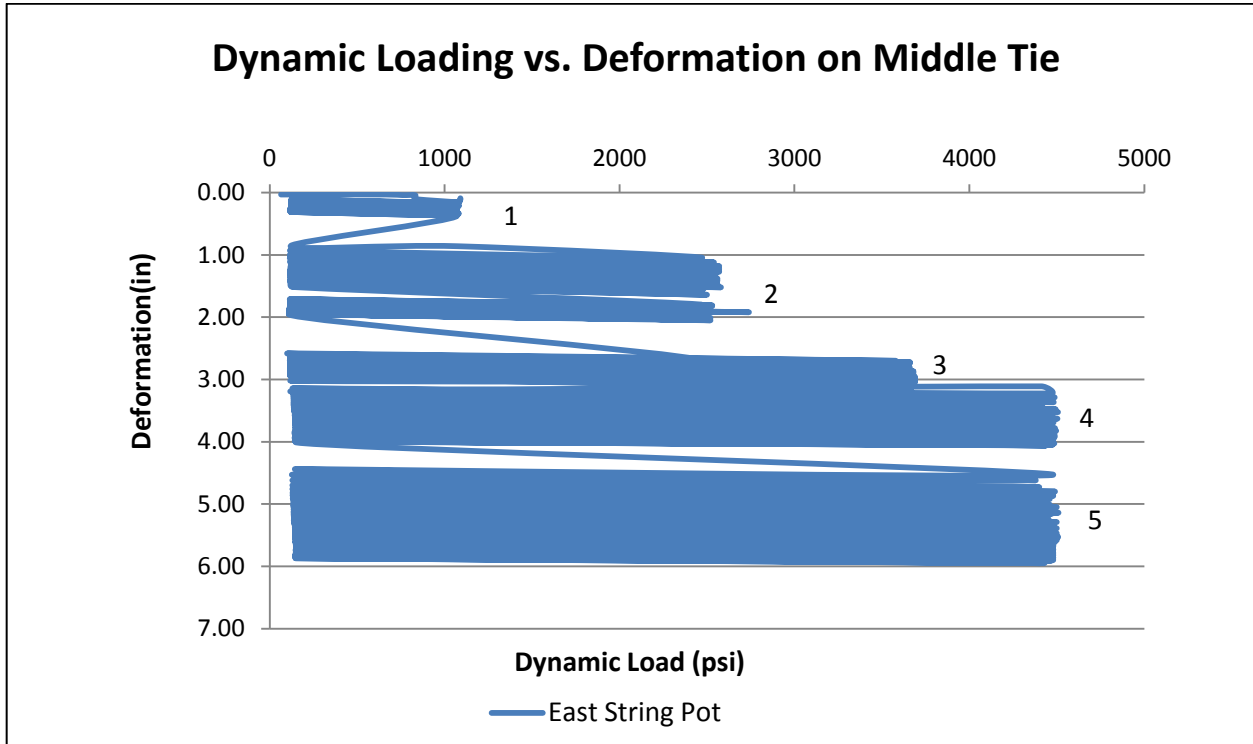


Figure 4.4 Dynamic loading vs. deformation (east string pot)

4.1.2 East String Pot versus Dynamic Loading at 1100 psi (9 psi Tie Bearing Pressure)

Seventy-nine cycles were applied on the railroad section at 1100 psi, resulting in a total accumulated deformation after 79 cycles of 0.37 in. Figure 4.5 shows deformations (settlement) recorded by the east string pot for a dynamic loading of 1100 psi.

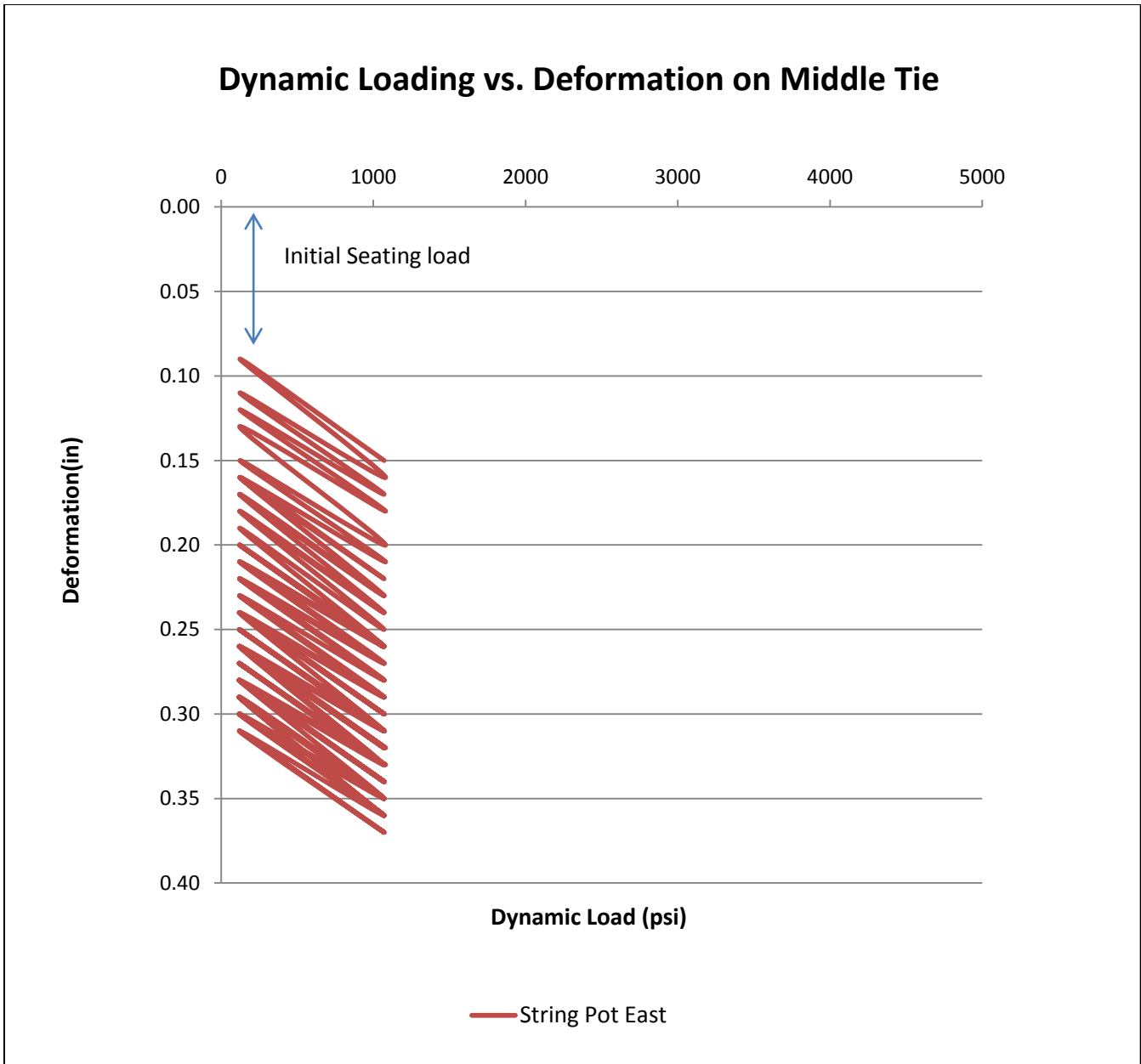


Figure 4.5 East string pot deformations versus dynamic loading at 1100 psi

4.1.3 East String Pot versus Dynamic Loading at 2500 psi (21 psi Tie Bearing Pressure)

One hundred sixteen cycles were applied to the railroad section at 2500 psi. The total accumulated deformation after 116 cycles was 2 in. More permanent deformation was observed during the early cycles of each step. As the number of cycles increased, a higher percentage of the

deformation was elastic. Figure 4.6 shows the east string pot reading versus dynamic loading at 2500 psi.

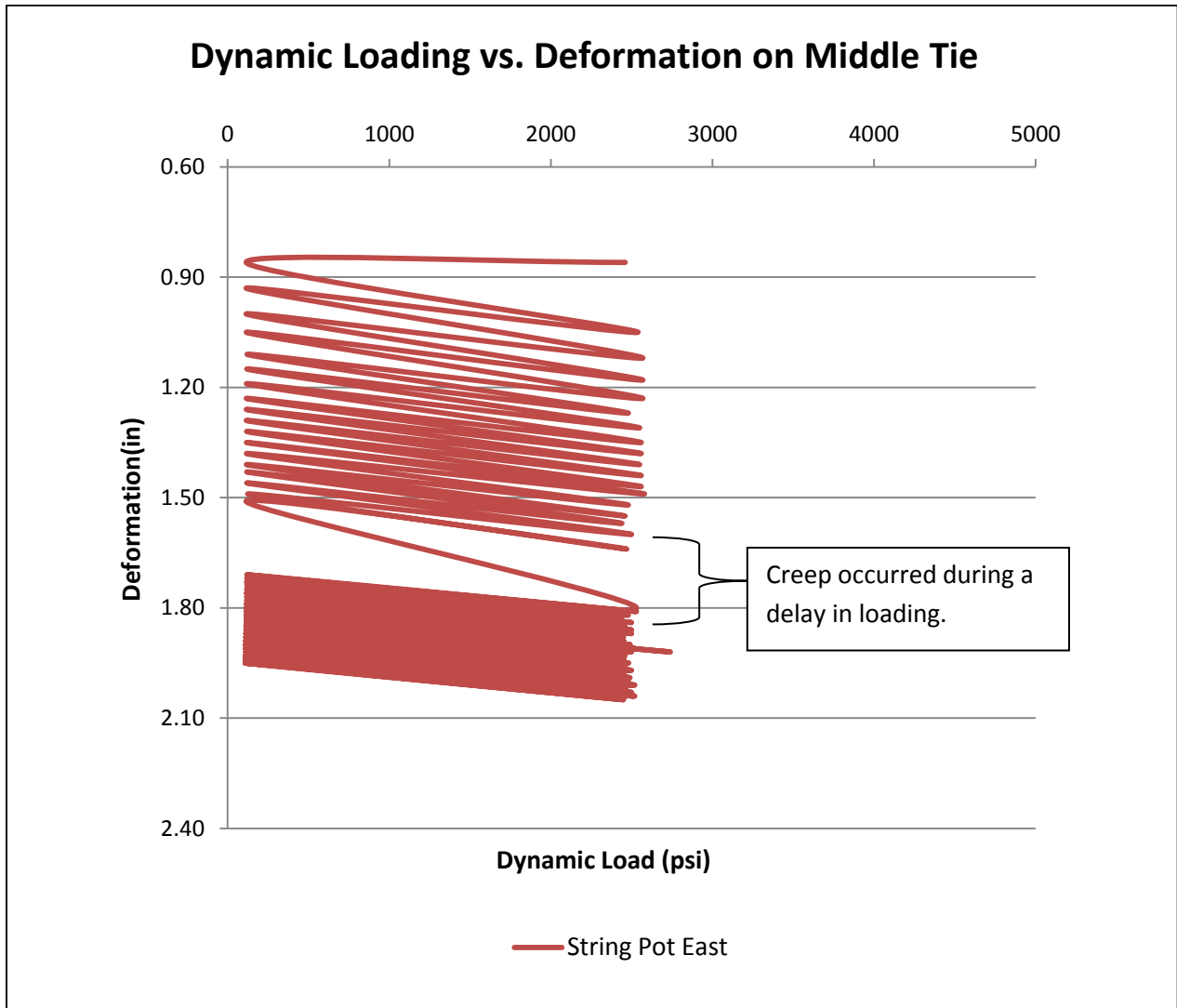


Figure 4.6 East string pot versus dynamic loading at 2500 psi

4.1.4 East String Pot versus Dynamic Loading at 3500 psi (31 psi Tie Bearing Pressure)

Fifty-two cycles were applied to the railroad section at 3500 psi for a total accumulated deformation after 52 cycles of 3.05 in. Figure 4.7 shows the east string pot reading versus dynamic loading at 3500 psi.

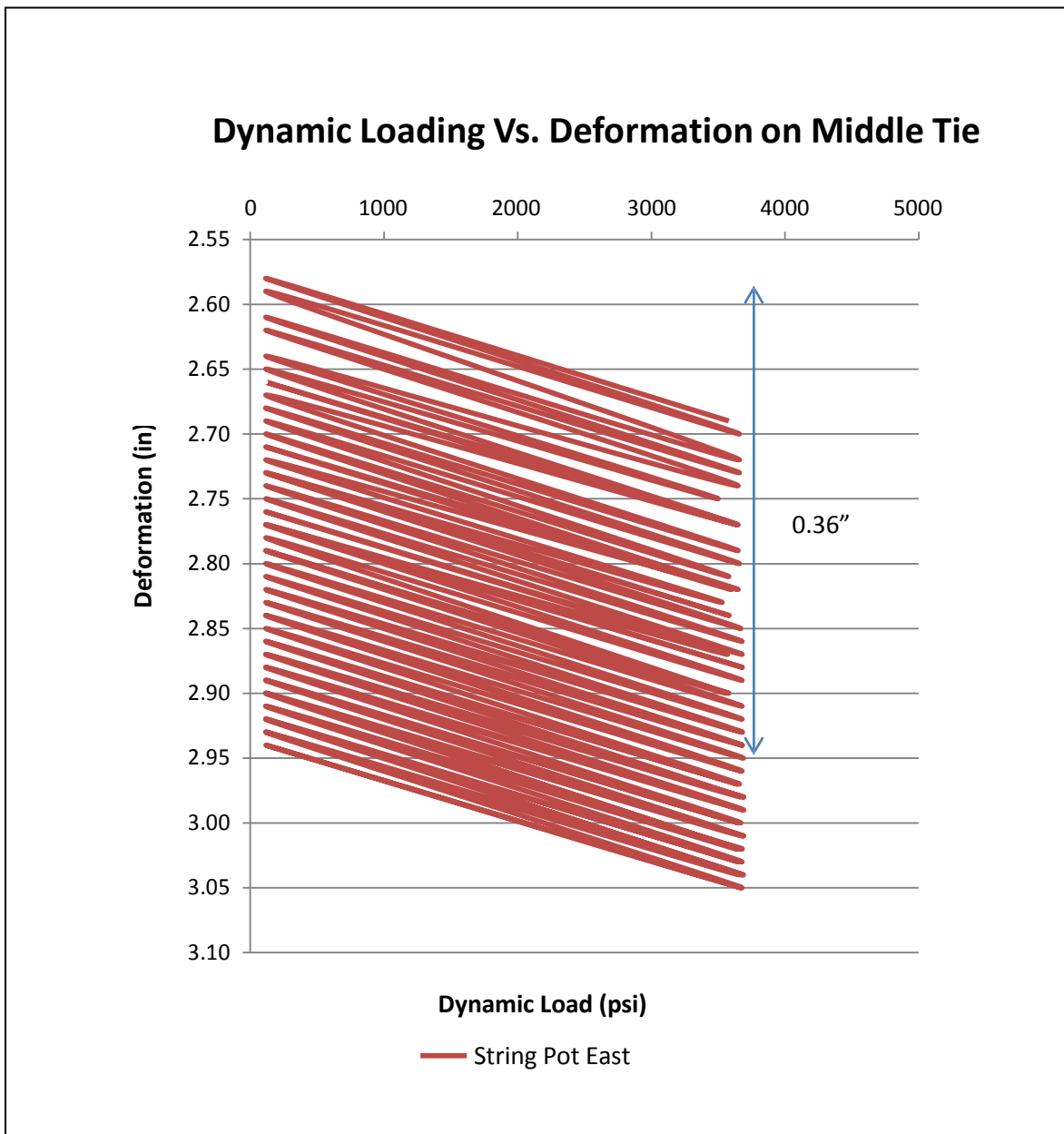


Figure 4.7 East string pot versus dynamic loading at 3500 psi

4.1.5 East String Pot versus Dynamic Loading at 4500 psi (38 psi Tie Bearing Pressure)

One hundred cycles were applied to the railroad section at 4500 psi. The total accumulated deformation after 100 cycles was 4.05 in. Figure 4.8 shows the east string pot reading versus dynamic loading at 4500 psi. More permanent deformation was observed for the early cycles. As the number of cycles increased, more elastic deformation was observed.

As figure 4.8 shows, at the beginning of the loading step the total deformation is the difference between number 1 on figure 4.8 and number 2, which is about 0.12 in. On the same graph the difference between numbers 1 and 3 is the permanent deformation for the same cycle, which is 0.04 in, while the difference between points 2 and 3 is the elastic deformation. This elastic deformation is 0.08 in. As the number of cycles increases the permanent and total deformations per cycle decrease, and a higher percentage of the deformation is elastic.

Dynamic Loading vs. Deformation on Middle Tie

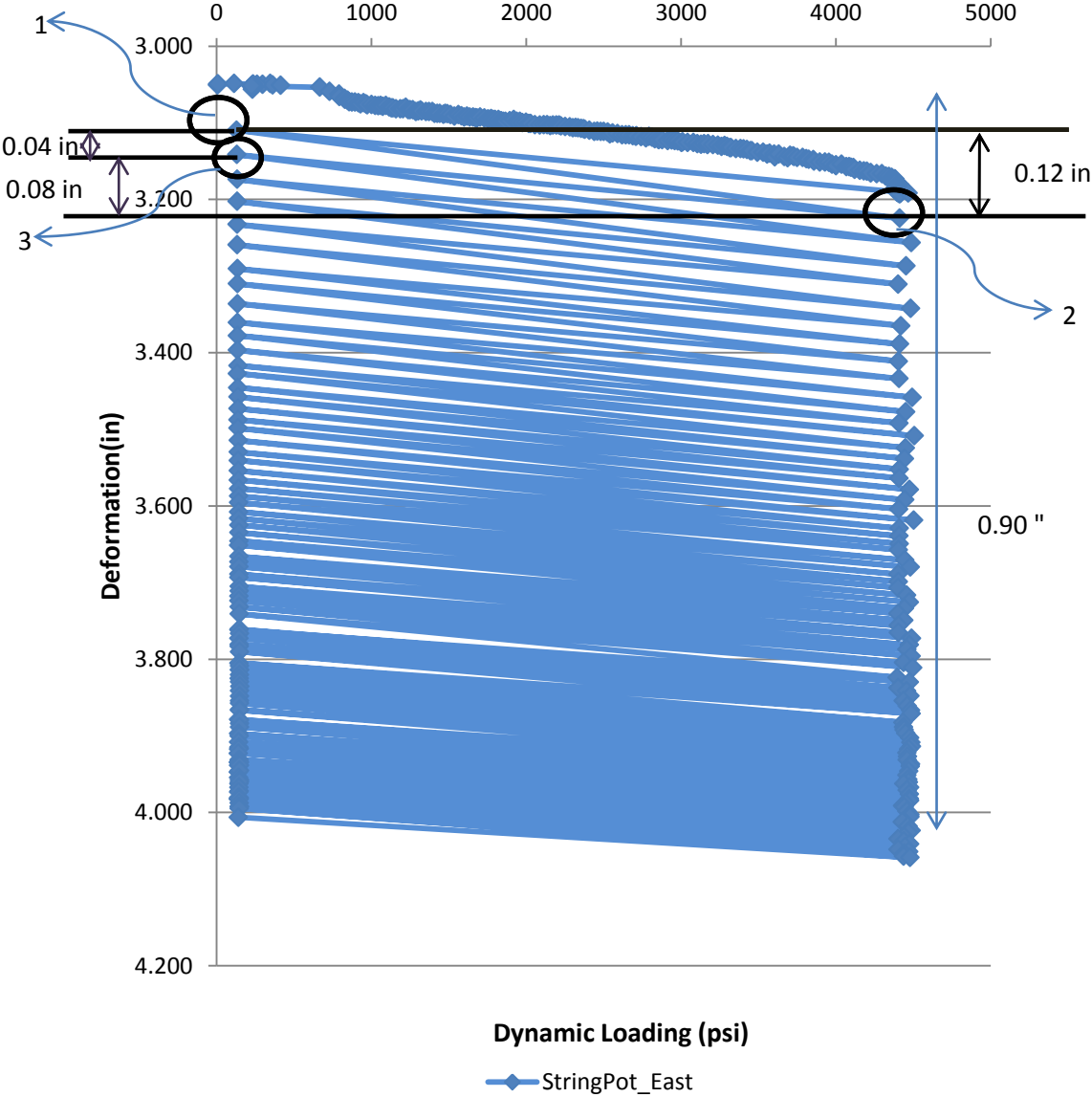


Figure 4.8 East string pot versus dynamic loading at 4500 psi (not soaked)

4.1.6 East String Pot versus Dynamic Loading at 4500 psi (Soaked) (40 psi Tie Bearing Pressure)

Fifty gallons of water were added to the section via garden hose over period of 15 minutes. The section was left overnight for water to penetrate into the soil. One-hundred cycles were applied to the railroad section at 4500 psi the following day. The total accumulated deformation after 100 cycles was 5.95 in. As with the earlier steps, the beginning cycles resulted in more permanent deformation per cycle. As the number of cycles increased more elastic deformation was observed. Figure 4.9 shows the east string pot reading versus dynamic loading at 4500 psi, soaked.

As shown in figure 4.9, at the beginning of the loading step the difference between numbers 1 and 2 was the total deformation, or, 0.18 in., which was 50% more than was observed during the initial cycles when loading the section to 4500 psi without soaking, and 40% more than was observed at the end of the end of unsoaked loading. Most of the additional deformation per cycle was permanent. On the same graph, the difference between numbers 1 and 3 was the permanent deformation for the same cycle, which was 0.09 in. The elastic deformation is shown on the same graph, and was also 0.09 in. As with the previous loading step, the permanent and total deformations per cycle decreased as the number of cycles increased, and a higher percentage of the deformation was elastic.

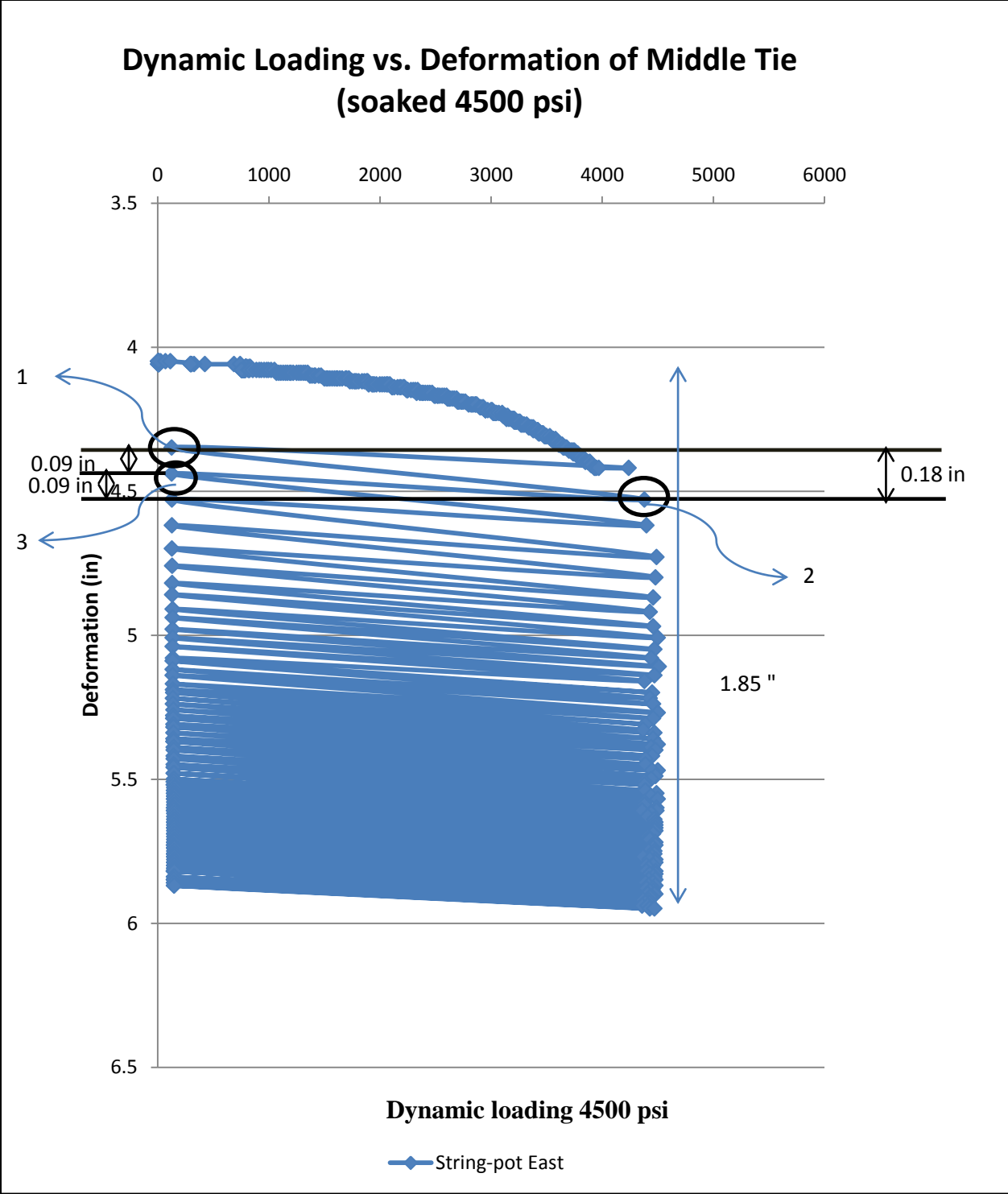


Figure 4.9 East string pot reading versus dynamic loading at 4500 psi soaked

4.1.7 West String Pot

Figures 4.10-4.15 show the recorded values on the west string pot. These deformations were generally consistent with those from the east string pot.

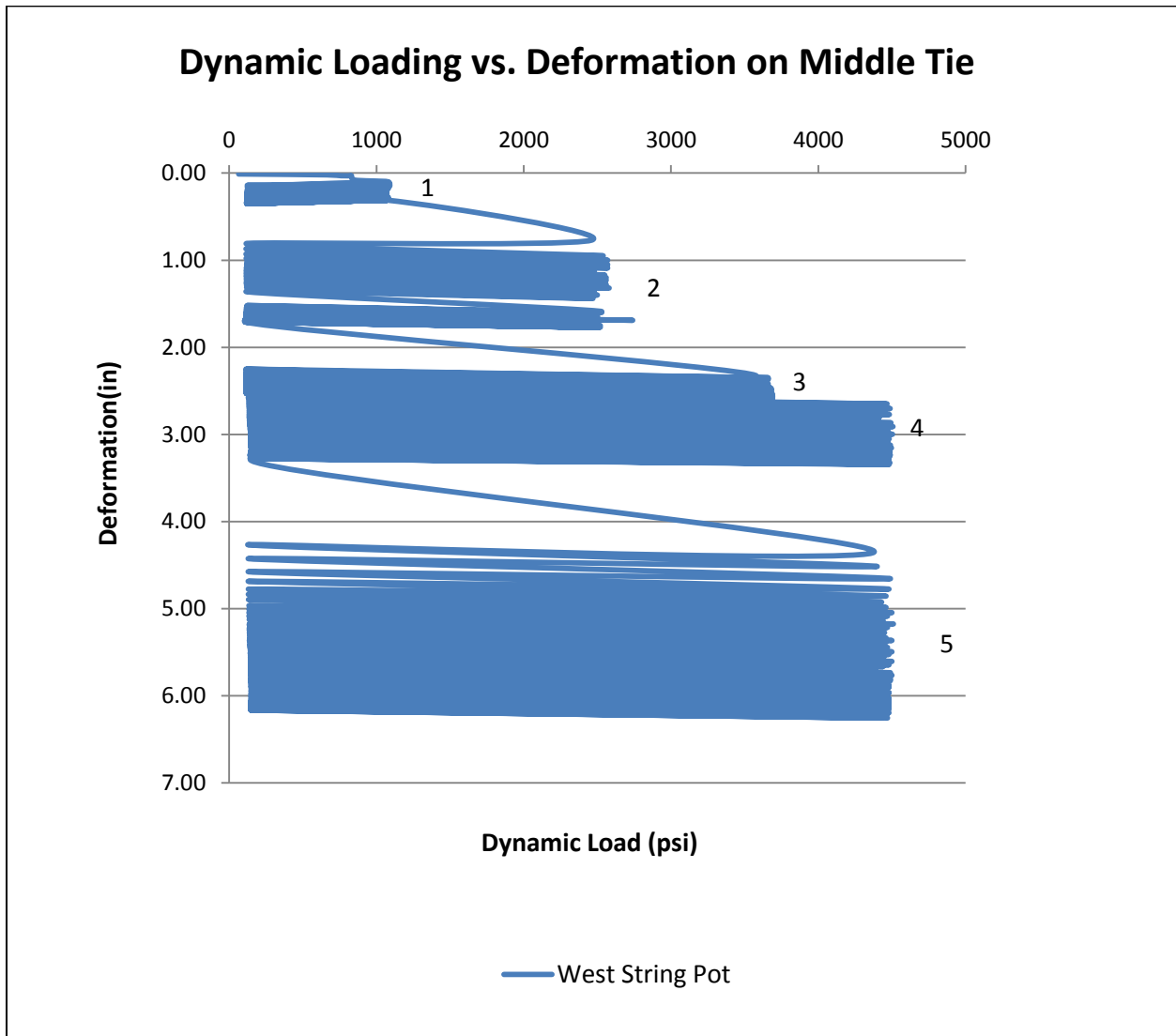


Figure 4.10 Dynamic loading vs. deformation (west string pot)

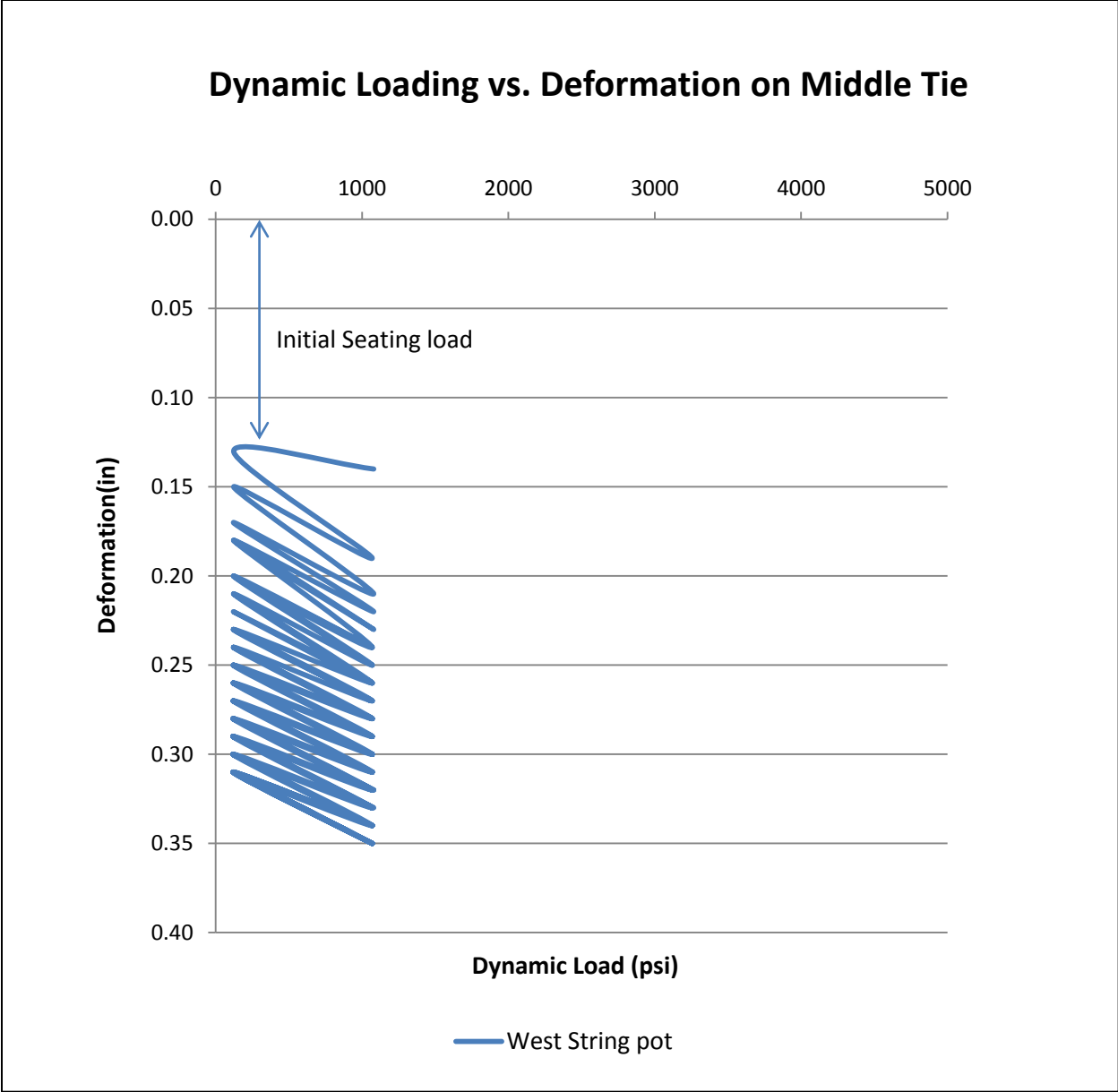


Figure 4.11 West string pot versus dynamic loading at 1100 psi

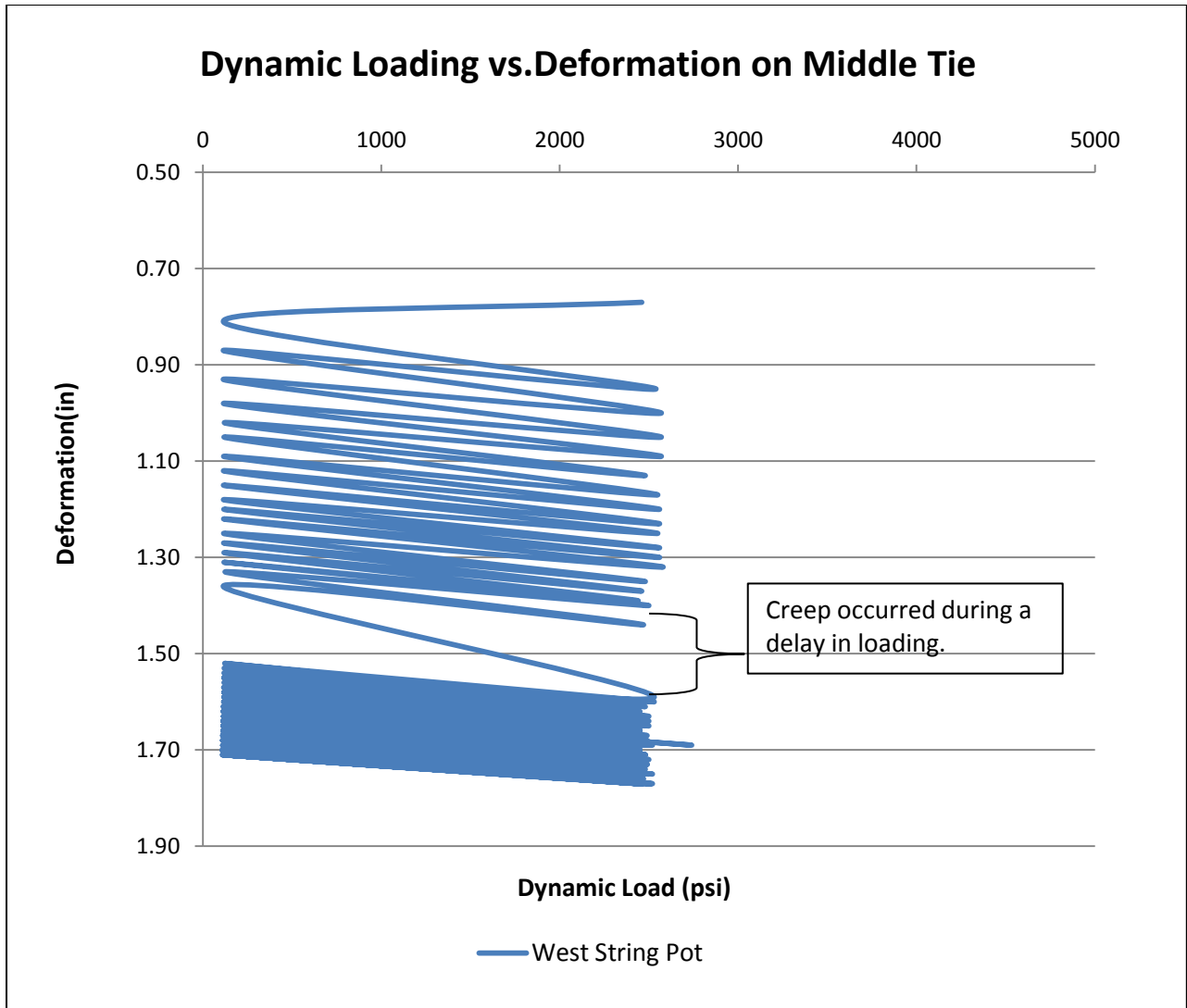


Figure 4.12 West string pot versus dynamic loading at 2500 psi

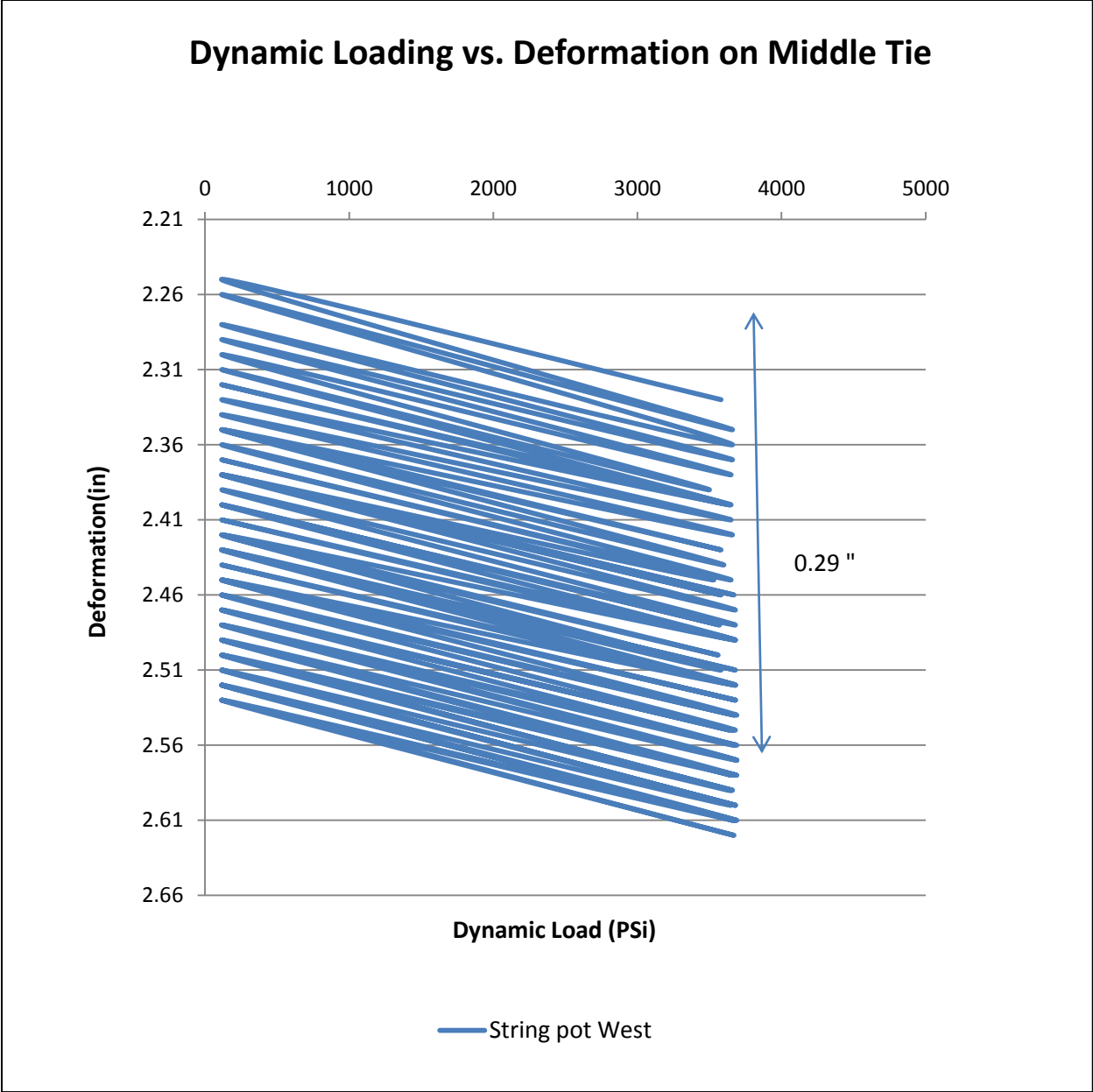


Figure 4.13 West string pot versus dynamic loading at 3500 psi

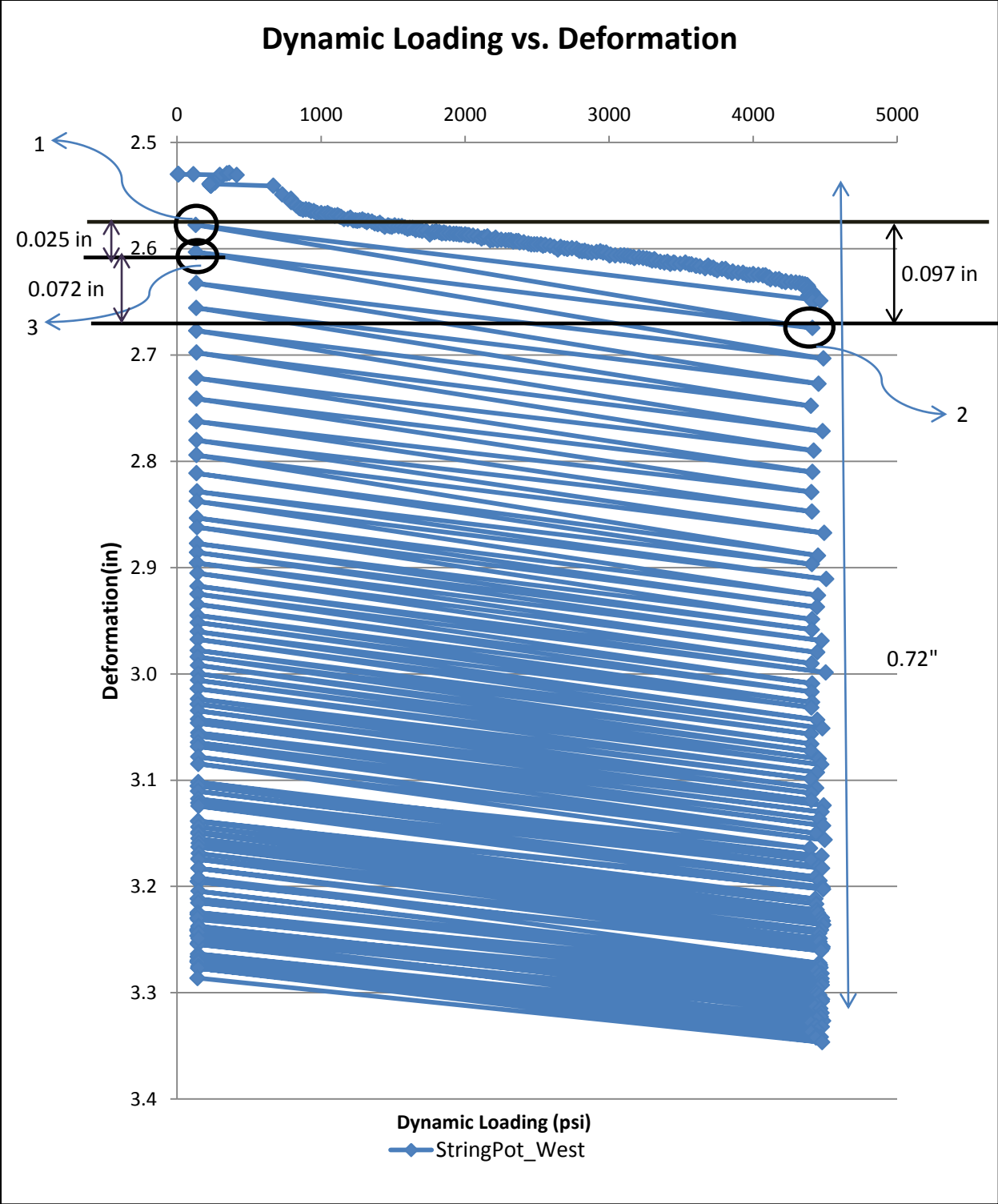


Figure 4.14 West string pot versus dynamic loading at 4500 psi (not soaked)

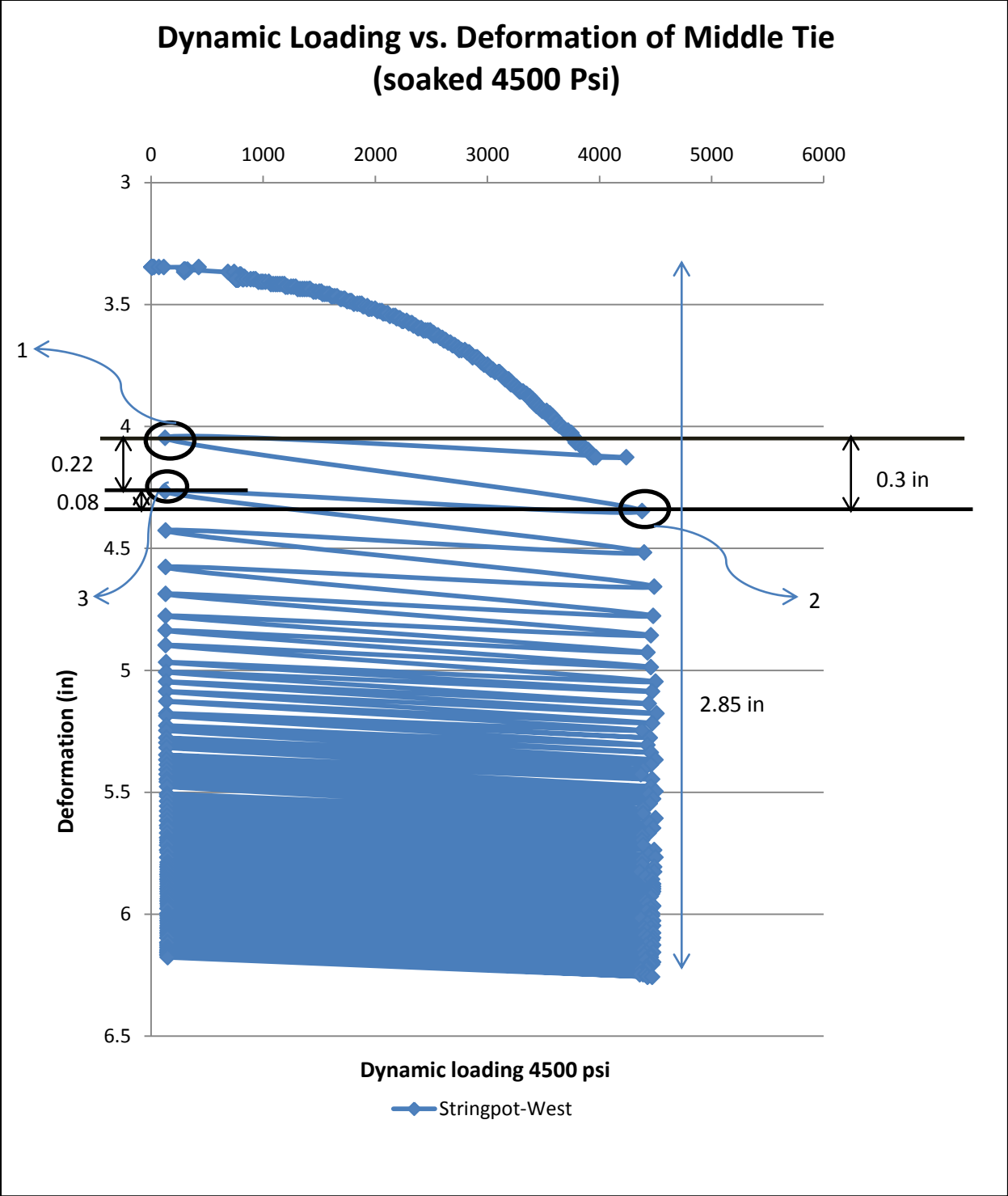


Figure 4.15 West string pot versus dynamic loading at 4500 psi (soaked)

4.1.8 Unreinforced Test (Displacement Transducers)

Four displacement transducers were installed on the railroad track to measure the deformation near the ends of each rail on the track panel. Figure 4.16 shows the transducer locations. Some sliding of transducer ends resulted in measurements that were not reliable. These results are not included in the analysis.

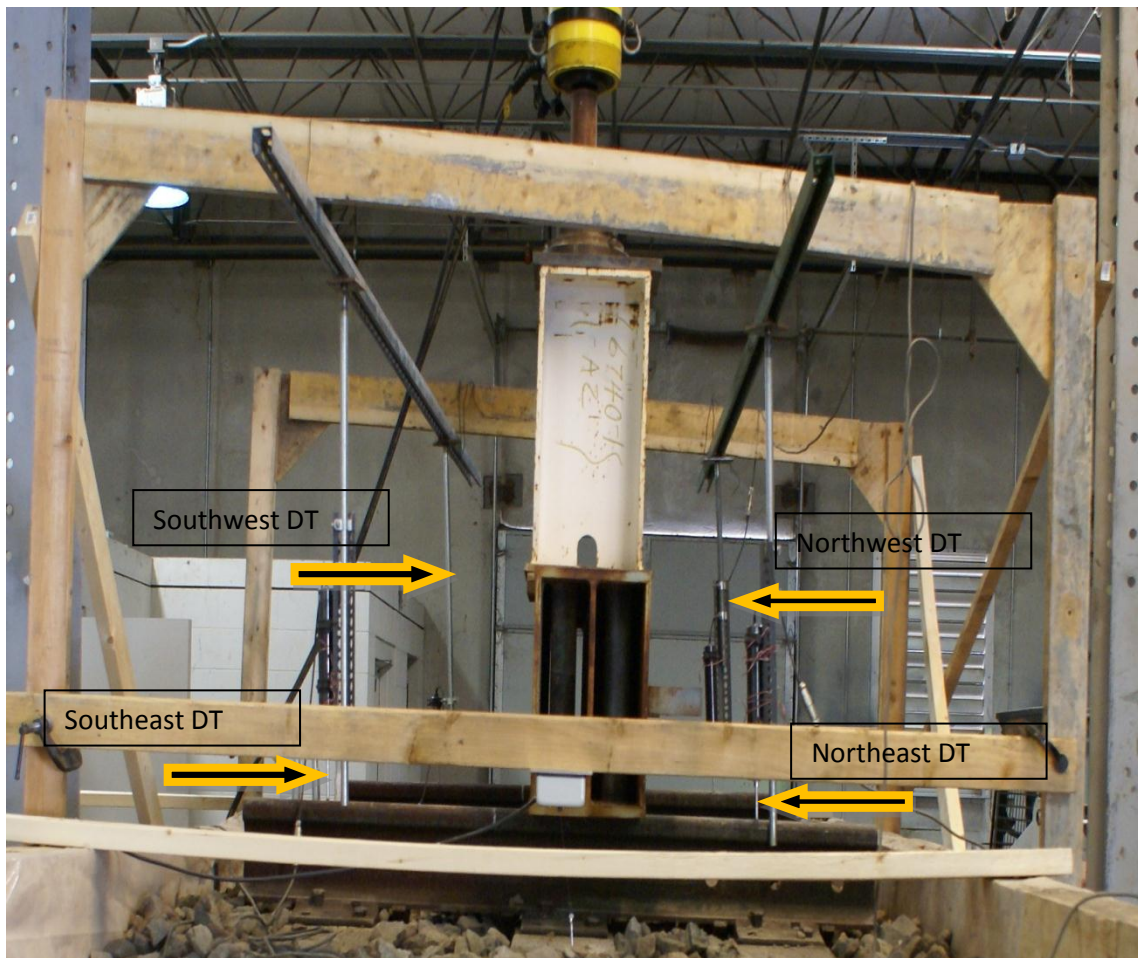


Figure 4.16 Displacement transducers

4.1.9 Displacement Transducers at 1100 psi (Southeast) (9 psi Tie Bearing Pressure)

Seventy-nine cycles were applied to the railroad section at 1100 psi. The total deformation accumulated after 79 cycles was 0.41 in. Figures 4.17-4.20 show DT reading versus dynamic loading at 1100 psi.

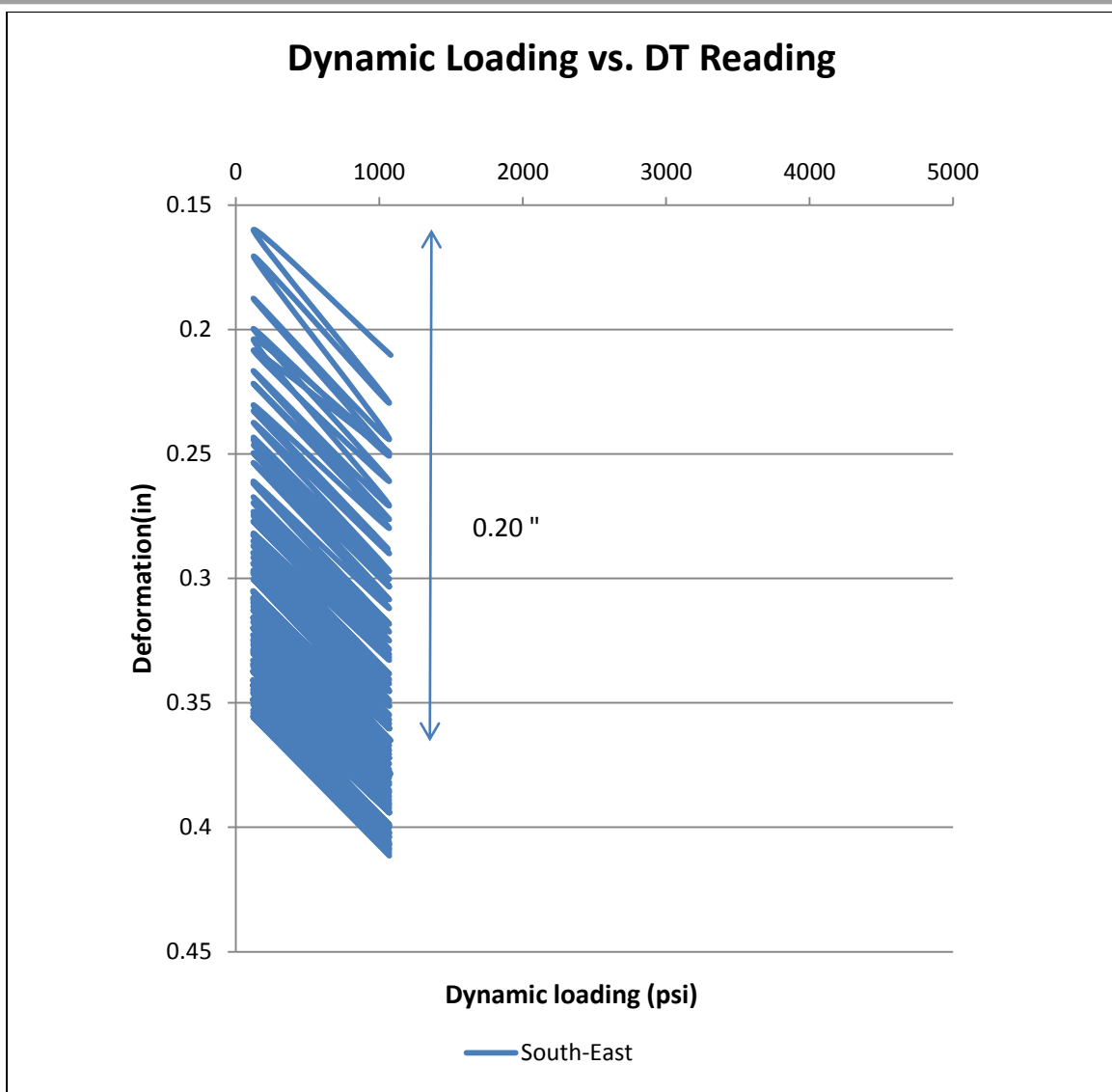


Figure 4.17 Displacement transducer reading at 1100 psi (southeast)

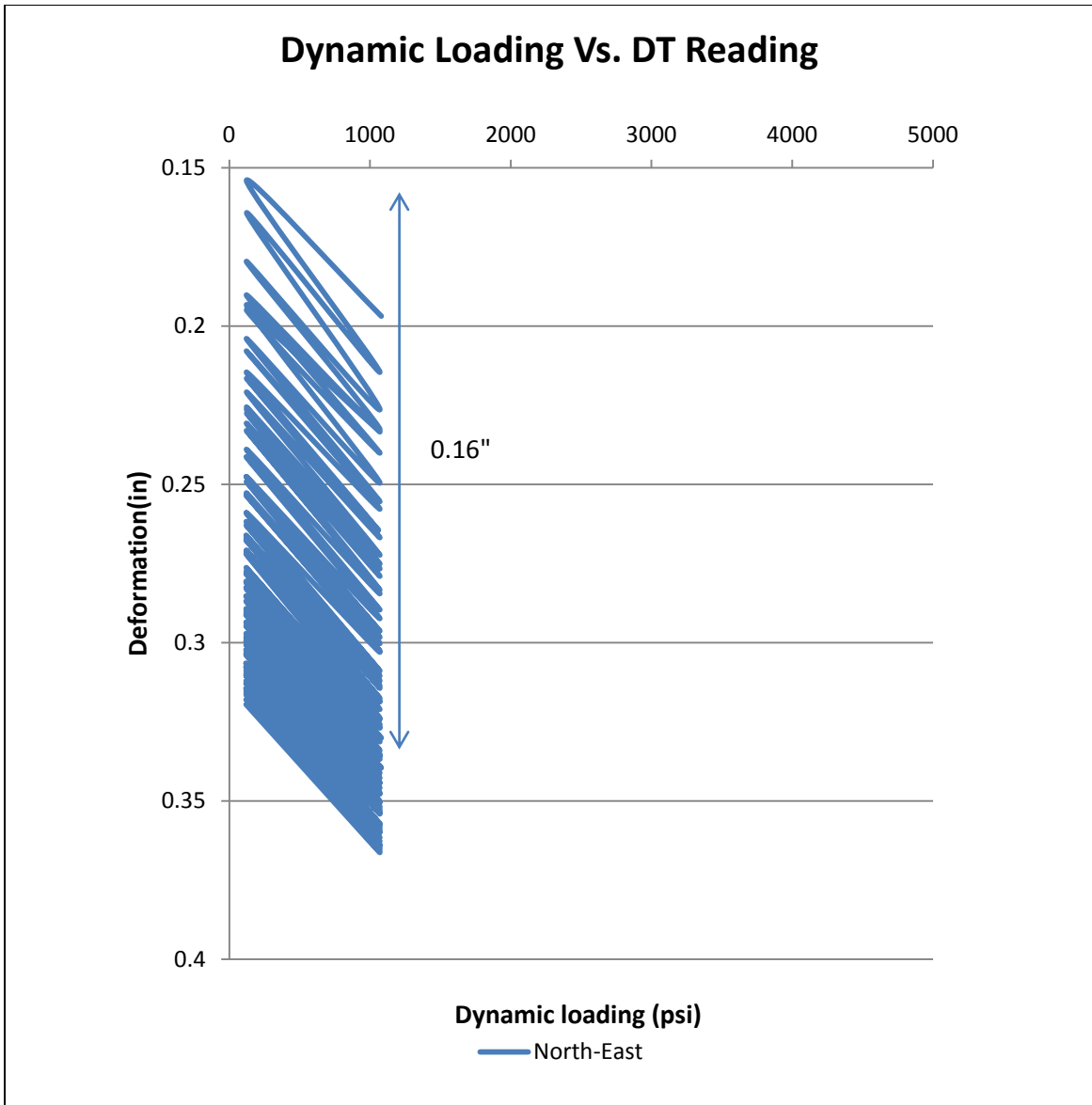


Figure 4.18 Displacement transducer reading at 1100 psi (northeast)

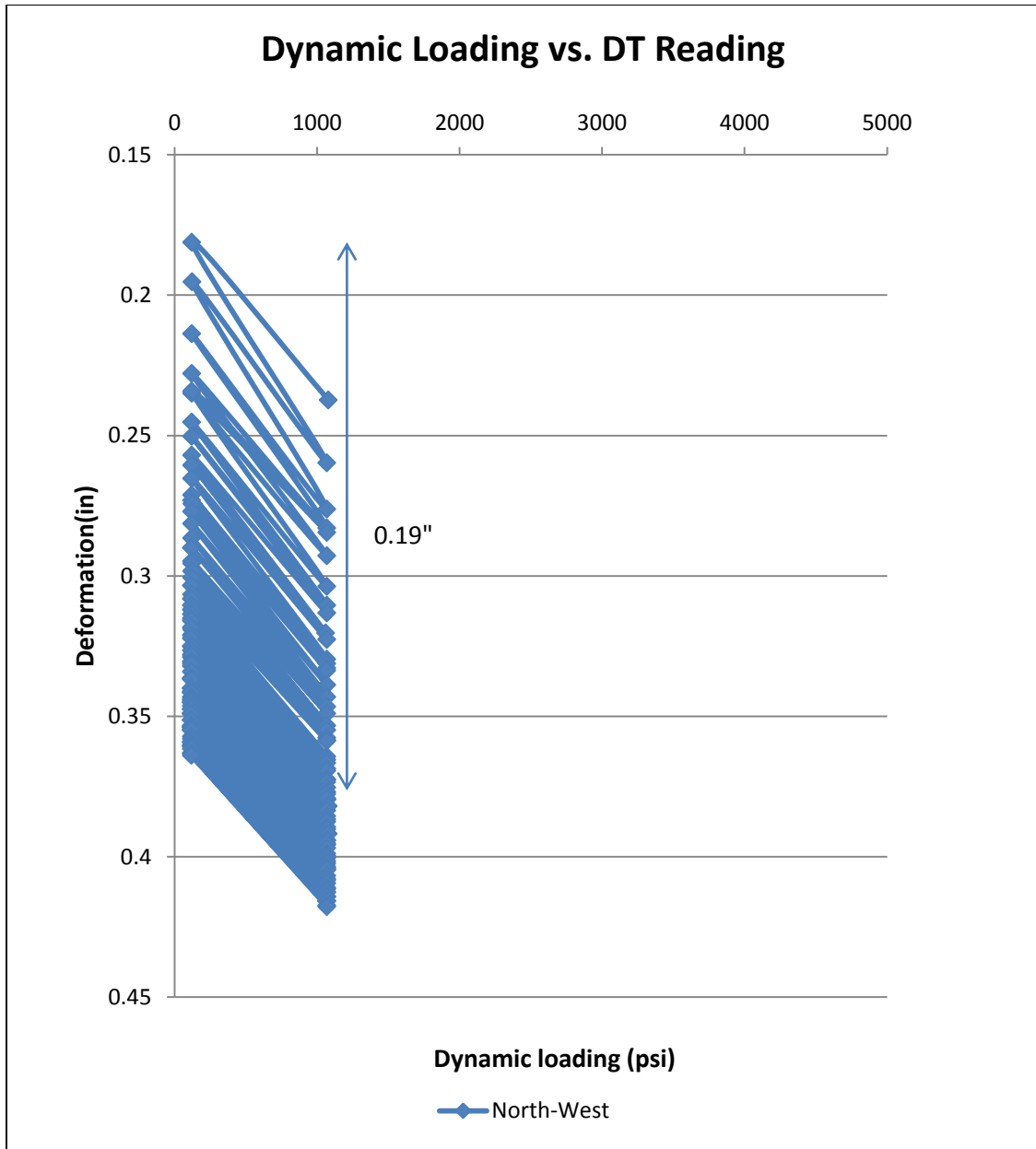


Figure 4.19 Displacement transducer reading at 1100 psi (northwest)

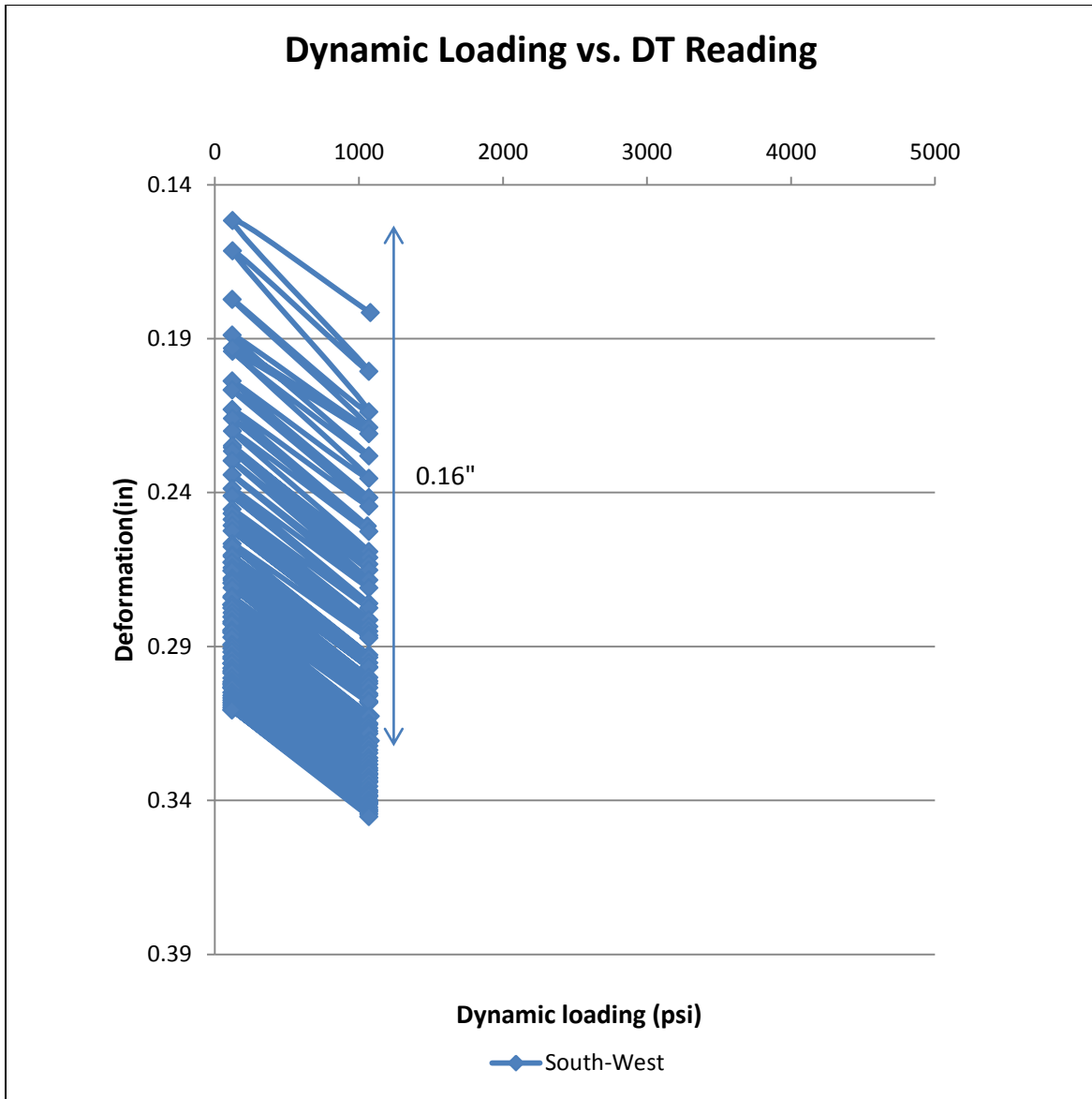


Figure 4.20 Displacement transducer reading at 1100 psi (southwest)

Due to slippage of the displacement transducers, data for the 2500 psi and 3500 psi load levels were not reliable and were not included.

4.1.10 Displacement Transducers at 4500 psi Dry (Southeast)

One-hundred cycles were applied to the railroad section at 4500 psi unsoaked, resulting in a total accumulated deformation after one 100 cycles of 3.7 in. Permanent deformations were large during early cycles in the load step. As the number of cycles increased, the total deformation per cycle decreased and a higher percentage of the deformation was elastic. Deformations at each of the four corners of the track panel are shown in figures 4.21-4.24.

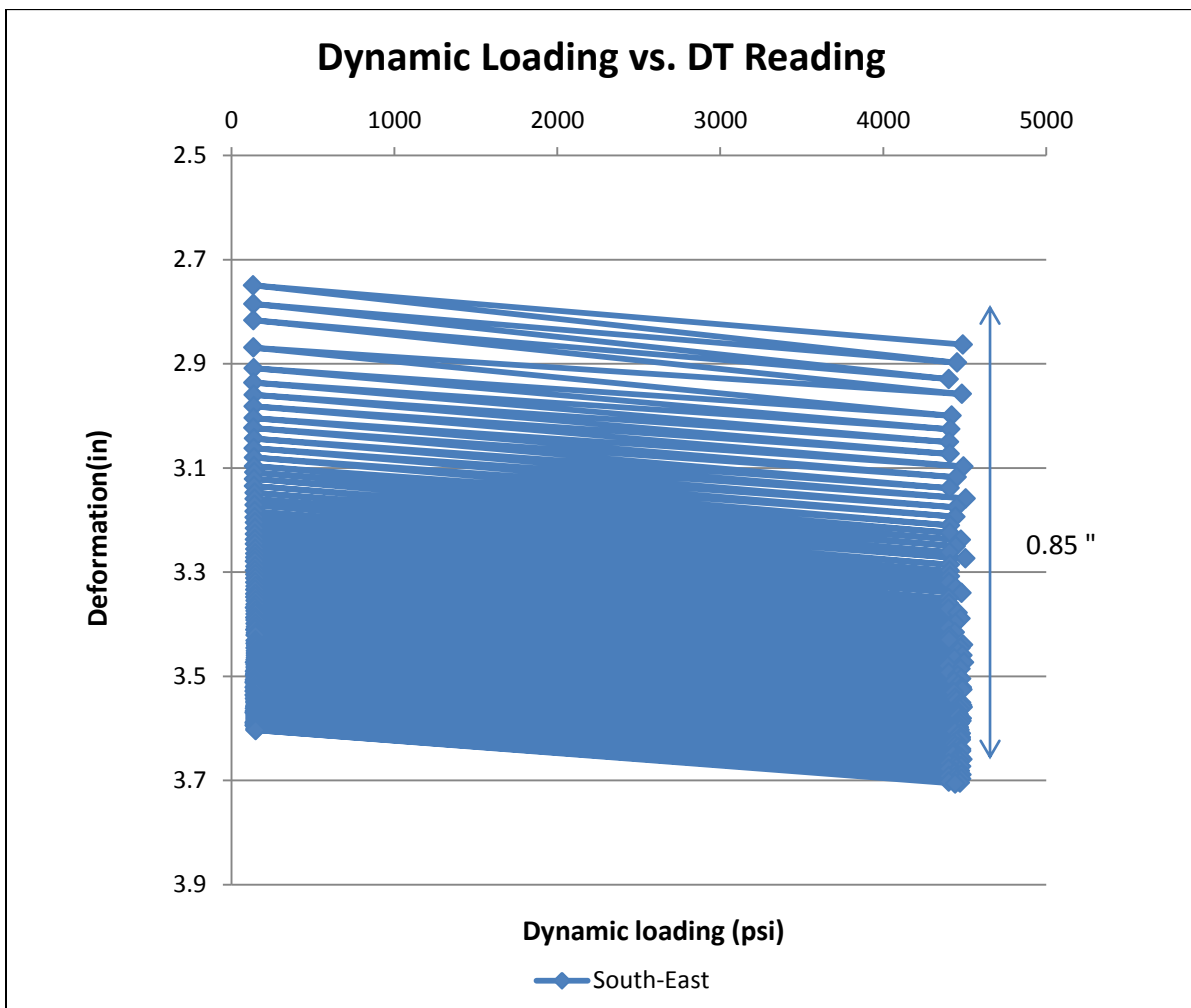


Figure 4.21 Displacement transducer reading at 4500 psi not soaked (southeast)

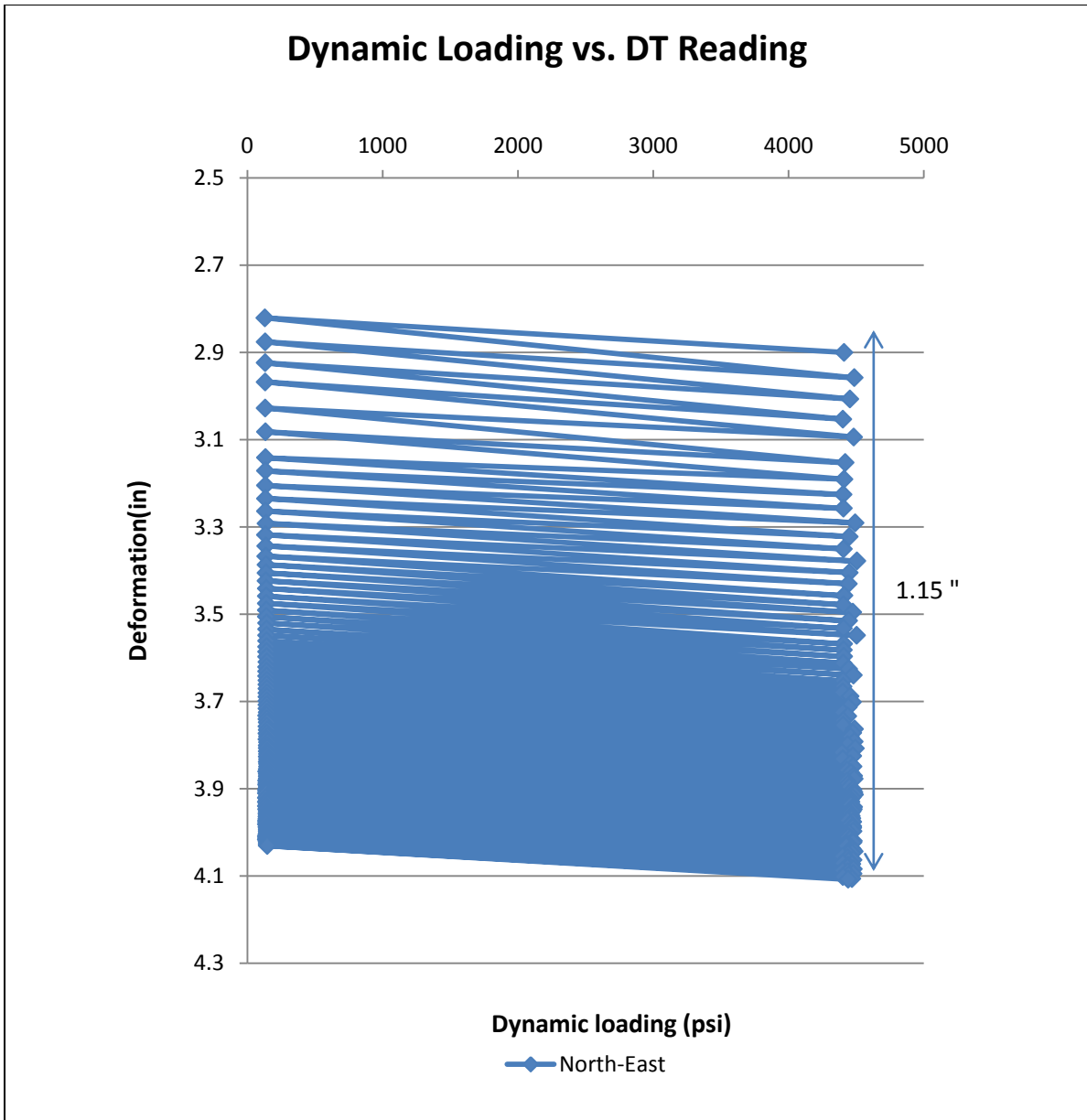


Figure 4.22 Displacement transducer reading at 4500 psi not soaked (northeast)

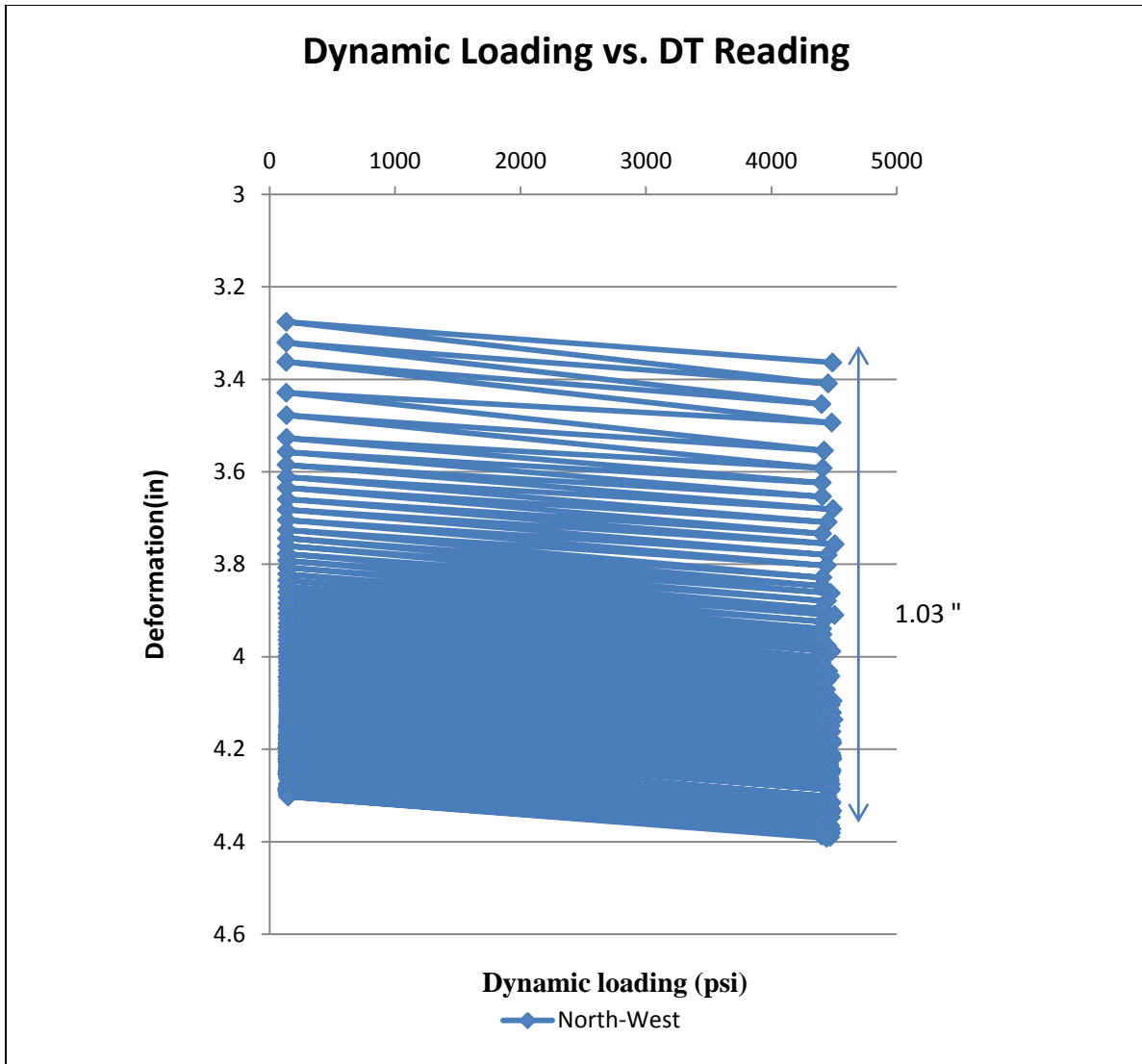


Figure 4.23 Displacement transducer reading at 4500 psi not soaked (northwest)

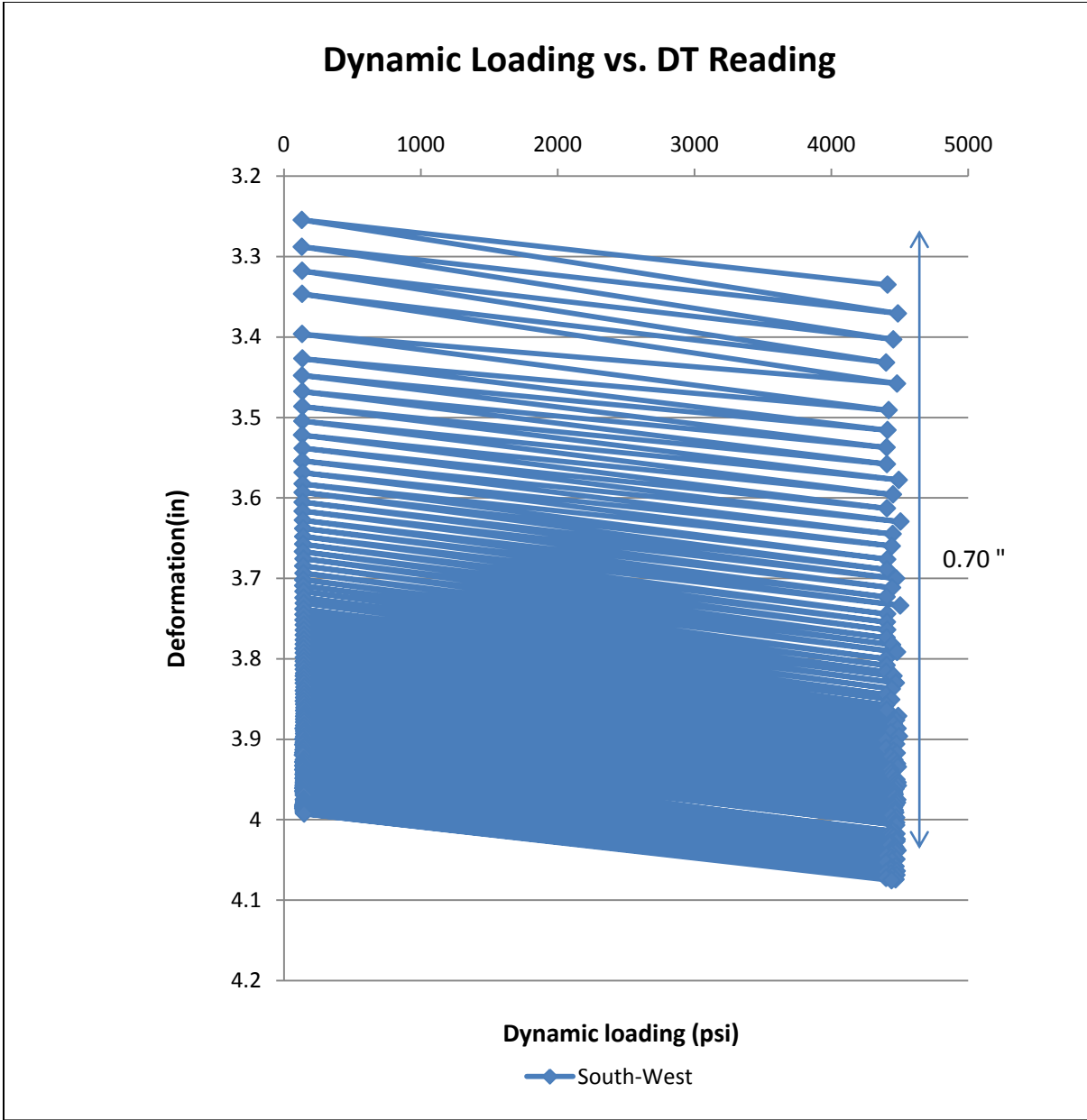


Figure 4.24 Displacement transducer reading at 4500 psi not soaked (southwest)

4.1.11 Displacement Transducers at 4500 psi Soaked (40 psi Tie Bearing Pressure)

After completion of the 4500 psi (unsoaked) loading step, 50 gallons of water were added to the section and allowed to soak-in overnight. One-hundred cycles were then applied to the railroad section at 4500 psi dry. Total deformation accumulated after 100 cycles was 5.85 in. Deformations were larger during the early cycles of the load step. As the number of cycles increased, a higher percentage of the deformations were elastic. Deformations at each of the four corners of the track panel are shown in figures 4.25-4.28.

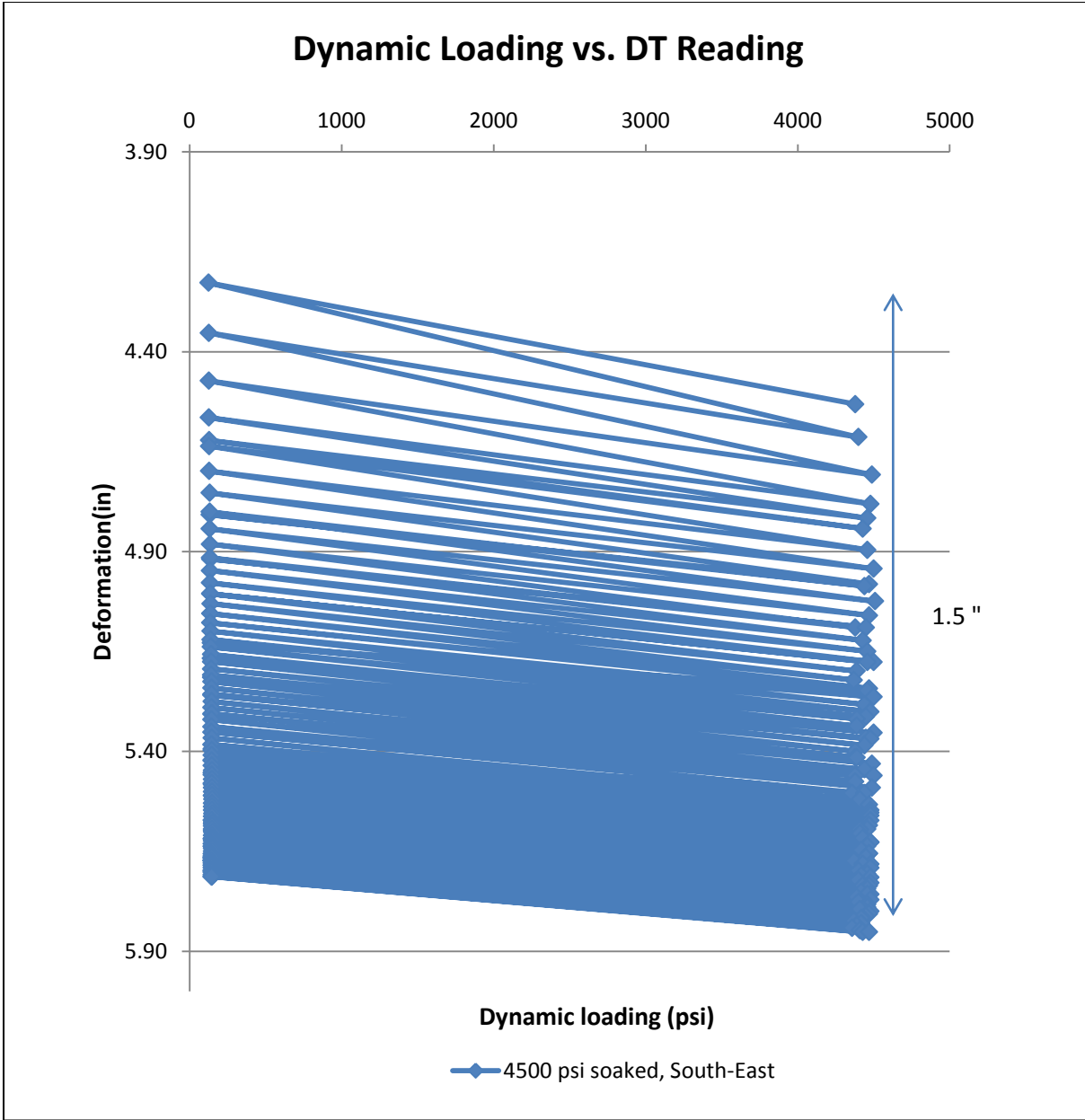


Figure 4.25 Displacement transducer reading at 4500 psi soaked (southeast)

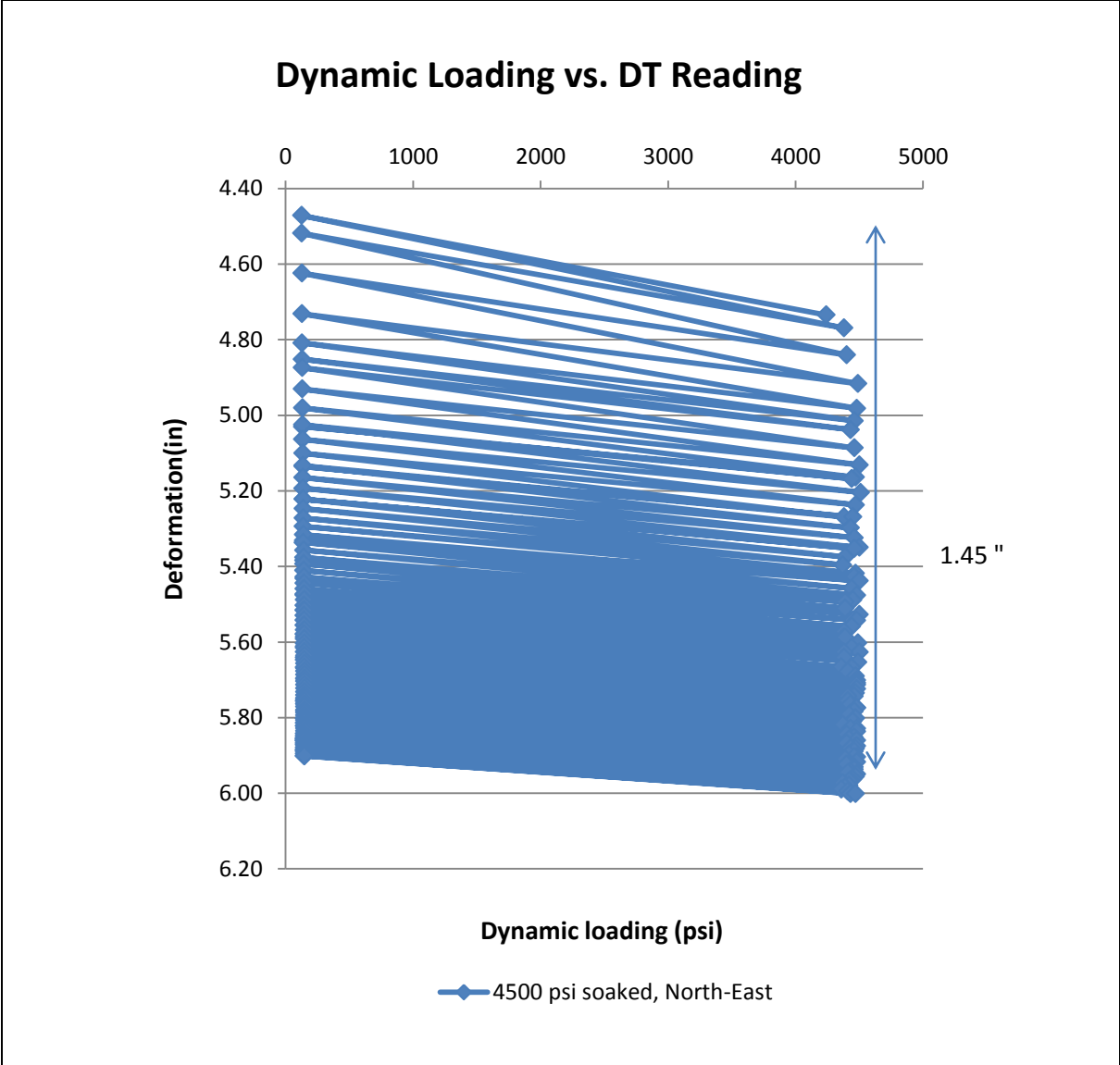


Figure 4.26 Displacement transducer reading at 4500 psi soaked (northeast)

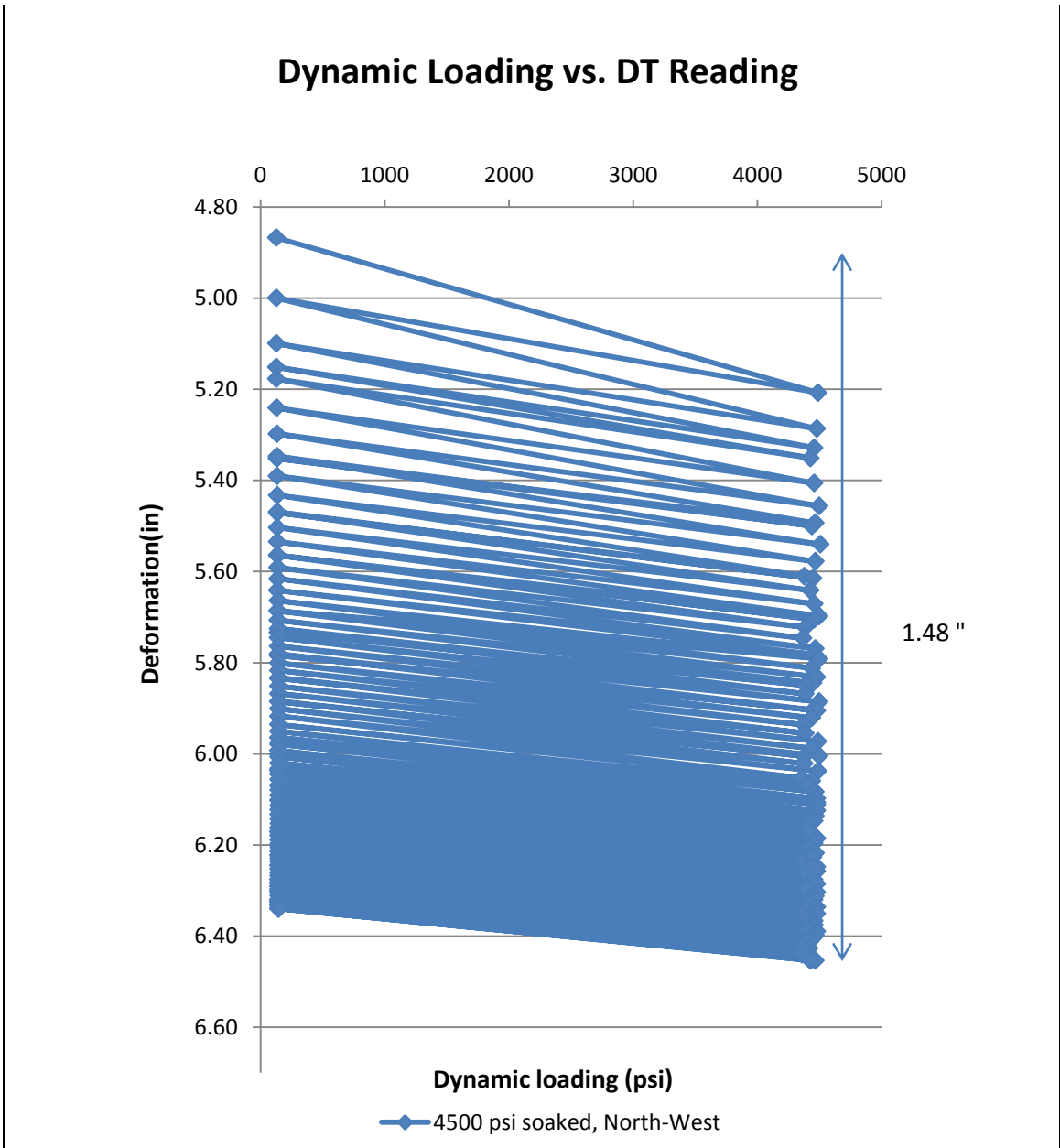


Figure 4.27 Displacement transducer reading at 4500 psi soaked (northwest)

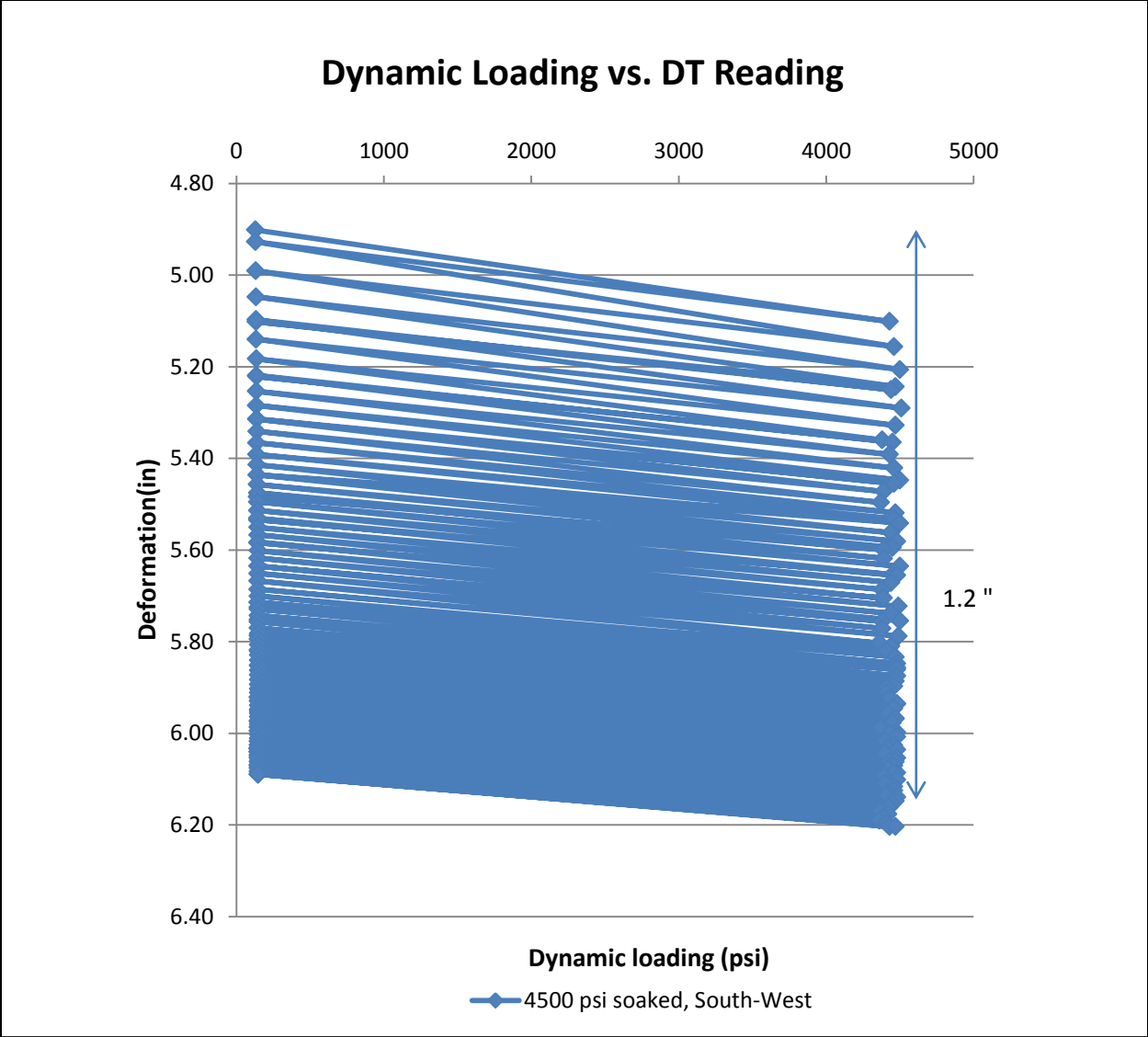


Figure 4.28 Displacement transducer reading at 4500 psi soaked (southwest)

4.1.12 Pressure Cell Results for Unreinforced Test

Five pressure cells were installed, as shown in figure 4.29. Pressure cells 1, 2 and 3 were installed at the interface of subgrade and ballast under the middle tie (1 and 3 were right below the rails). Pressure cells 4 and 5 were installed under the right tie with Cell 4 beneath the rail and Cell 5 beneath the center of the tie.

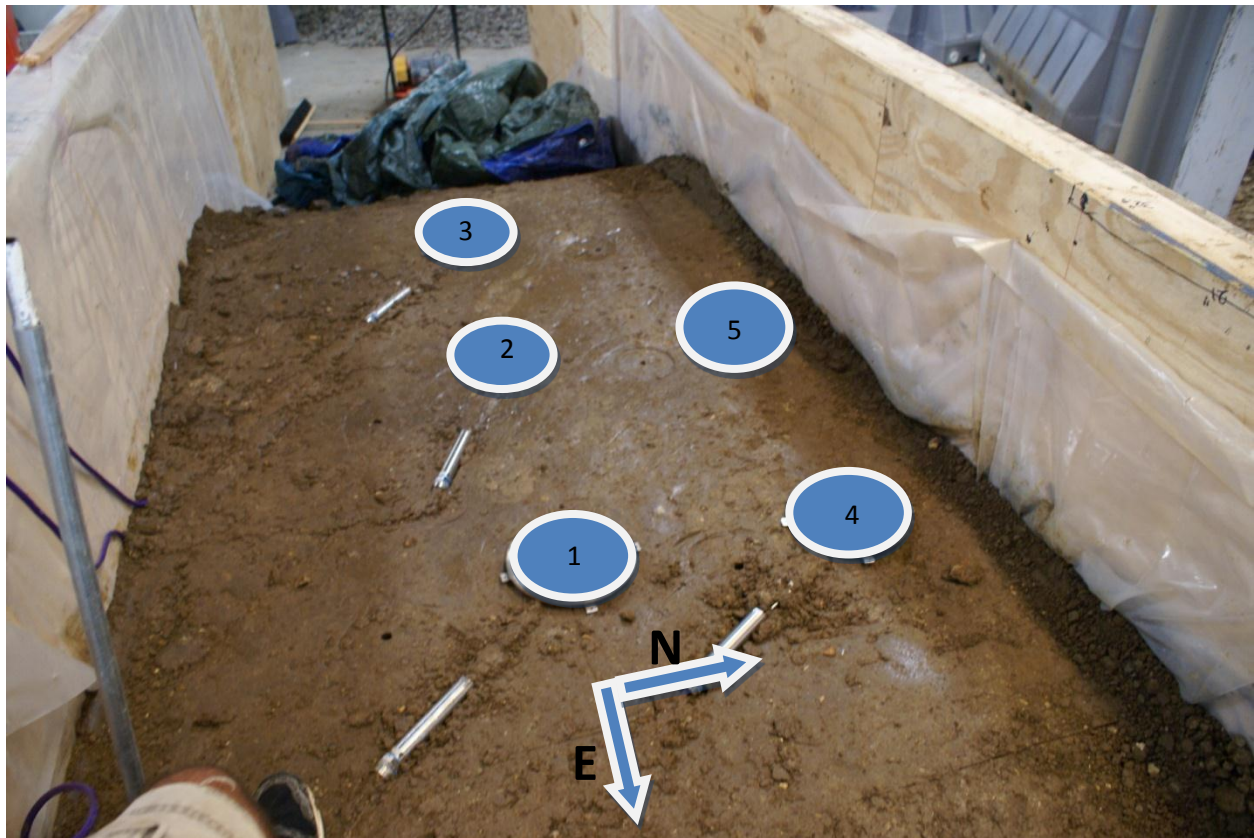


Figure 4.29 Pressure cells

Table 4.2 and figure 4.30 show pressure cell response versus hydraulic pressure in the jack. Pressure cell 1 measured the highest vertical stress observed, of 19 psi. When subgrade pressure at the location of pressure cell 1 reached 18 psi, the subgrade began to yield (fail). Pressure cell 4 experienced subgrade failure at a pressure of 12 psi. The soil beneath these pressure cells began to yield as the hydraulic pressure was increased to 4500 psi. The subgrade did not experience failure at the locations of pressure cells 2, 3, or 5 until it was soaked with 50 gallons of water and reloaded. Pressure cell 3 experienced lower pressure due to the movement of the tie or the pressure cell itself. Table 4.3 and figure 4.31 show the same plot with tie bearing pressure on the x-axis (actual pressure).

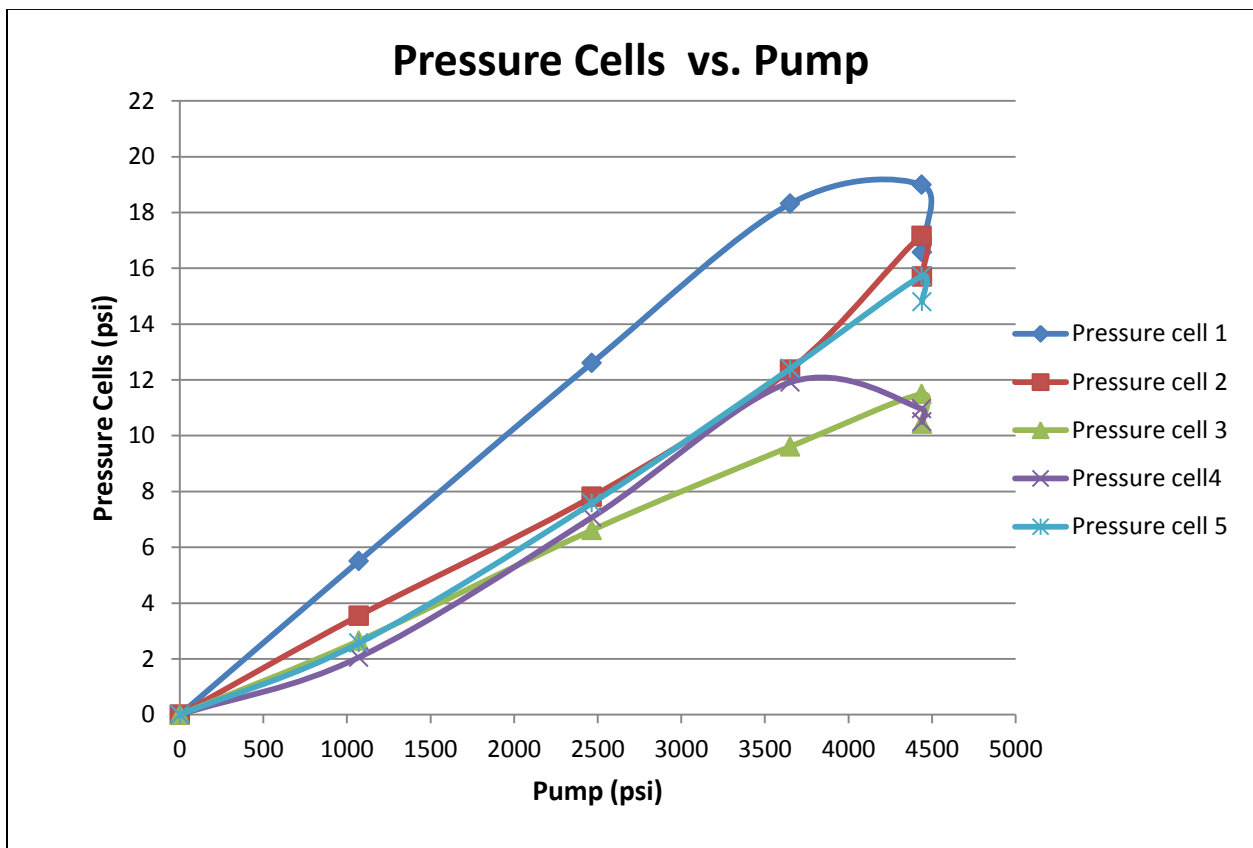


Figure 4.30 Pressure cells vs. pump pressure at subgrade level (target pressure)

Table 4.2 Pressure cells vs. pump pressure at subgrade level (unreinforced test)

Load (lb)	Pressure Transducer (psi)	Pressure cell 1 (psi)	Pressure cell 2 (psi)	Pressure cell 3 (psi)	Pressure cell 4 (psi)	Pressure cell 5 (psi)
0	0	0.0	0.0	0.0	0.0	0.0
22053	1071	5.5	3.5	2.6	2.1	2.6
50778	2465	12.6	7.8	6.6	7.1	7.6
75221	3652	18.3	12.4	9.6	11.9	12.4
91405	4437	19.0	17.2	11.5	11.0	15.7
91466	4440	16.6	15.7	10.4	10.5	14.8

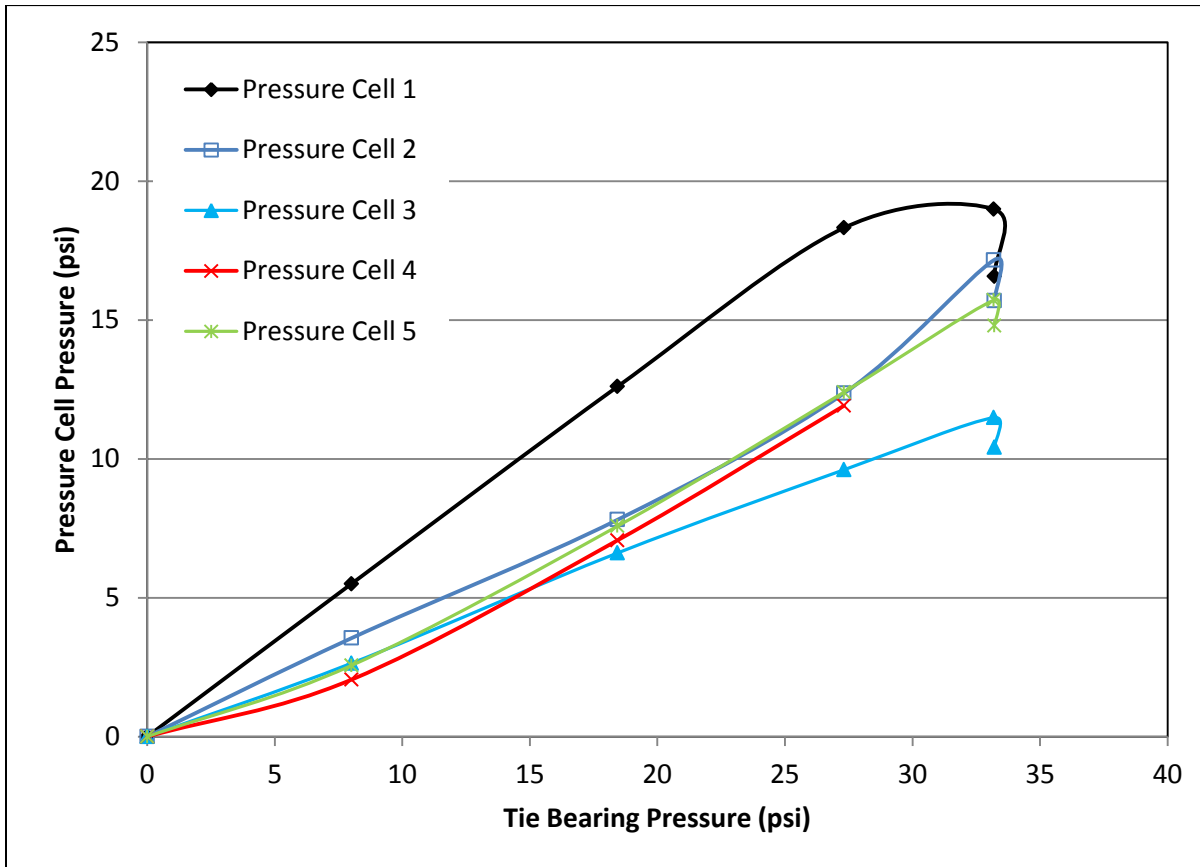


Figure 4.31 Pressure cells vs. tie bearing pressure on ballast

Table 4.3 Pressure cells vs. tie bearing pressure (unreinforced)

Right below ties						
Load (lb)	Tie Bearing Pressure (psi)	Pressure cell 1 (psi)	Pressure cell 2 (psi)	Pressure cell 3 (psi)	Pressure cell 4 (psi)	Pressure cell 5 (psi)
0	0.0	0.0	0.0	0.0	0.0	0.0
22053	8.0	5.5	3.5	2.6	2.1	2.6
50778	18.4	12.6	7.8	6.6	7.1	7.6
75221	27.3	18.3	12.4	9.6	11.9	12.4
91405	33.2	19.0	17.2	11.5	failed?	15.7
91466	33.2	16.6	15.7	10.4	failed?	14.8

4.2 Reinforced Test Section

For the reinforced section, dynamic loading was conducted in five steps as shown in table

4.4 while using triaxial geogrid to reinforce the ballast section. The number of cycles for each test matches number used for the unreinforced section.

Table 4.4 Loading information for reinforced test

Load Step	Cycles	Loading Rate (Sec/Cycle)	Target Supply Pressure (psi)	Actual Average Total Load (lb)	Tie Bearing Pressure (psi)
1	79	5	1100	23100	8
2	116	6	2500	51600	19
3	52	20	3500	72300	26
4	100	22	4500 (dry)	97100	35
5	100	24	4500 (soaked)	97500	35

4.2.1 East String Pot (Reinforced Test)

Figure 4.32 shows the dynamic loading at different loading steps versus deformation.

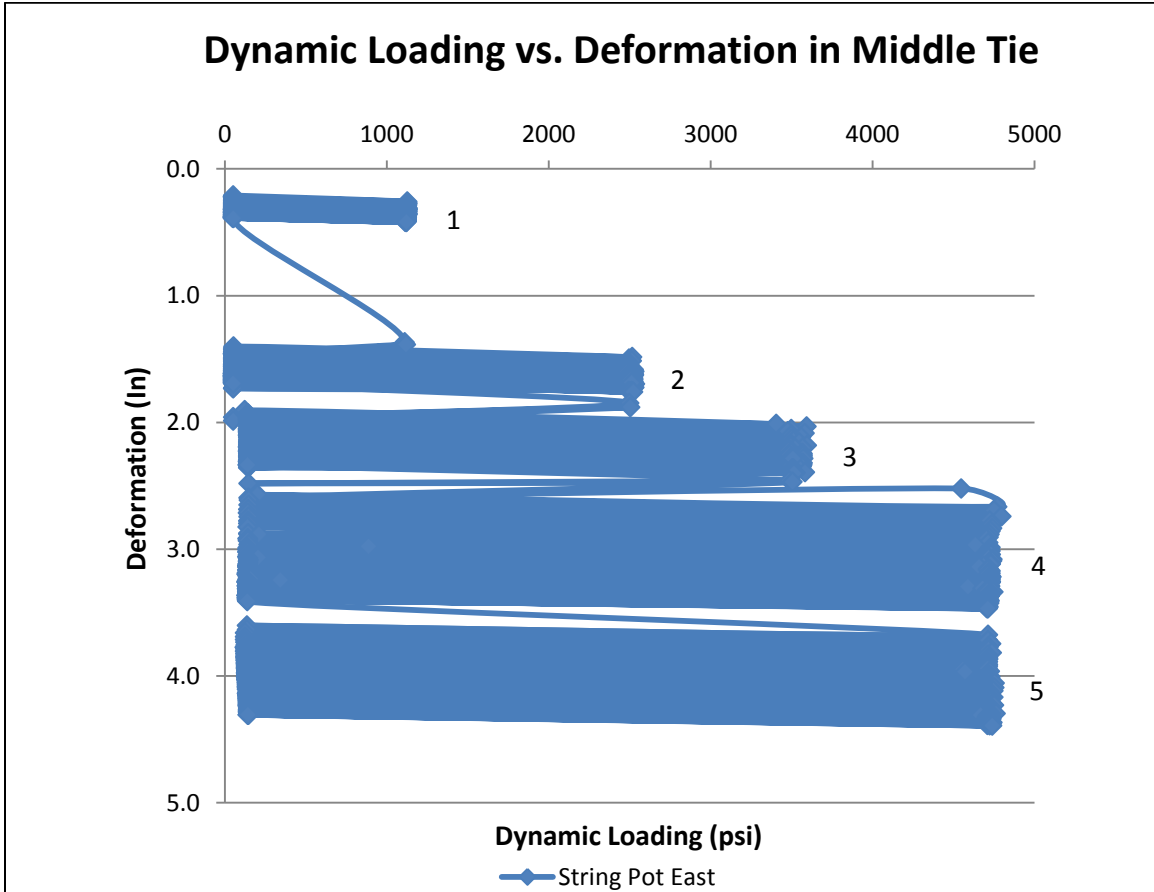


Figure 4.32 Dynamic loading vs. deformation (reinforced test)

4.2.2 East String Pot versus Dynamic Loading at 1100 psi – Reinforced (9 psi Tie Bearing Pressure)

Seventy-nine cycles were applied on the railroad section at 1100 psi, resulting in a total accumulated deformation after 79 cycles of 0.42 in. Figure 4.33 shows deformations (settlement) recorded by the east string pot for a dynamic loading of 1100 psi.

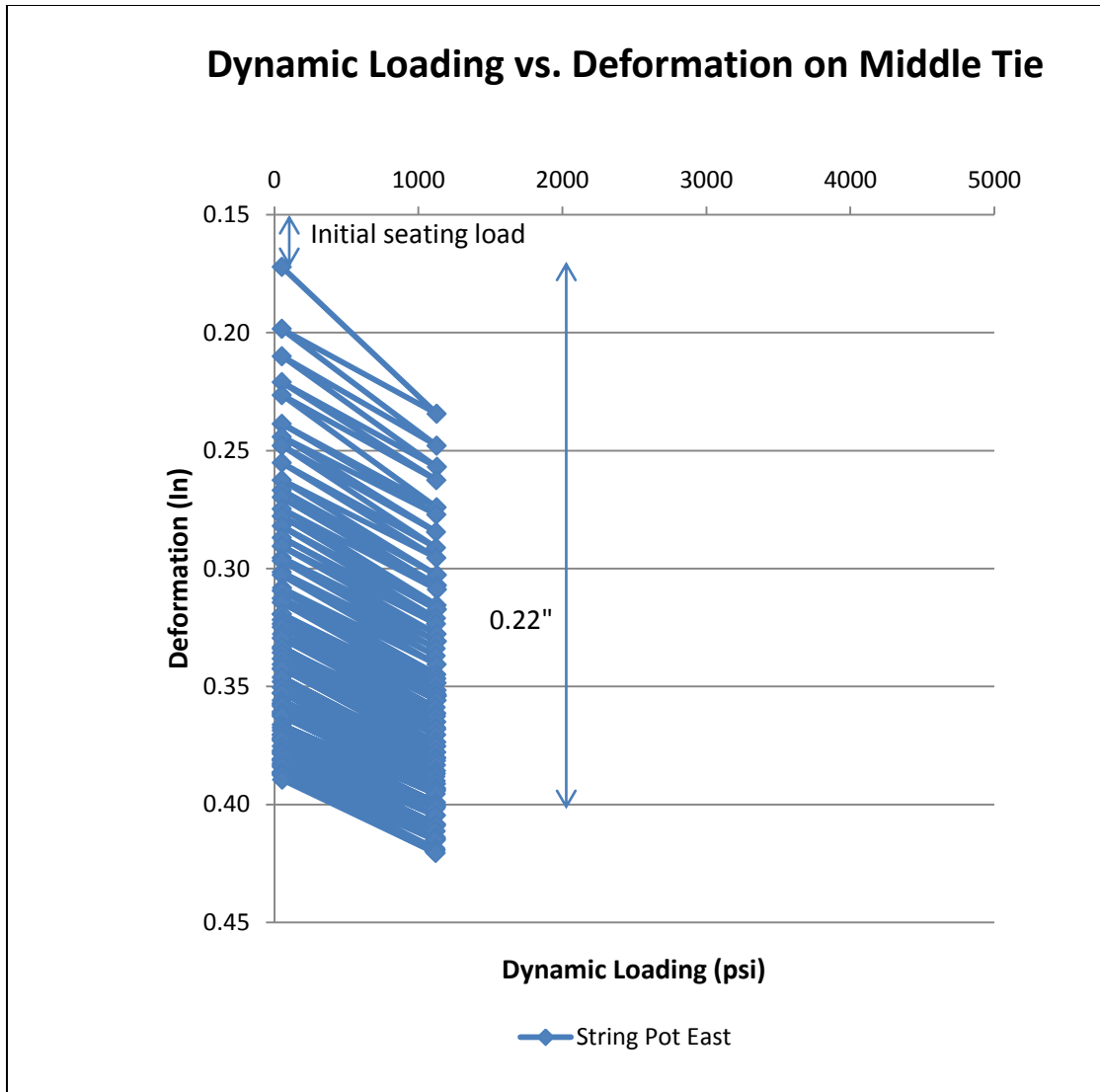


Figure 4.33 East string pot deformations versus dynamic loading at 1100 psi

4.2.3 East String Pot versus Dynamic Loading at 2500 psi – Reinforced (21 psi Tie Bearing Pressure)

One-hundred-sixteen cycles were applied on the railroad section at 2500 psi. The total deformation accumulated after 116 cycles was 1.79 in. More permanent deformation per cycle was observed for the early cycles. As the number of cycles increased a greater percentage of the

total deformation per cycle was elastic deformation. Figure 4.34 shows east string pot reading versus dynamic loading at 2500 psi.

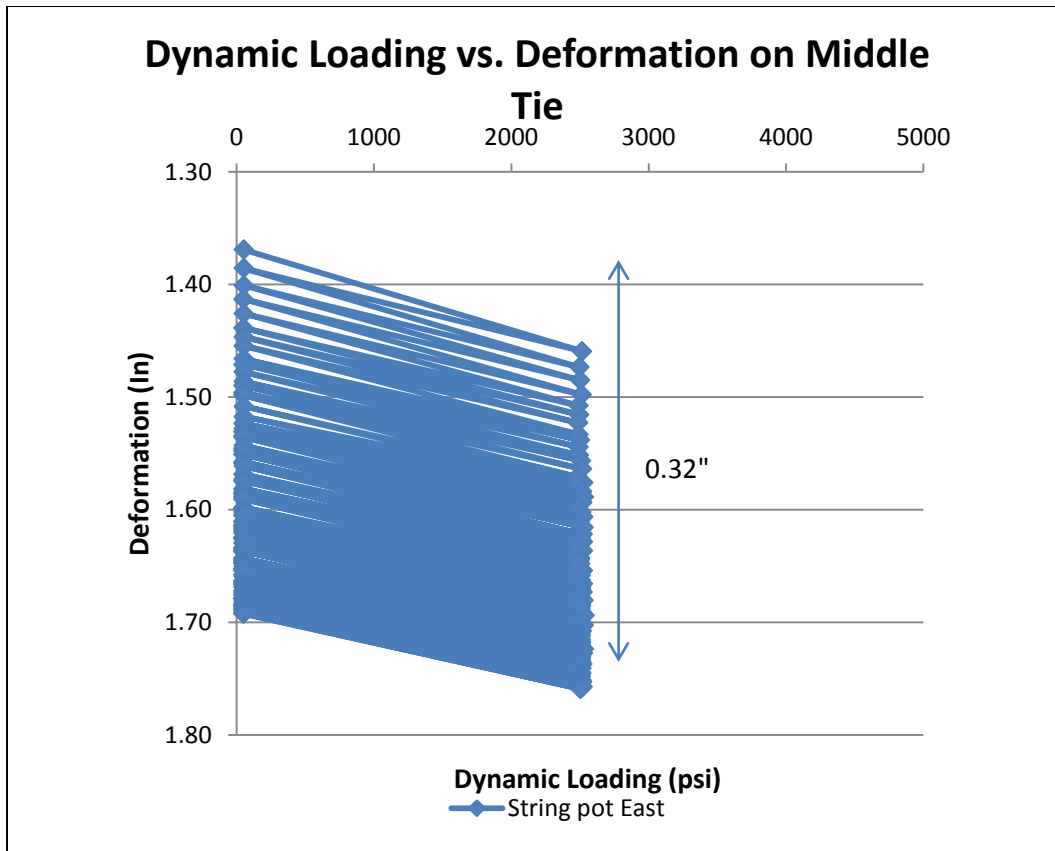


Figure 4.34 East string pot deformations versus dynamic loading at 2500 psi

4.2.4 East String Pot versus Dynamic Loading at 3500 psi – Reinforced (29 psi Tie Bearing Pressure)

Fifty-two cycles were applied to the railroad section at 3500 psi for a total accumulated deformation after 52 cycles of 2.4 in. Figure 4.35 shows the east string pot reading versus dynamic loading at 3500 psi.

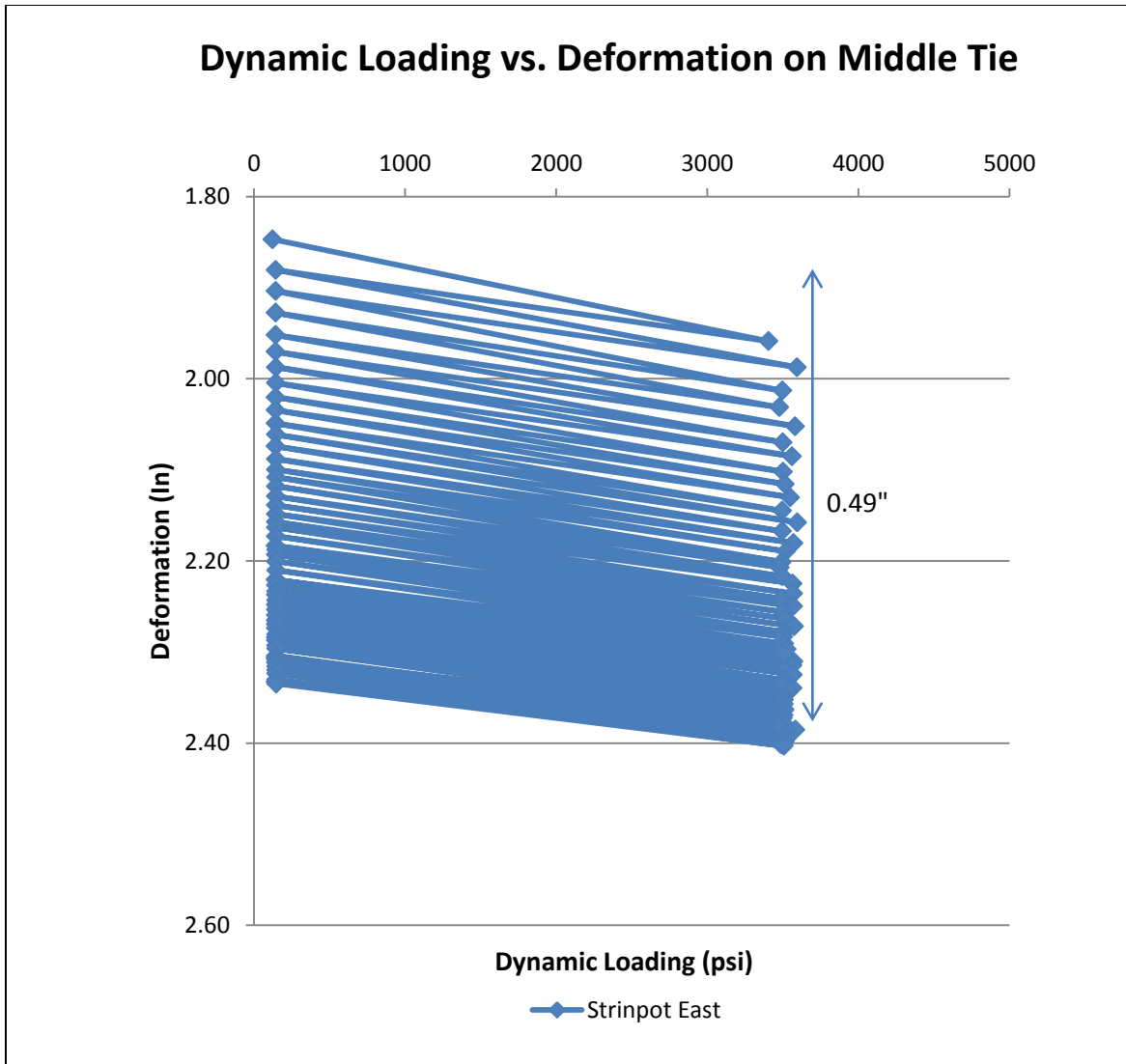


Figure 4.35 East string pot deformations versus dynamic loading at 3500 psi

4.2.5 East String Pot versus Dynamic Loading at 4500 psi – Reinforced (Not Soaked, 39 psi Tie Bearing Pressure)

One-hundred cycles were applied to the railroad section at 4500 psi. The total accumulated deformation after 100 cycles was 3.46 in. Figure 4.36 shows the east string pot reading versus dynamic loading at 4500 psi. More permanent deformation was observed for the early cycles. As the number of cycles increased, more elastic deformation was observed.

As figure 4.36 (below) shows, at the beginning of the loading step the total deformation is the difference between numbers 1 and 2 on figure 4.36, which is about 0.124 in. On the same graph, the difference between numbers 1 and 3 is the permanent deformation for the same cycle, which is 0.043 in., while the difference between points 2 and 3 is the elastic deformation. This elastic deformation is 0.081 in. As the number of cycles, increases the permanent and total deformations per cycle decrease and a higher percentage of the deformation is elastic.

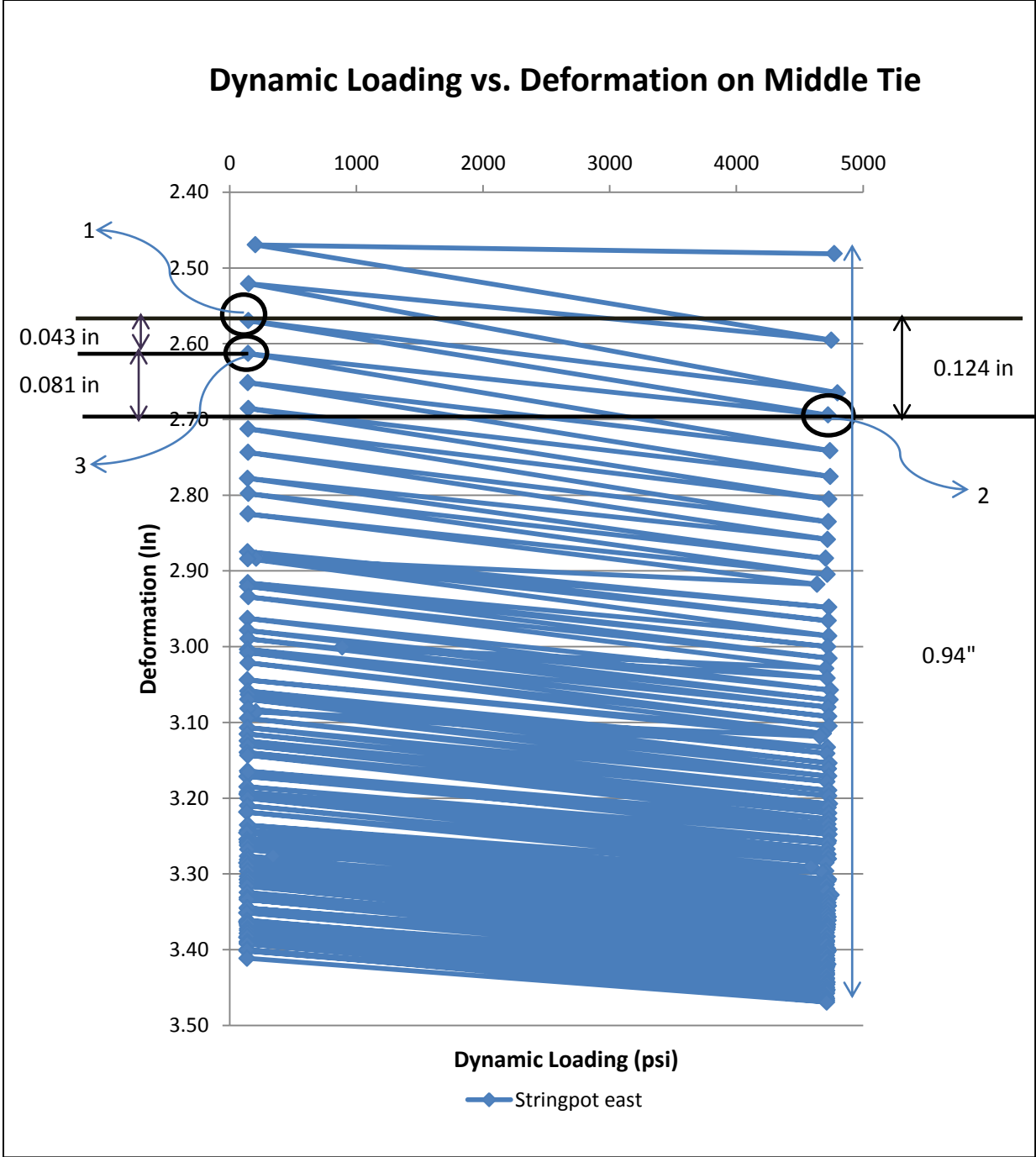


Figure 4.36 East string pot versus dynamic loading at 4500 psi (not soaked)

4.2.6 East String Pot versus Dynamic Loading at 4500 psi – Reinforced (Soaked, 39 psi Tie Bearing Pressure)

Fifty gallons of water were added to the section via garden hose over period of 15 minutes. The section was left overnight for water to penetrate into the soil. One-hundred cycles were applied to the railroad section at 4500 psi the following day. The total accumulated deformation after 100 cycles was 4.39 in. As with the earlier steps, the beginning cycles resulted in more permanent deformation per cycle. As the number of cycles increased, a higher percentage of the deformation was elastic. Figure 4.37 shows the east string pot reading versus dynamic loading at 4500 psi soaked.

As figure 4.5.6 shows, at the beginning of the loading step the difference between numbers 1 and 2 in figure 4.37 was the total deformation, observed as 0.11, which was 50% more than was observed during the initial cycles when loading the section to 4500 psi without soaking, and 40% more than was observed at the end of the end of unsoaked loading. Most of the additional deformation per cycle was permanent. On the same graph the difference between numbers 1 and 3 was the permanent deformation for the same cycle, or 0.08 in. The elastic deformation is shown on the same graph, and was 0.03 in. As with the previous loading step, the permanent and total deformations per cycle decreased and a higher percentage of the deformation was elastic.

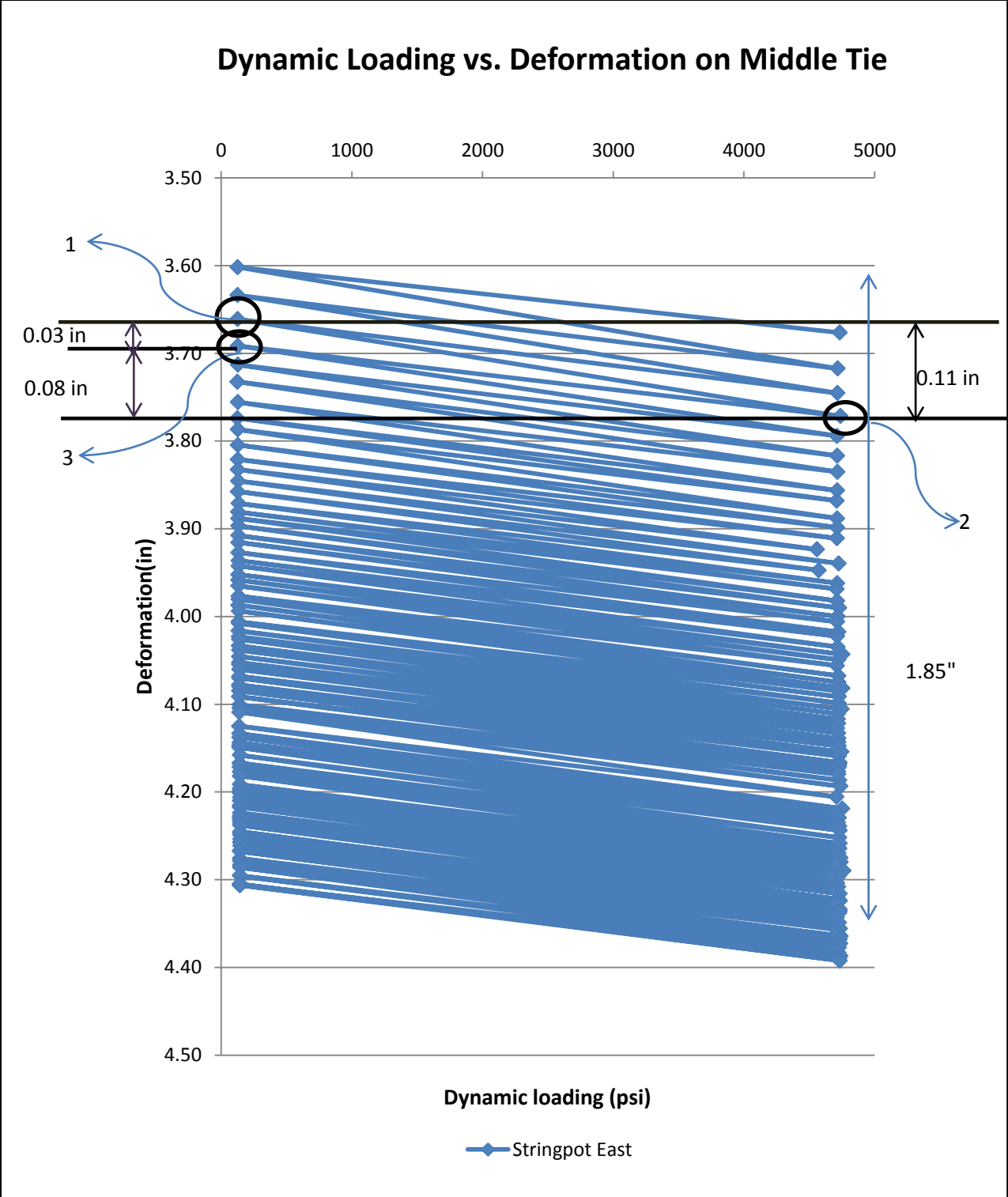


Figure 4.37 East string pot versus dynamic loading at 4500 psi (soaked)

4.2.7 West String Pot (Reinforced Test)

Figures 4.38-4.43 show the recorded values on the west string pot.

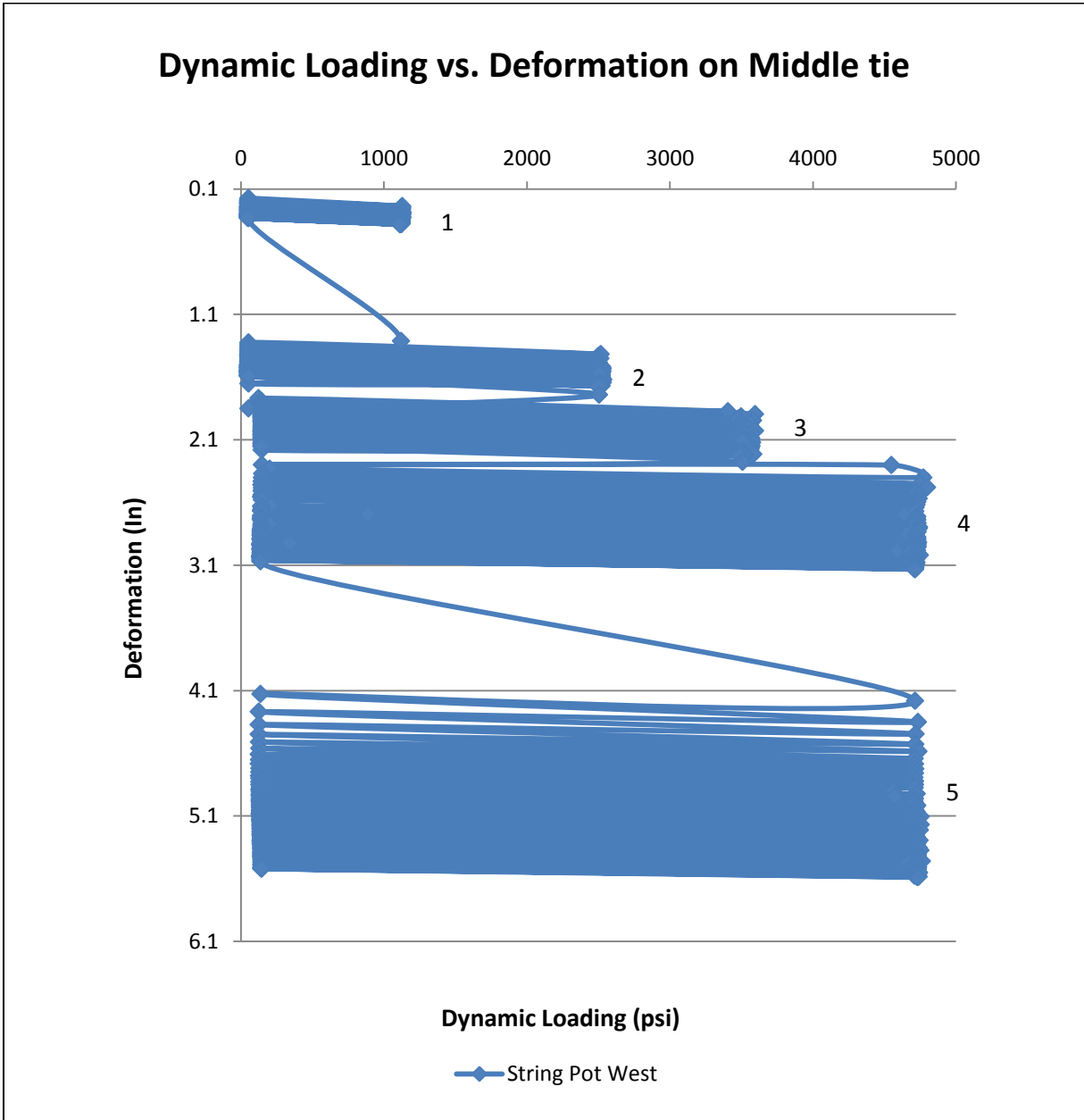


Figure 4.38 Dynamic loading vs. deformation. (reinforced test)

Dynamic Loading vs. Deformation on Middle tie

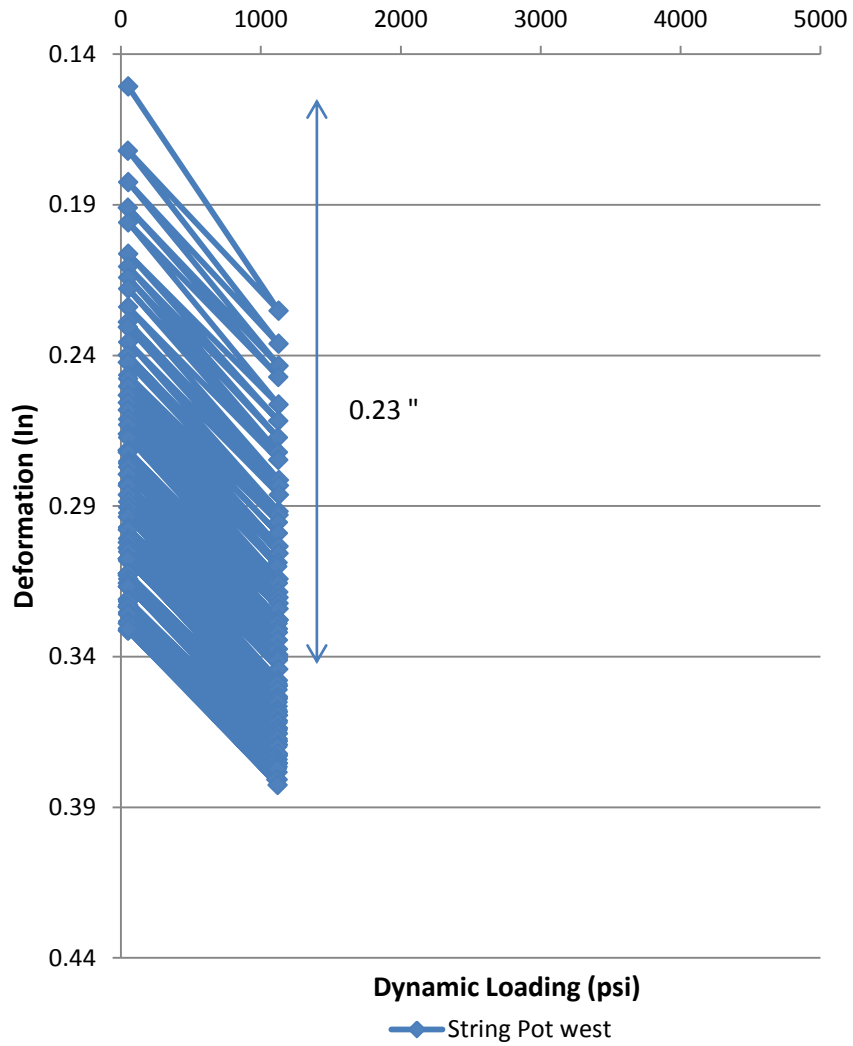


Figure 4.39 West string pot versus dynamic loading at 1100 psi

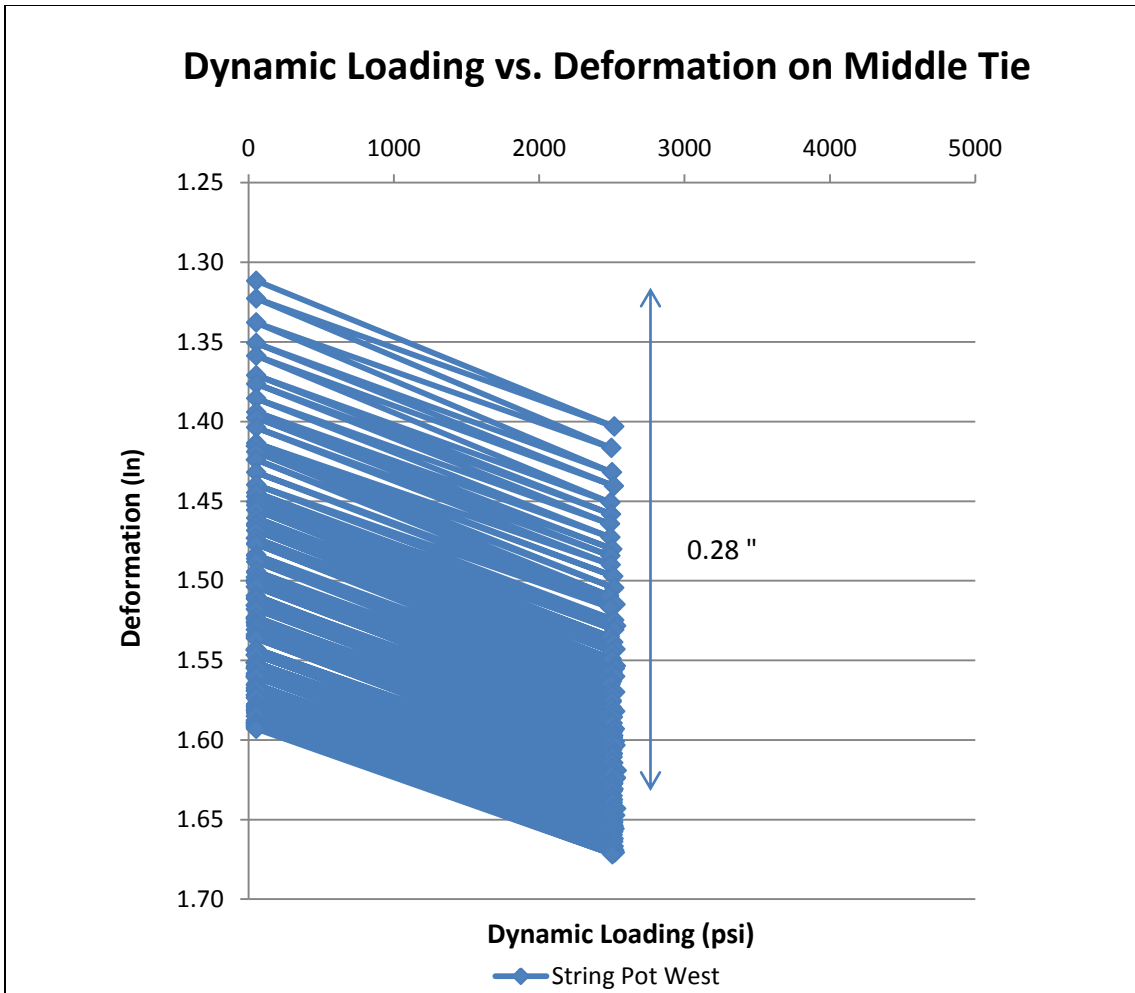


Figure 4.40 West string pot versus dynamic loading at 2500 psi

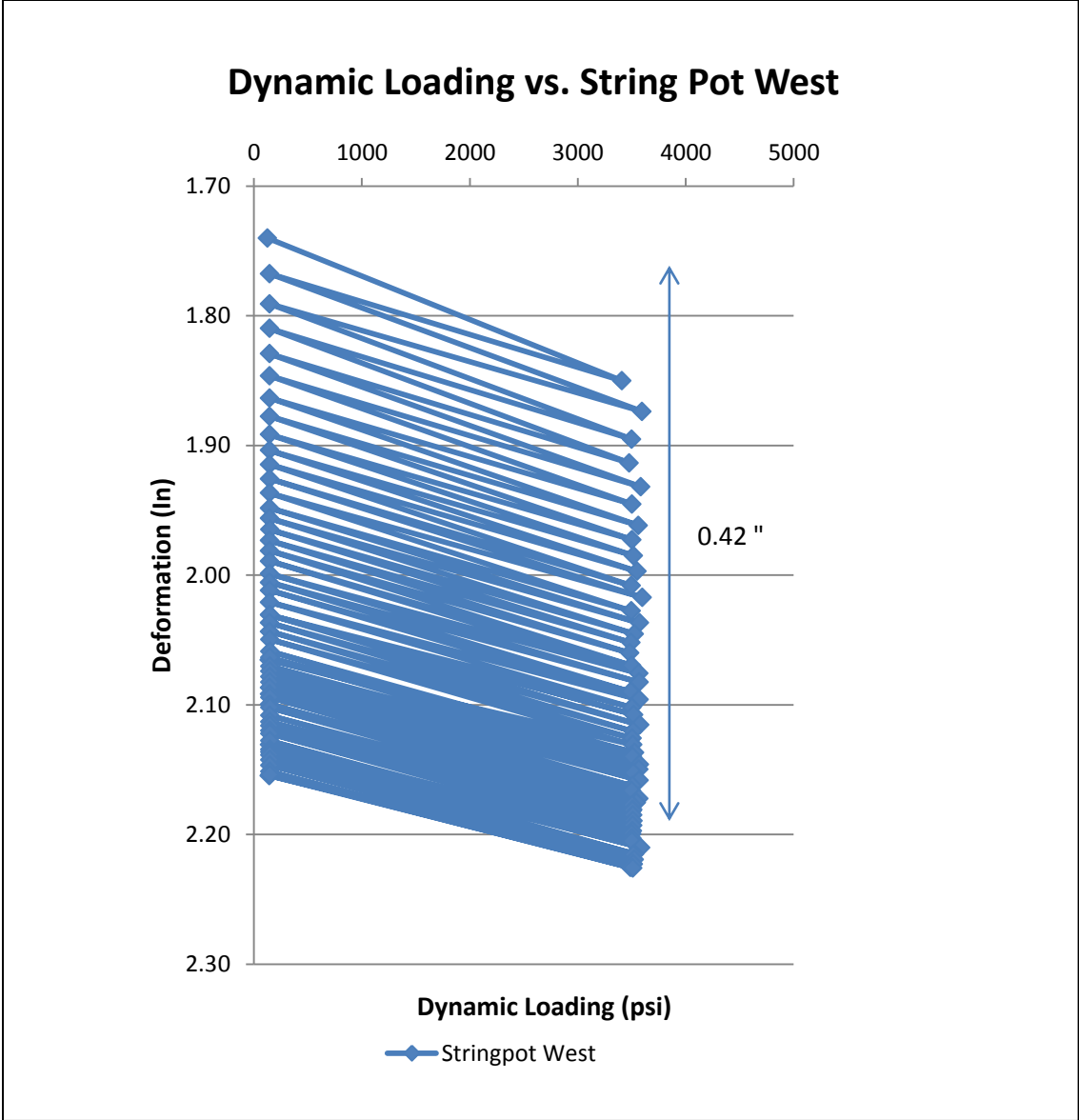


Figure 4.41 West string pot versus dynamic loading at 3500 psi

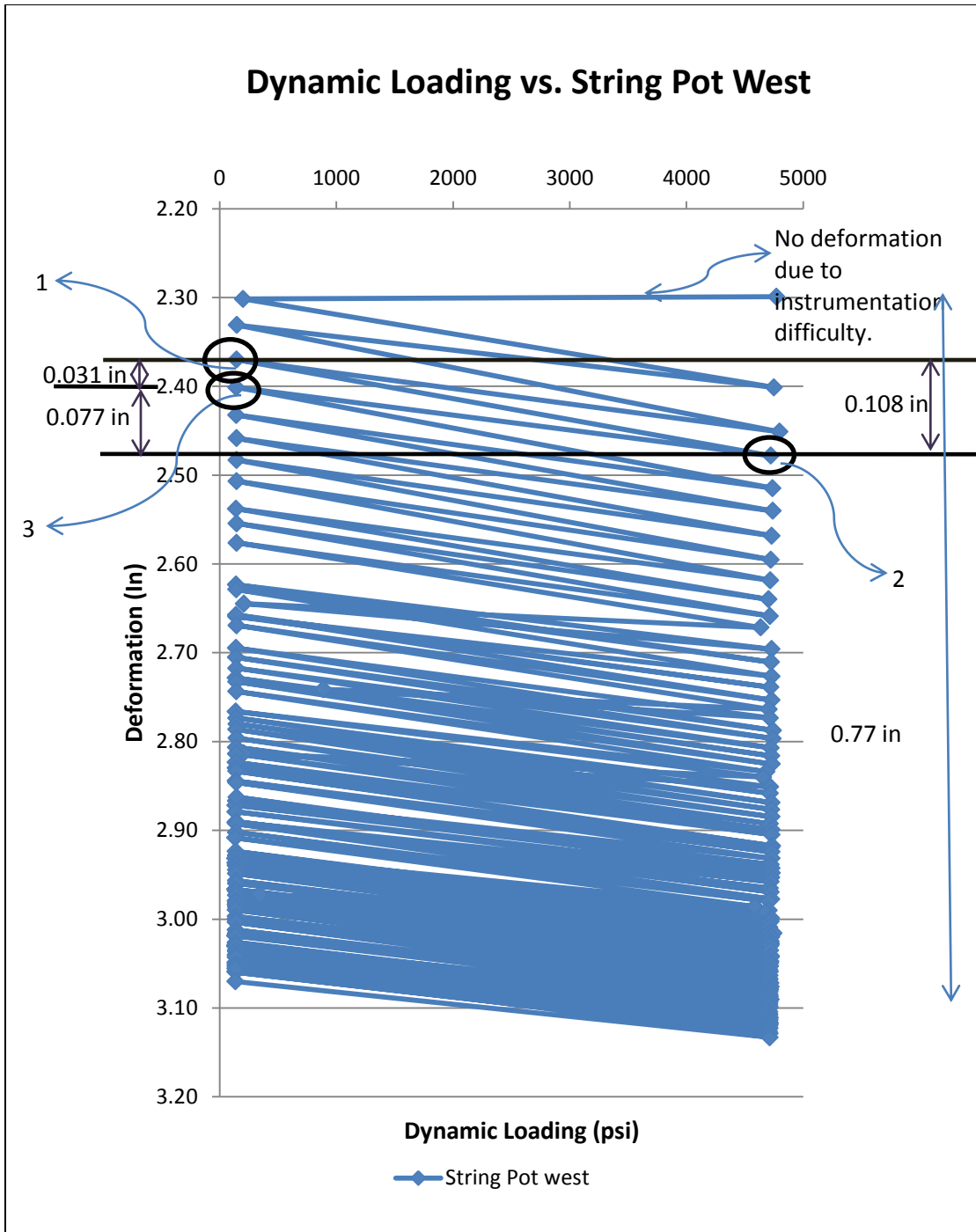


Figure 4.42 West string pot versus dynamic loading at 4500 psi (not soaked)

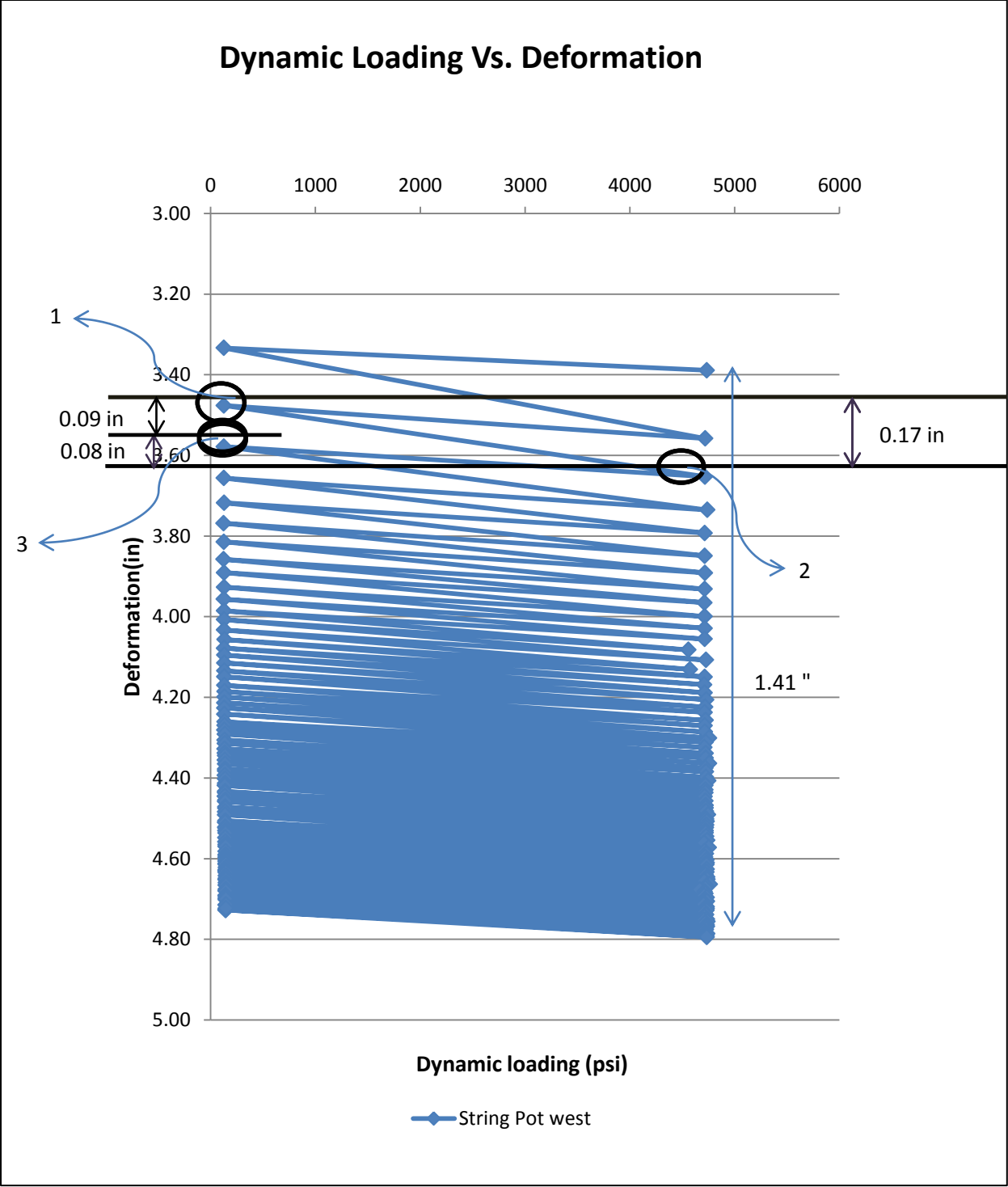


Figure 4.43 West string pot versus dynamic loading at 4500 psi (soaked)

4.2.8 Reinforced Test (Displacement Transducers)

Four displacement transducers were installed on the railroad track to measure the deformation near the ends of each rail on the track panel. Figure 4.44 shows the transducer locations. Some sliding of transducer ends during some load steps resulted in measurements that were not reliable. These results are not included in the analysis.

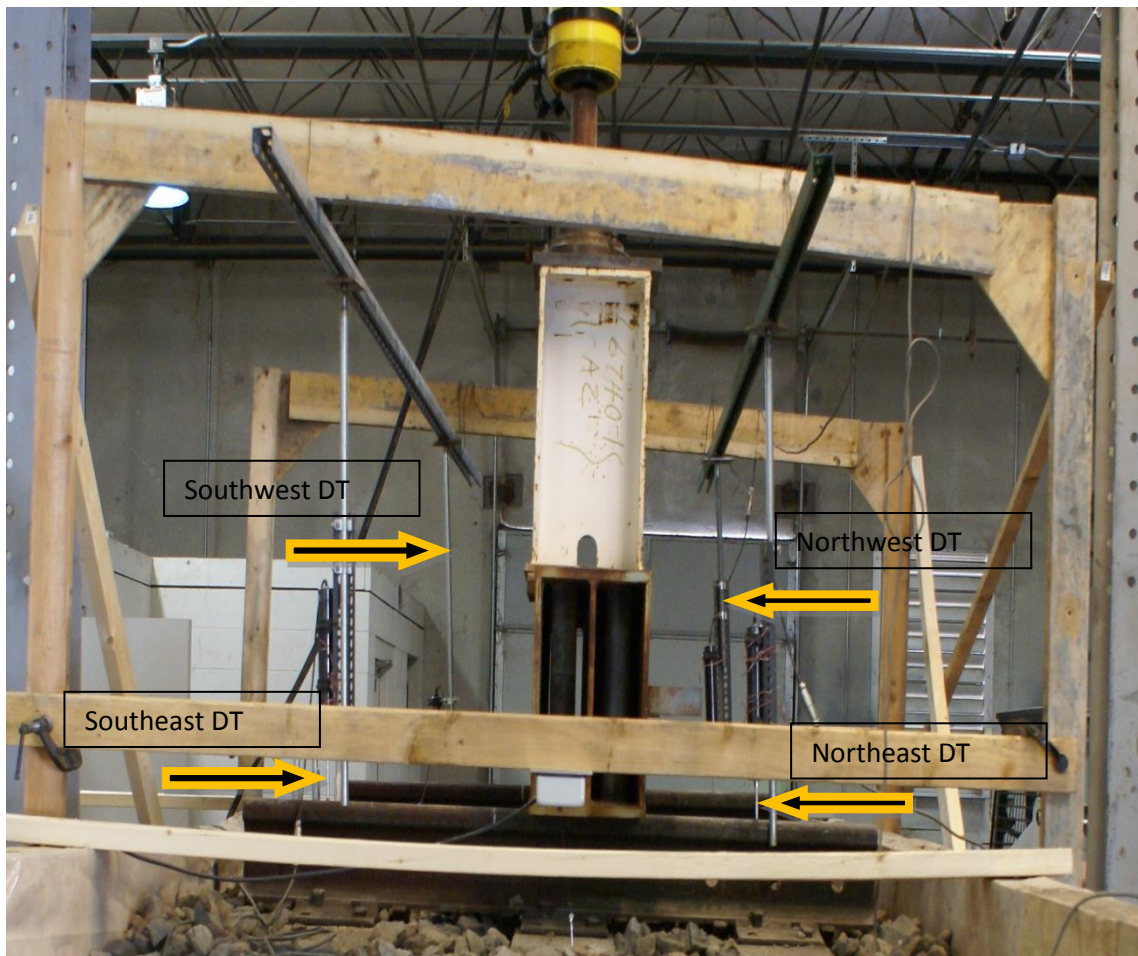


Figure 4.44 Displacement transducers

4.2.9 Displacement Transducers (DT) at 1100 psi (Southeast, 9 psi Bearing Pressure)

Seventy-nine cycles were applied to the railroad section at 1100 psi. The total deformation measured by the southeast DT after 79 cycles was 0.55 in. Displacements of 0.36 and 0.33 were recorded at the northwest and southwest corners, respectively. The reading at the northeast corner was unreliable. No reliable readings were recorded at any of the later load steps. Figures 4.45 through 4.47 (below) show DT readings versus dynamic loading.

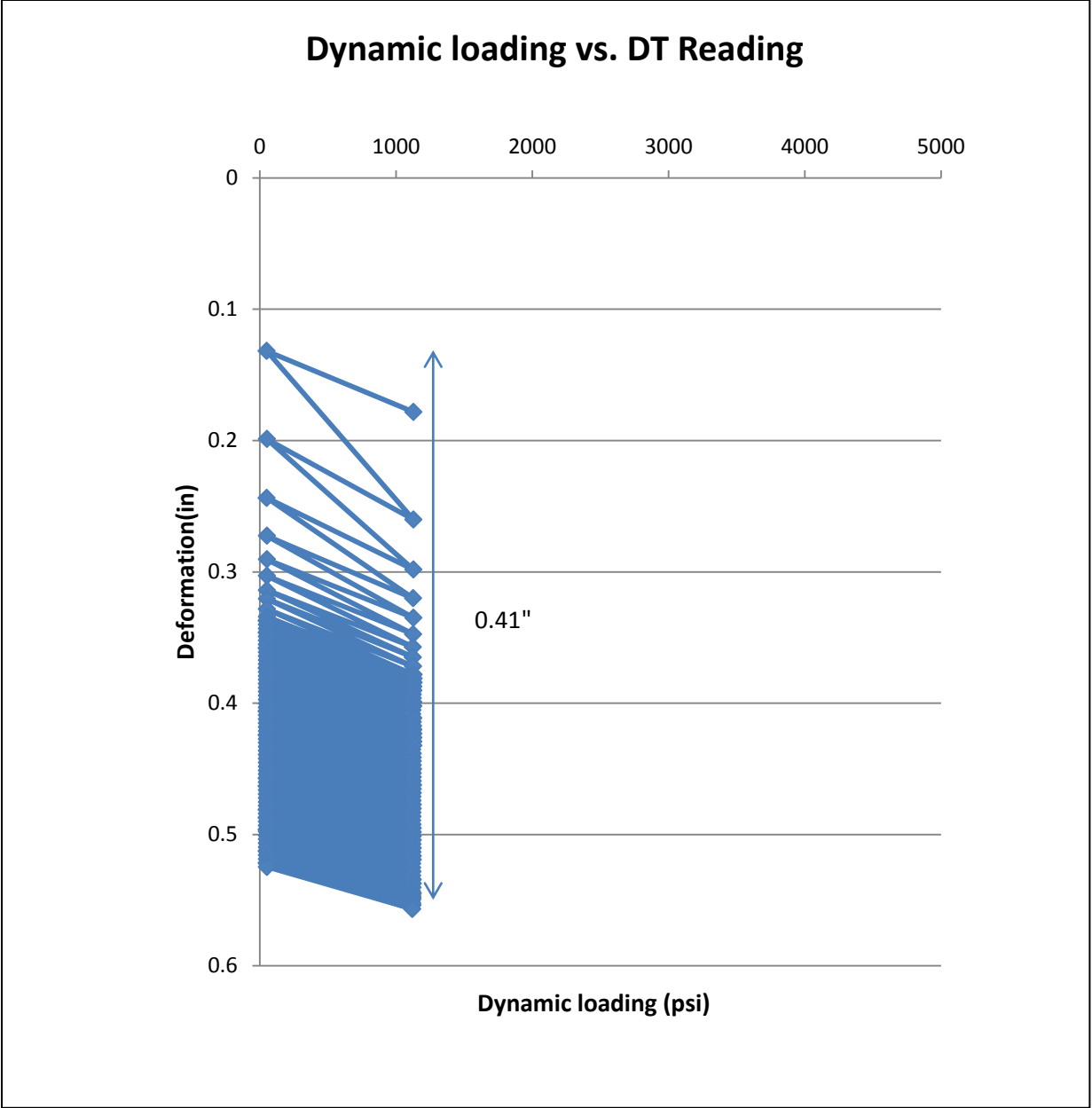


Figure 4.45 Displacement transducer readings at 1100 psi (southeast)

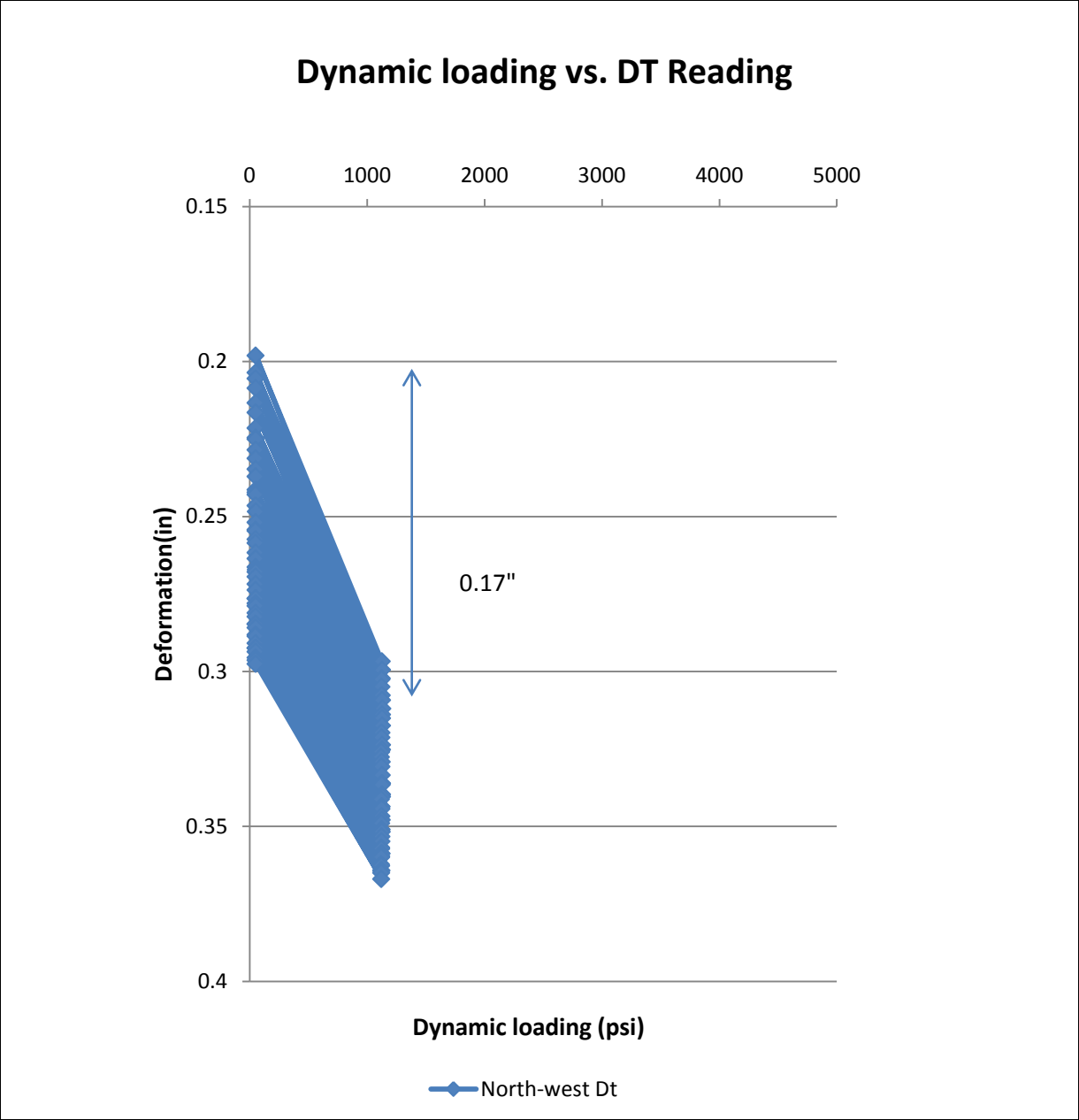


Figure 4.46 Displacement transducer readings at 1100 psi (northwest)

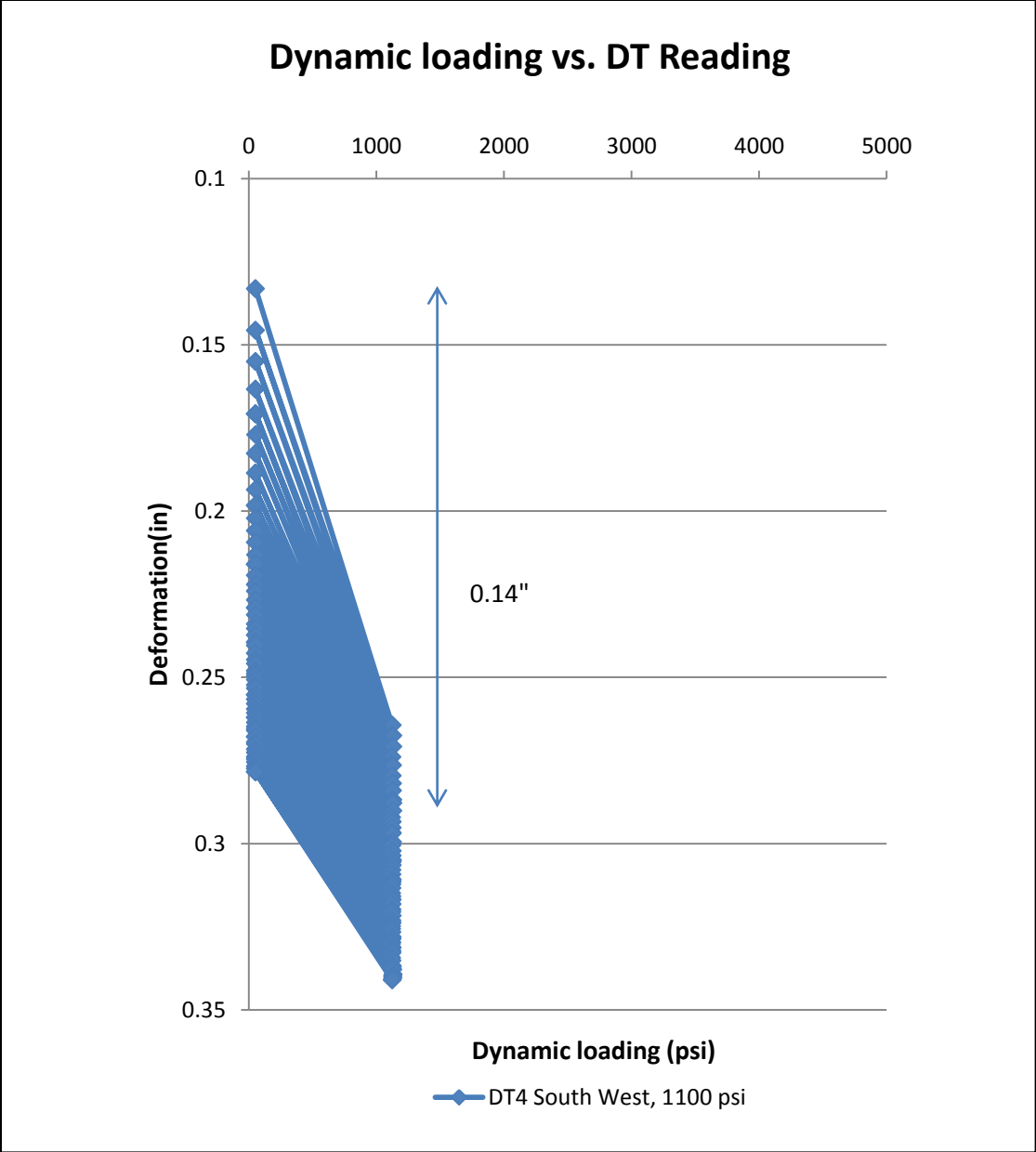


Figure 4.47 Displacement transducer readings at 1100 psi (southwest)

4.2.10 Pressure Cells Results for Reinforced Test

Five pressure cells were installed as shown in figure 4.48. Pressure cells 1, 2 and 3 were installed at the interface of subgrade and ballast below the middle tie (1 and 3 were right below the rails road track). Pressure cells 4 and 5 were installed under the right tie.

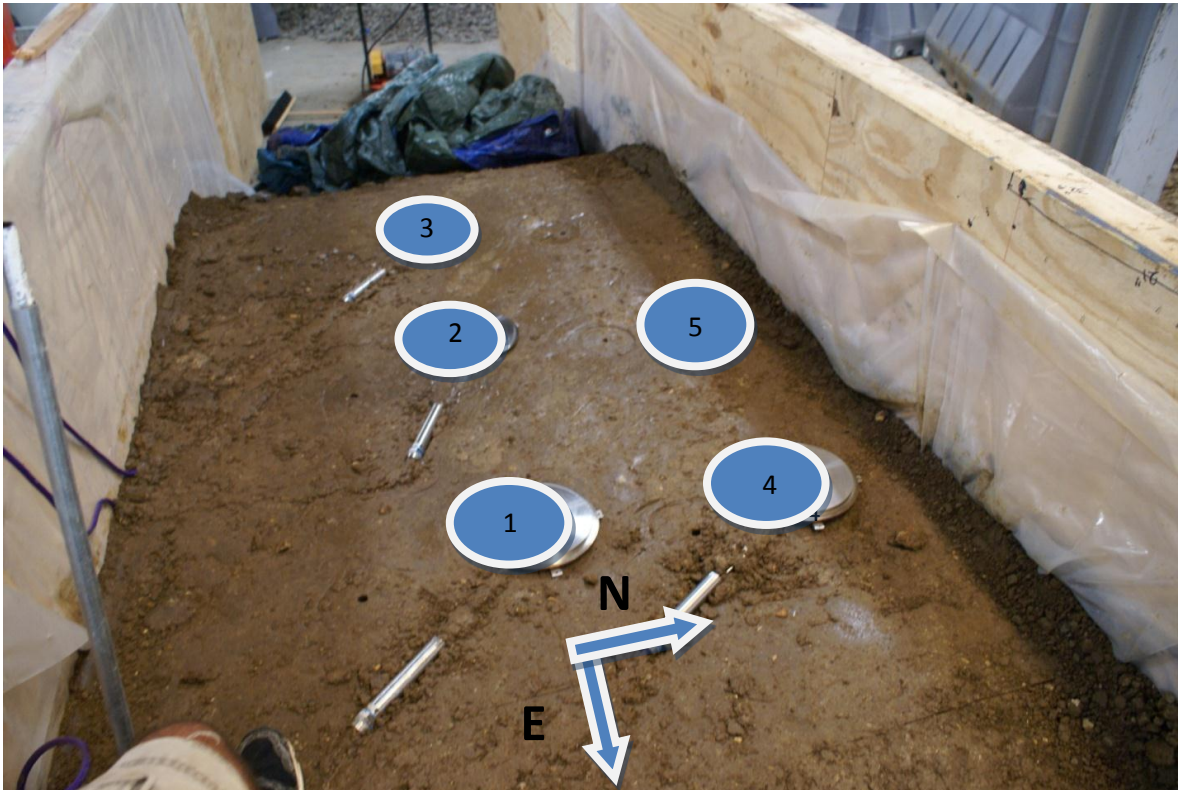


Figure 4.48 Pressure cells

4.2.11 Pressure Cell Results at Subgrade Level

Figure 4.49 and table 4.5 and show the pressure cell data versus pressure transducer data for the reinforced case. Pressure cell 4 data was not recorded due to the failure of pressure cell 4. For this test, unlike the unreinforced case, the subgrade did not fail at any location until it was soaked with 50 gallons of water. Pressure cell 2 experienced the highest pressure at approximately 21 psi. Figure 4.50 and table 4.6 present the similar information vs. tie bearing pressure.

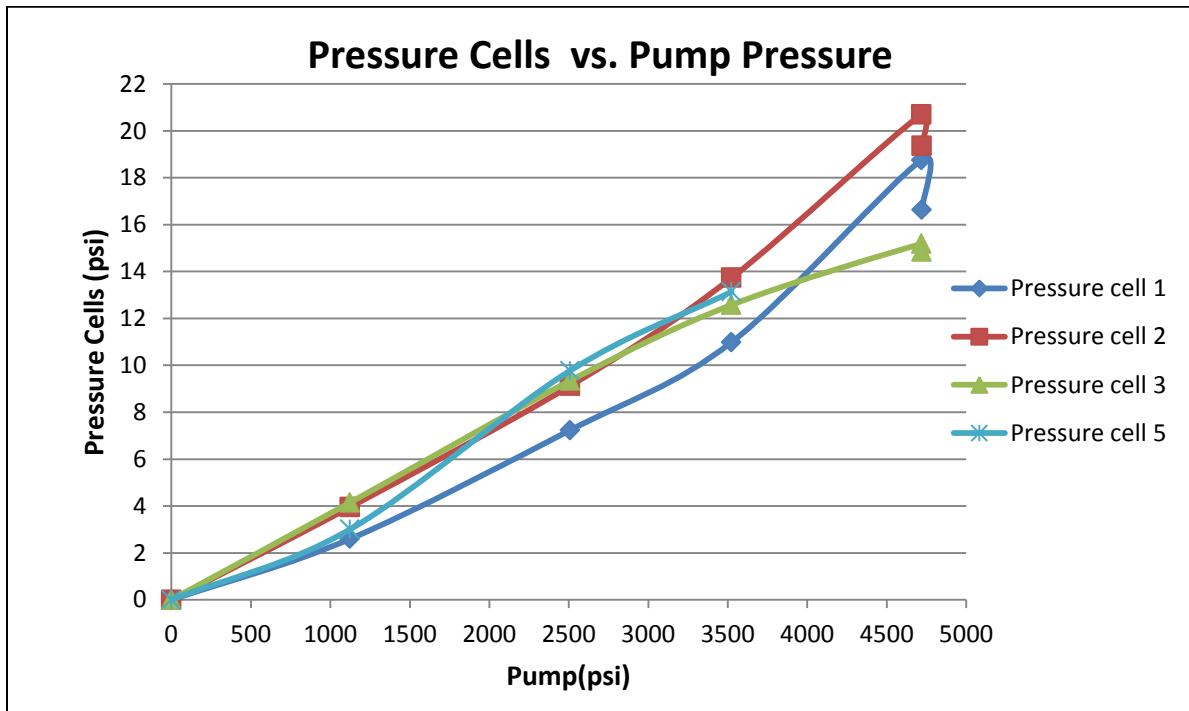


Figure 4.49 Pressure cells vs. pump pressure at subgrade level

Table 4.5 Pressure cells vs. pump pressure at subgrade level

Load (lb)	Pressure Transducer (psi)	Pressure cell 1 (psi)	Pressure cell 2 (psi)	Pressure cell 3 (psi)	Pressure cell 4 (psi)	Pressure cell 5 (psi)
0	0	0.0	0.0	0.0	0.0	0.0
23157	1124	2.6	4.0	4.1	1.3	3.0
51665	2508	7.2	9.1	9.3	1.6	9.8
72592	3524	11.0	13.7	12.6	1.8	13.1
97211	4719	18.8	20.7	15.2	2.1	no reading
97253	4721	16.6	19.4	14.8	2.0	no reading

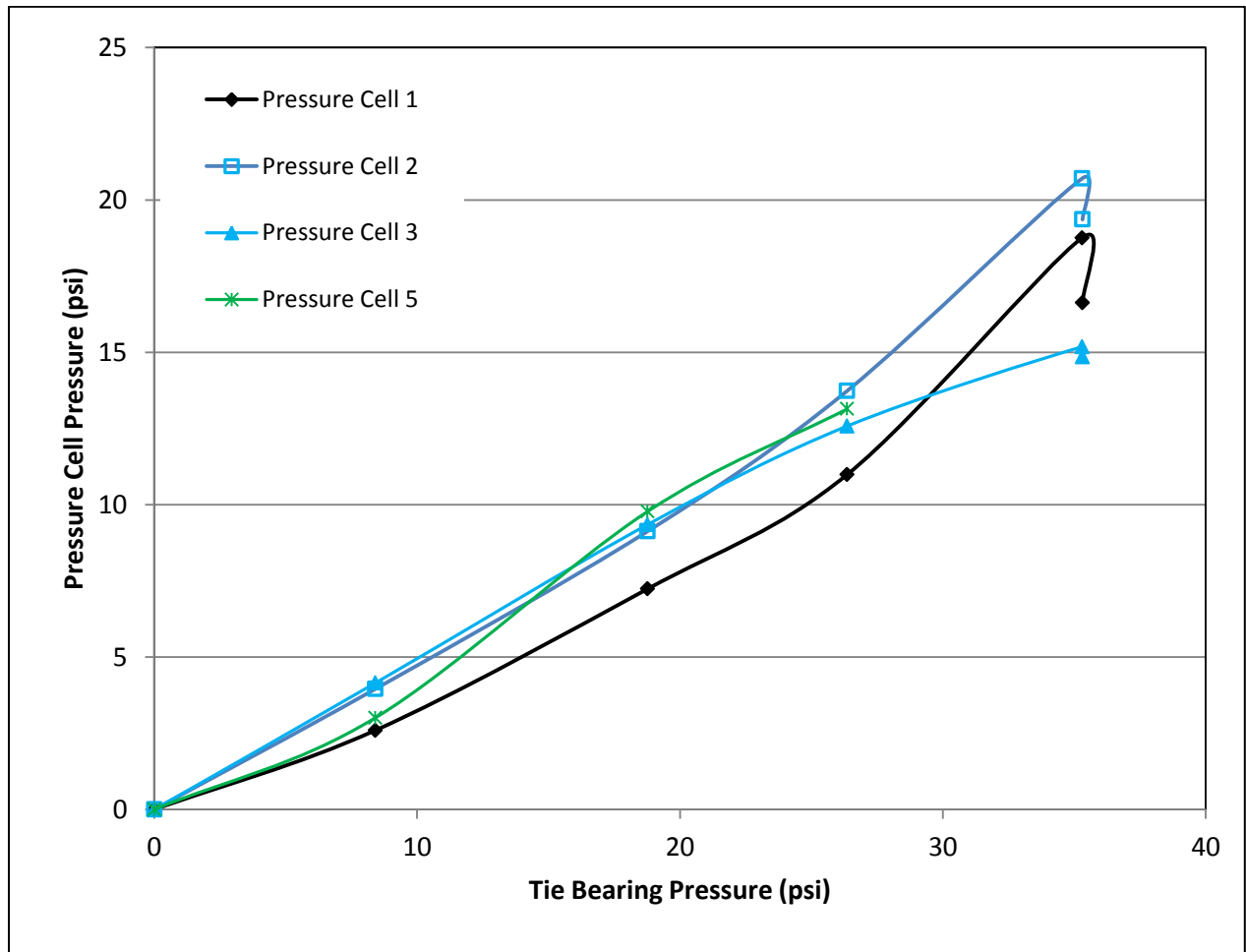


Figure 4.50 Pressure cells vs. tie bearing pressure

Table 4.6 Pressure cells vs. tie bearing pressure (reinforced)

Right below ties						
Load (lb)	Tie Bearing Pressure (psi)	Pressure cell 1 (psi)	Pressure cell 2 (psi)	Pressure cell 3 (psi)	Pressure cell 4 (psi)	Pressure cell 5 (psi)
0	0.0	0.0	0.0	0.0	no reading	0.0
23157	8.4	2.6	4.0	4.1	no reading	3.0
51665	18.8	7.2	9.1	9.3	no reading	9.8
72592	26.4	11.0	13.7	12.6	no reading	13.1
97211	35.3	18.8	20.7	15.2	no reading	no reading
97253	35.3	16.6	19.4	14.8	no reading	no reading

4.3 Unreinforced vs. Reinforced: Settlement Comparison

Table 4.7 shows the comparison between unreinforced and reinforced test for unit weight and number of cycles.

Table 4.7 Comparison of loading cycles and subgrade conditions

	Unreinforced	Reinforced
Prior to Test Unit Weight (lb/ft³)	91.5	93
Number of Cycles	447	447
Moisture Content Before Test	26	27
Moisture Content After Test	26.5	27.5
% Proctor	92%	93%

The results of the two tests are compared in this section. As shown in figure 4.51 and table 4.8, the reduction in settlement for the reinforced section is noticeable for both the west and east string pots. The improvement was minimal for the light early loading but became more significant as loading and settlements became larger.

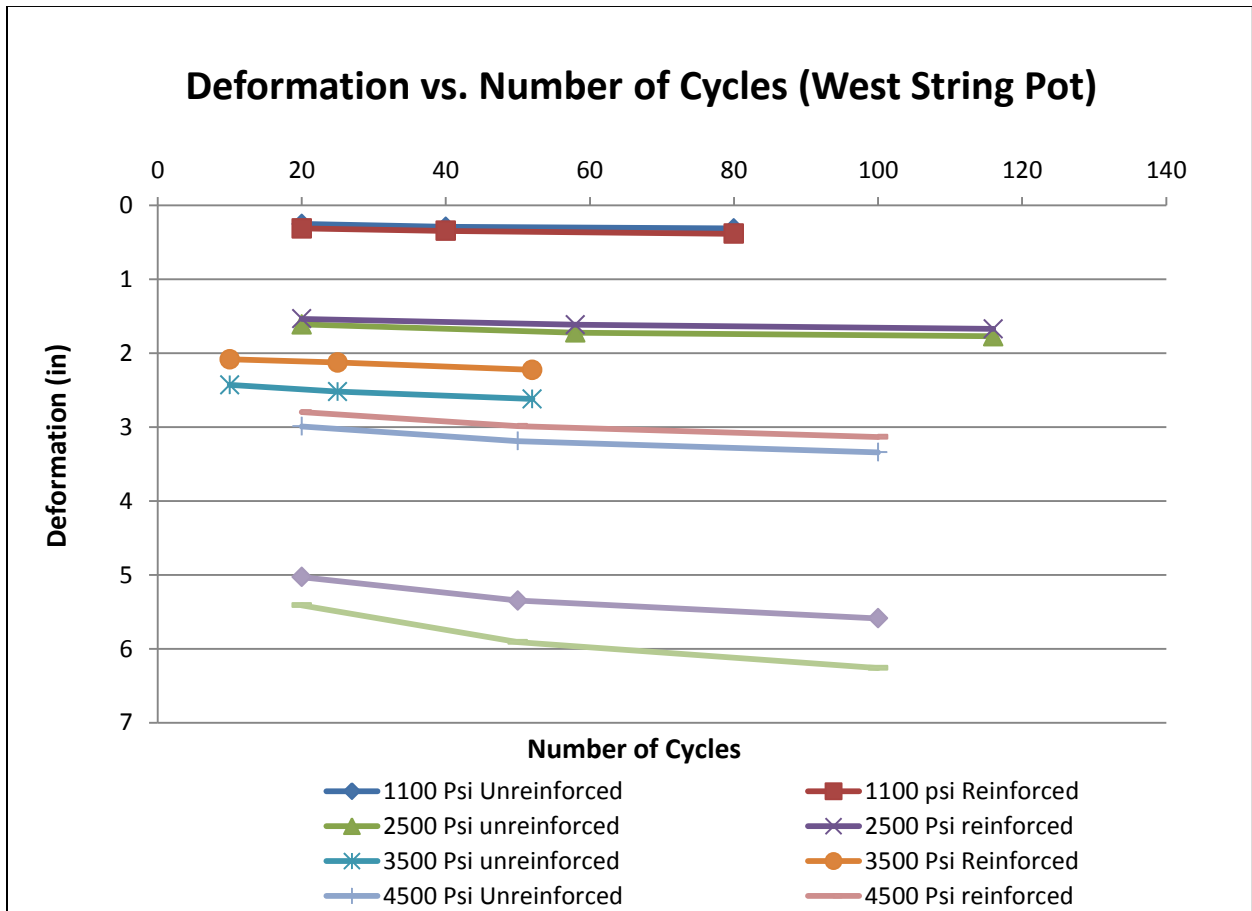


Figure 4.51 West string pot result comparison

Table 4.8 Comparison of settlement between the reinforced test and unreinforced test (west string pot)

Pressure (psi)	Deformation(in) West Stringpot		Number Of cycles	Actual Pressure applied Reinforced (psi)	Actual Pressure applied Unreinforced (psi)
	Unreinforced	Reinforced			
1100(Beginning)	0.25	0.31	20	1120	1070
1100(Middle)	0.29	0.34	40	1126	1080
1100(End)	0.31	0.38	80	1121	1070
2500(Beginning)	1.61	1.54	20	2487	2480
2500(Middle)	1.72	1.61	58	2512	2440
2500(End)	1.77	1.67	116	2505	2450
3500(Beginning)	2.43	2.08	10	3570	3580
3500(Middle)	2.52	2.13	25	3505	3680
3500(End)	2.62	2.23	52	3508	3670
4500(Beginning)	2.99	2.80	20	4741	4406
4500(Middle)	3.19	2.99	50	4590	4462
4500(End)	3.34	3.13	100	4714	4480
4500 Soaked(Beginning)	5.41	5.03	20	4715	4370
4501 Soaked(Middle)	5.91	5.35	50	4740	4470
4502 Soaked(End)	6.26	5.59	100	4735	4470

At the end of the 1100 psi loading step there was no substantial difference in settlement between the two sections. After the 2500 psi loading step an improvement of 0.09 in was observed for the reinforced case. The amount of improvement improved to 0.4 in after the 3500 psi loading step, 0.2 in after the 4500 psi loading step (not soaked) and 0.6 in after loading of the soaked section.

Figure 4.51 shows that the trends for the reinforced and unreinforced cases for 1100 psi loading are nearly identical. As larger loads were applied, the gap between the reinforced and unreinforced trends increased until the 3500 psi loading step. However, for the 4500 psi step, the gap got smaller. This is likely due to differences in the pressure applied for the unreinforced and reinforced cases. As shown in table 4.9, the pressure applied to the reinforced section was slightly less than that for the unreinforced section at the 3500 psi load step, and the reverse was true for the 4500 psi load step. This explains the larger gap for the 3500 psi load step and the smaller gap for the 4500 psi load step. Figure 4.52 shows the same data with settlements

adjusted to account for the difference in loading. As this figure shows, with each loading step the adjusted settlements show an increase in the difference in settlement between the two tests.

The full data set is reported in table 4.10.

Table 4.9 Reinforced loading vs. unreinforced loading

Reinforced Loads (lbs)	Unreinforced Loads (lbs)	Load difference in percentage
23088	22042	4.7%
51593	50470	2.2%
72269	75602	-4.4%
97115	92292	5.2%
97535	92082	5.9%

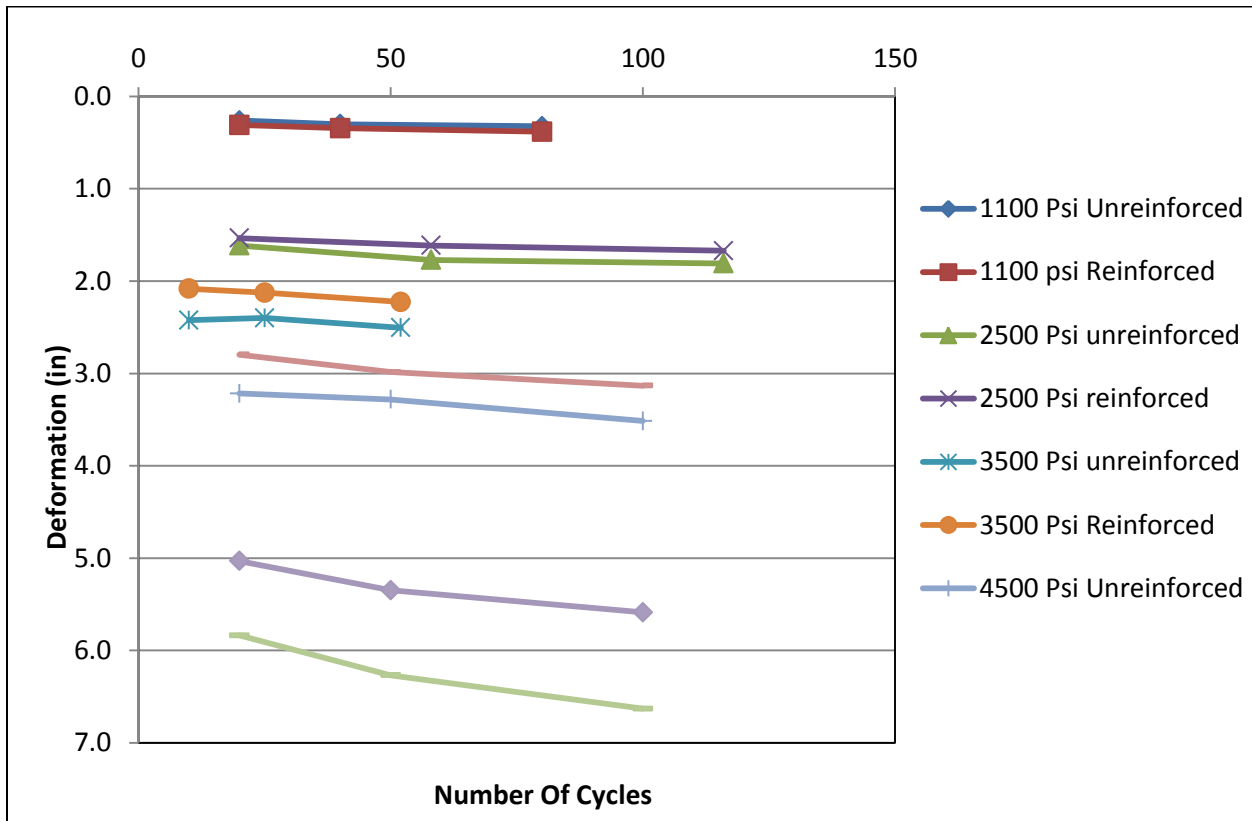


Figure 4.52 West string pot result comparison (after adjusting for load differences)

4.3.1 Reinforced vs. Unreinforced (East String Pot)

Figure 4.53 shows the deformation vs. number of cycles for the east string pot.

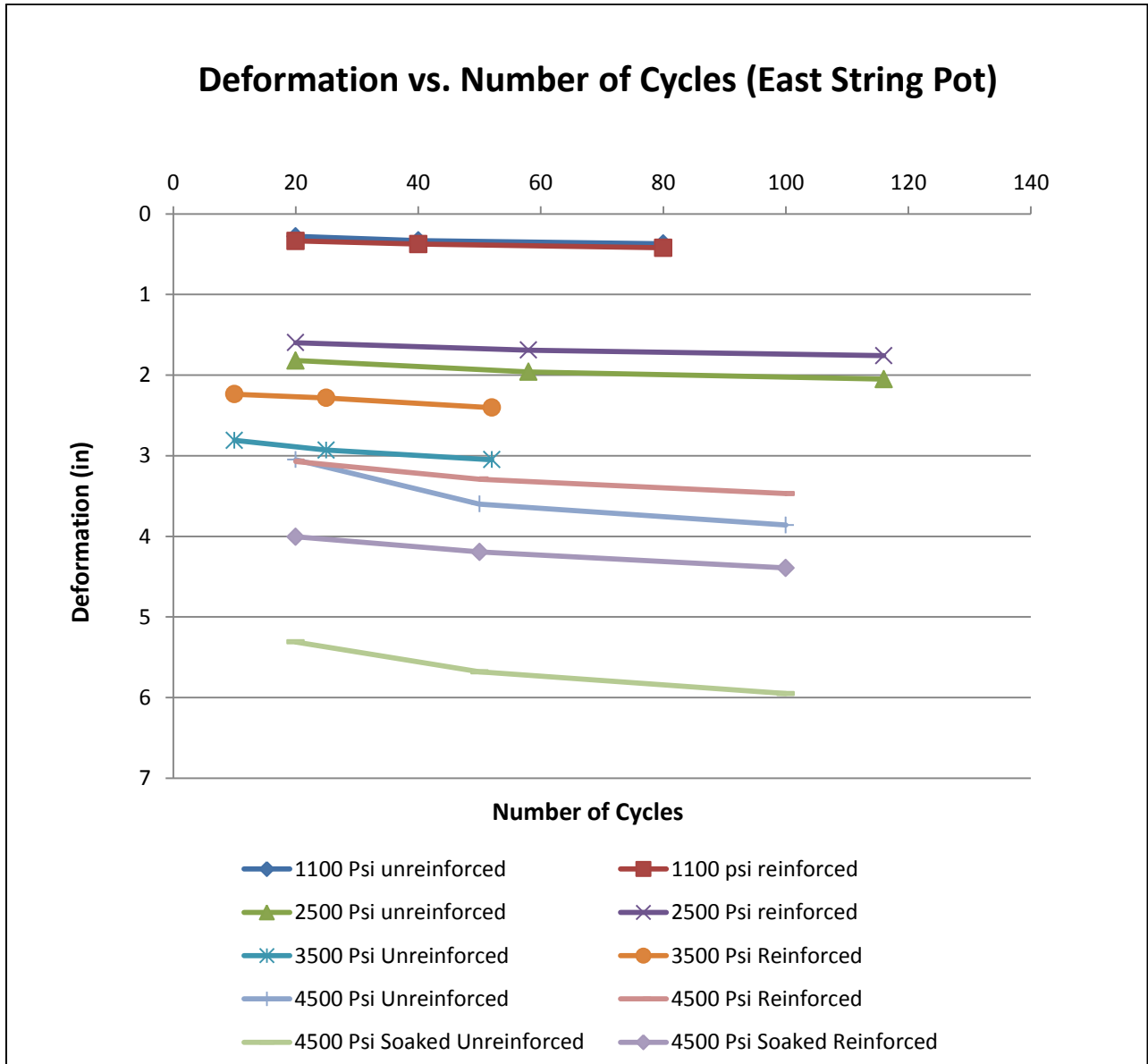


Figure 4.53 East string pot result comparison

Table 4.10 Comparison of settlement between reinforced test and unreinforced test (east string pot)

Pressure (psi)	Deformation(in) East Stringpot		Number Of cycles	Actual Pressure applied Reinforced (psi)	Actual Pressure applied Unreinforced (psi)
	Unreinforced	Reinforced			
1100(Beginning)	0.28	0.34	20	1120	1070
1100(Middle)	0.33	0.38	40	1126	1080
1100(End)	0.37	0.42	80	1121	1070
2500(Beginning)	1.82	1.60	20	2487	2480
2500(Middle)	1.96	1.69	58	2512	2440
2500(End)	2.05	1.76	116	2516	2450
3500(Beginning)	2.81	2.24	10	3570	3580
3500(Middle)	2.93	2.28	25	3505	3680
3500(End)	3.05	2.40	52	3508	3670
4500(Beginning)	3.6	3.07	20	4741	4406
4500(Middle)	3.86	3.29	50	4590	4462
4500(End)	4.05	3.47	100	4714	4480
4500 Soaked(Beginning)	5.31	4.01	20	4715	4370
4501 Soaked(Middle)	5.68	4.19	50	4740	4470
4502 Soaked(End)	5.95	4.39	100	4735	4470

As table 4.10 shows, at the end of the 1100 psi loading no improvement was observed. After the 2500 psi loading, a 0.3 in improvement in settlement was observed. After the 3500 psi loading, 0.64 in of settlement improvement was obtained; after 4500 psi loading (not soaked), about 0.58 in of settlement improvement was obtained, and the end of soaked section loading about 1.55 in of settlement improvement was obtained. Notice on figure 4.53 for the 1100 psi loading step how the reinforced and unreinforced curves are laid on top of each other. As the loads applied get bigger, the gap between the reinforced and unreinforced cases gets higher until the 3500 psi loading step. However, in the case of the 4500 psi, the loading step gap becomes smaller. This is because the pressure applied in the unreinforced and reinforced cases are not identical. Table 4.10 shows the percent difference in load applied in-between both unreinforced and reinforced cases. The test data were adjusted to account for the loading difference in loading using the same procedure, as was used in figure 4.52.

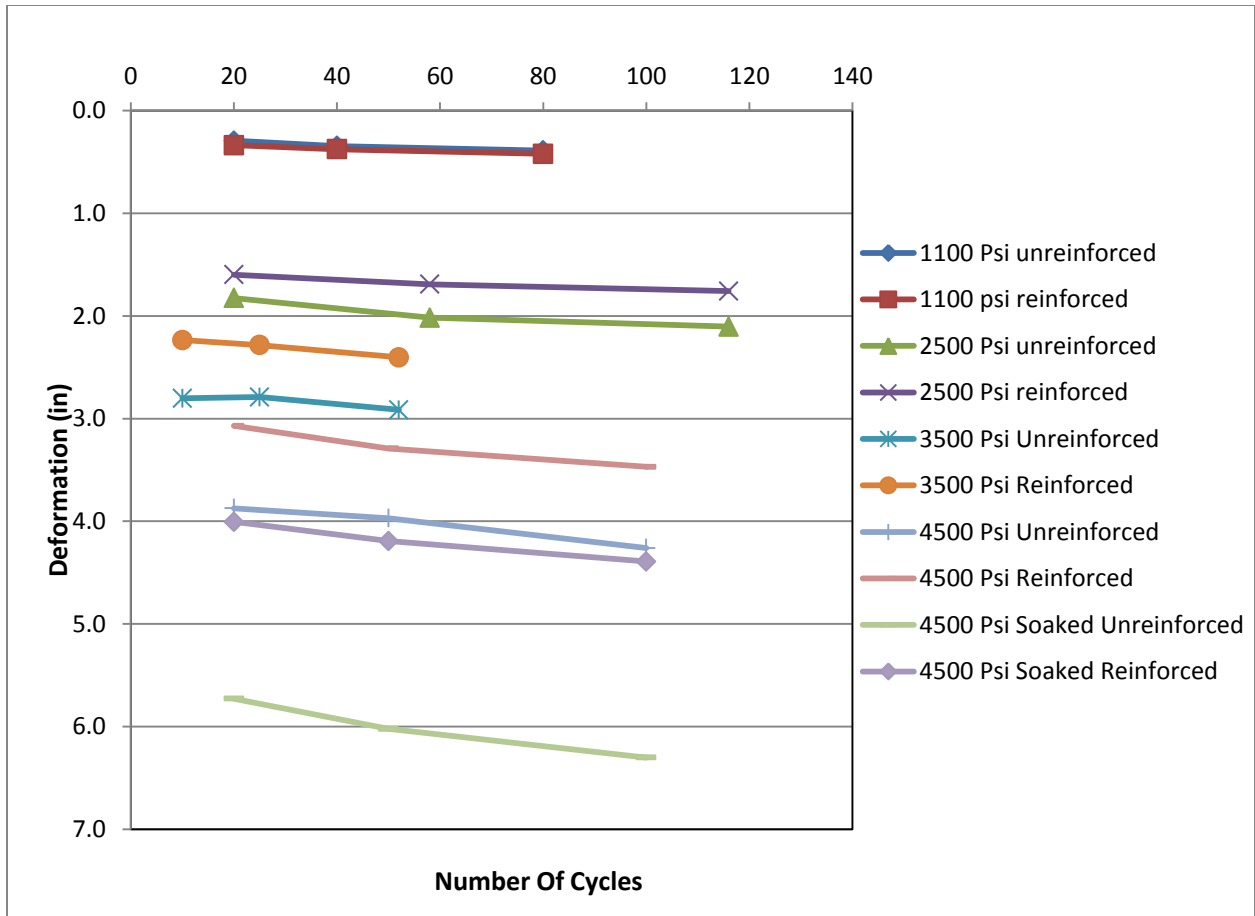


Figure 4.54 East string pot result comparison (after adjusting for load differences)

4.3.2 Number of Cycles versus Settlement (West String Pot)

Figures 4.55 and 4.56 show the settlement with cycles for both tests observed by west and east string pots. These figures also show less settlement for the reinforced section.

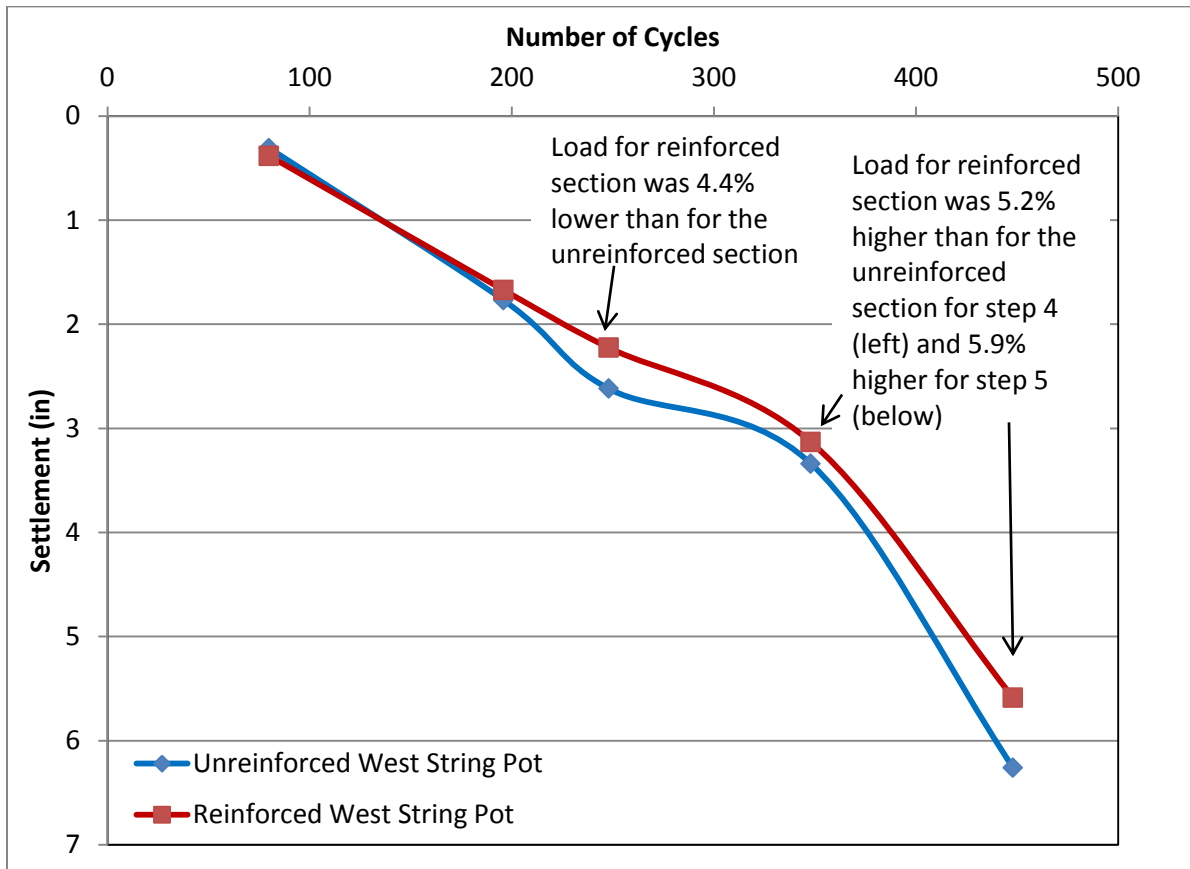


Figure 4.55 Number of cycles vs. settlement (west string pot)

4.3.3 Number of Cycles versus Settlement (East String Pot)

Figure 4.56 shows the improvement in settlement obtained in reinforced case base on west string pot.

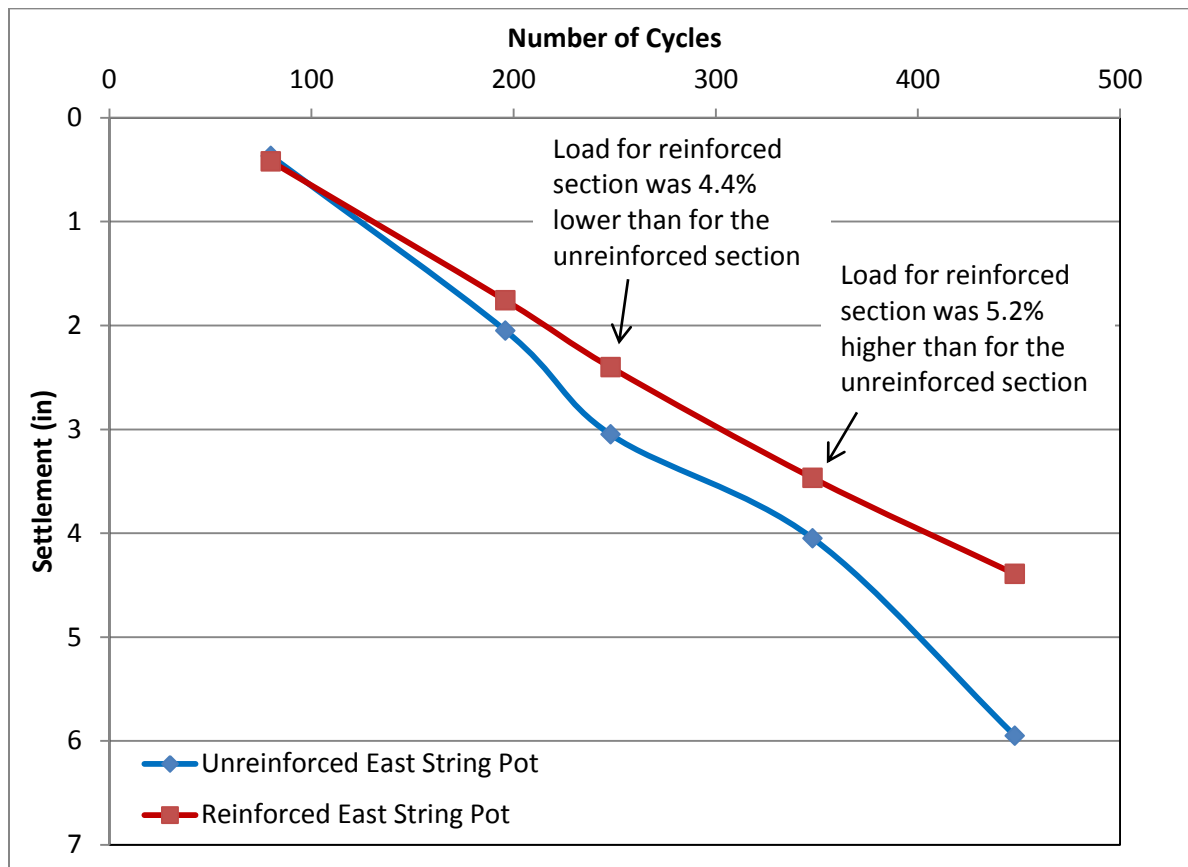


Figure 4.56 Number of cycles vs. settlement (east string pot)

4.3.4 Actual Pressure vs. Settlement

Figures 4.57-4.62 show the actual tie bearing pressure versus settlement for the early cycles, middle cycles, and later cycles.

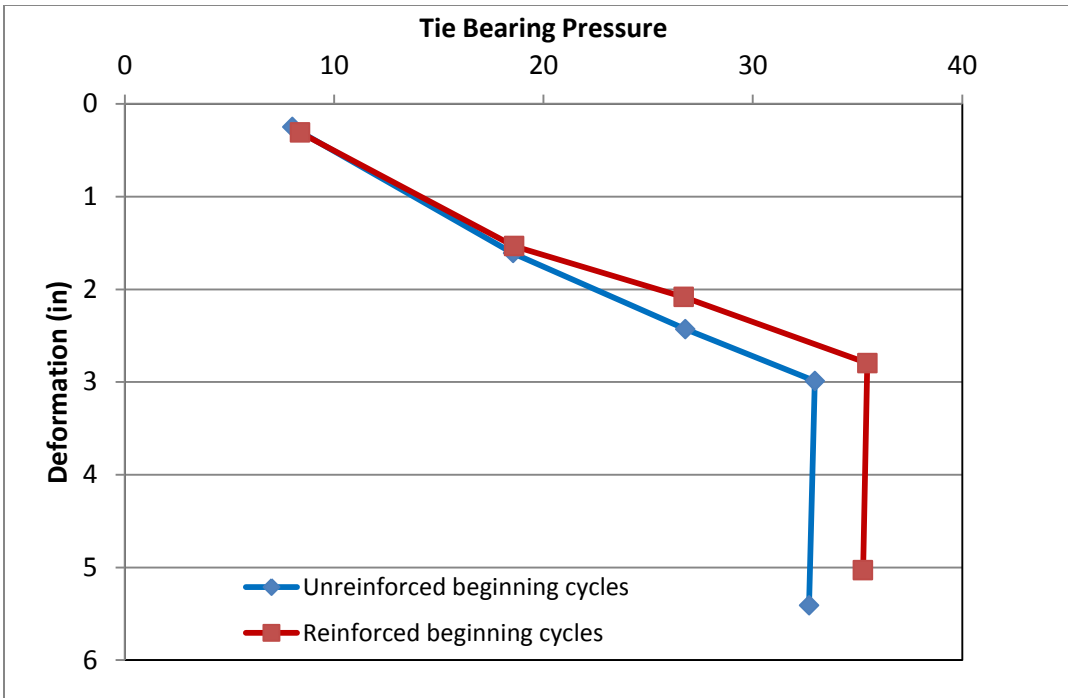


Figure 4.57 Deformation vs. actual tie bearing pressure at early cycles (west)

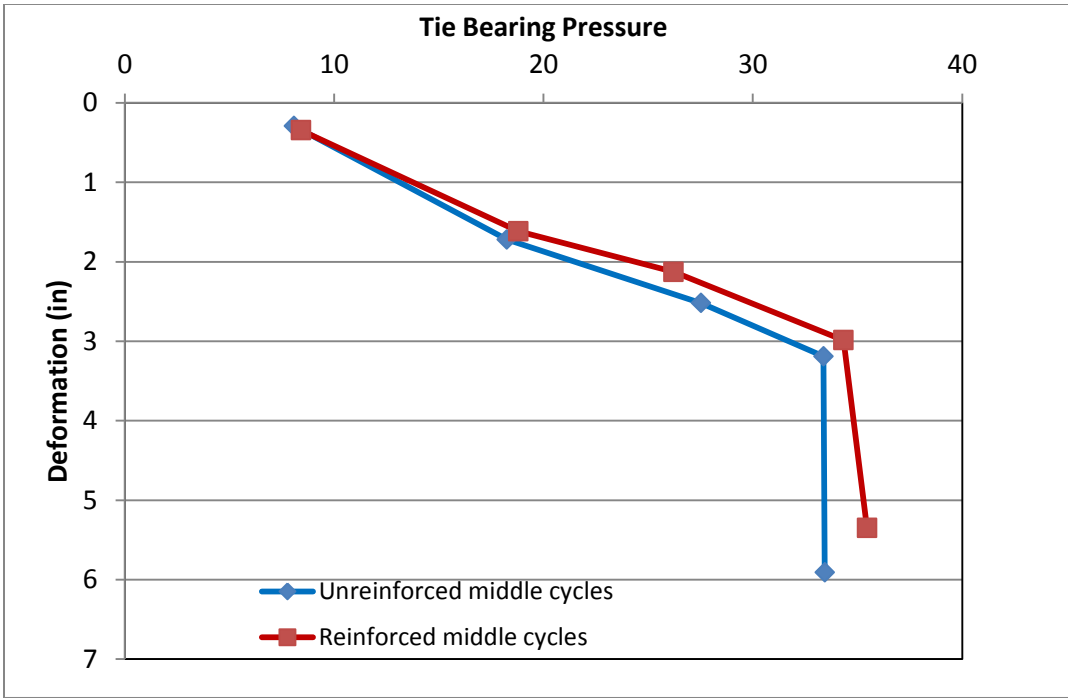


Figure 4.58 Deformation vs. actual tie bearing pressure at middle cycles (west)

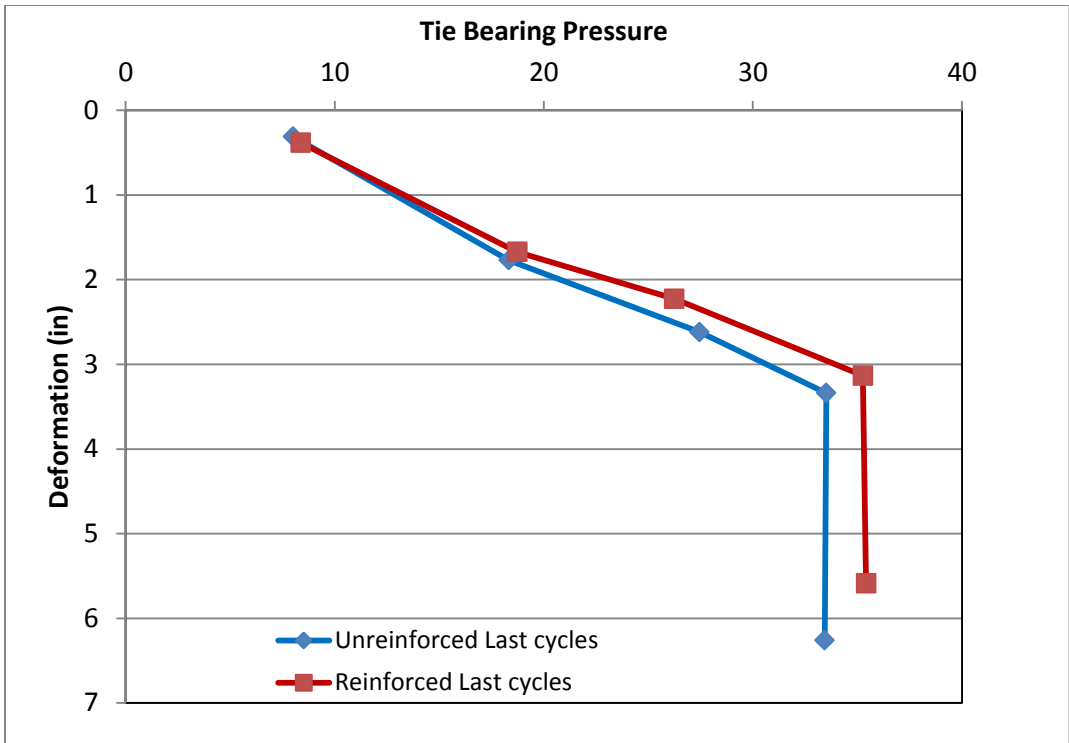


Figure 4.59 Deformation vs. actual tie bearing pressure at later cycles (west)

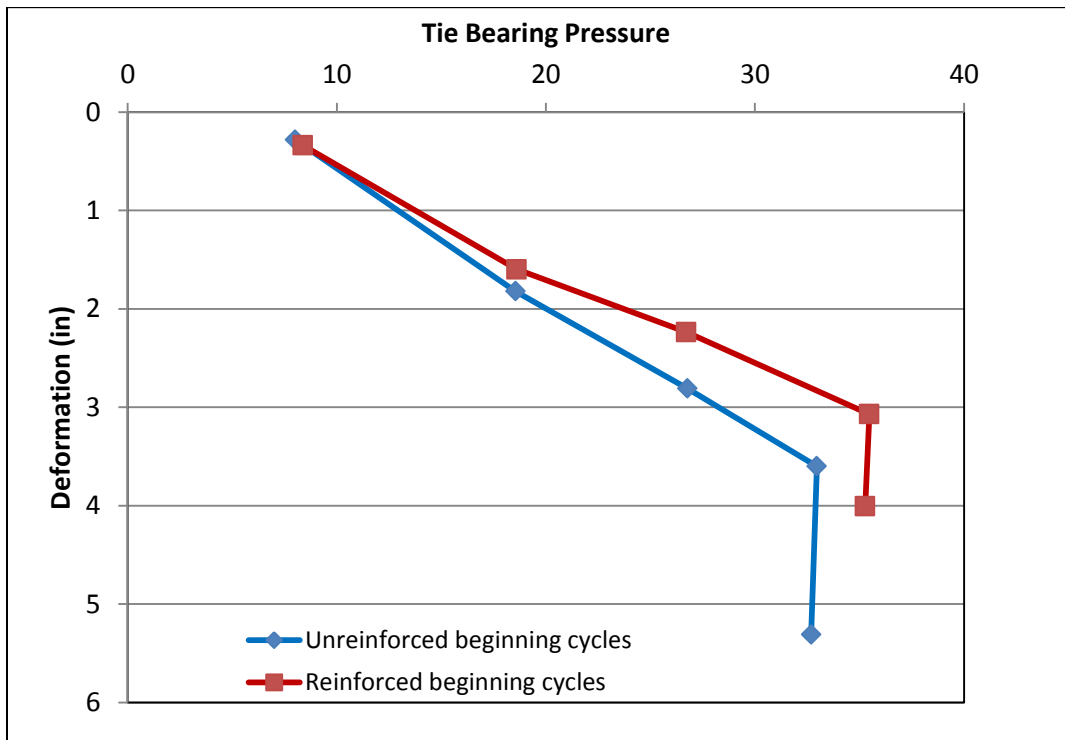


Figure 4.60 Deformation vs. actual tie bearing pressure at early cycles (east)

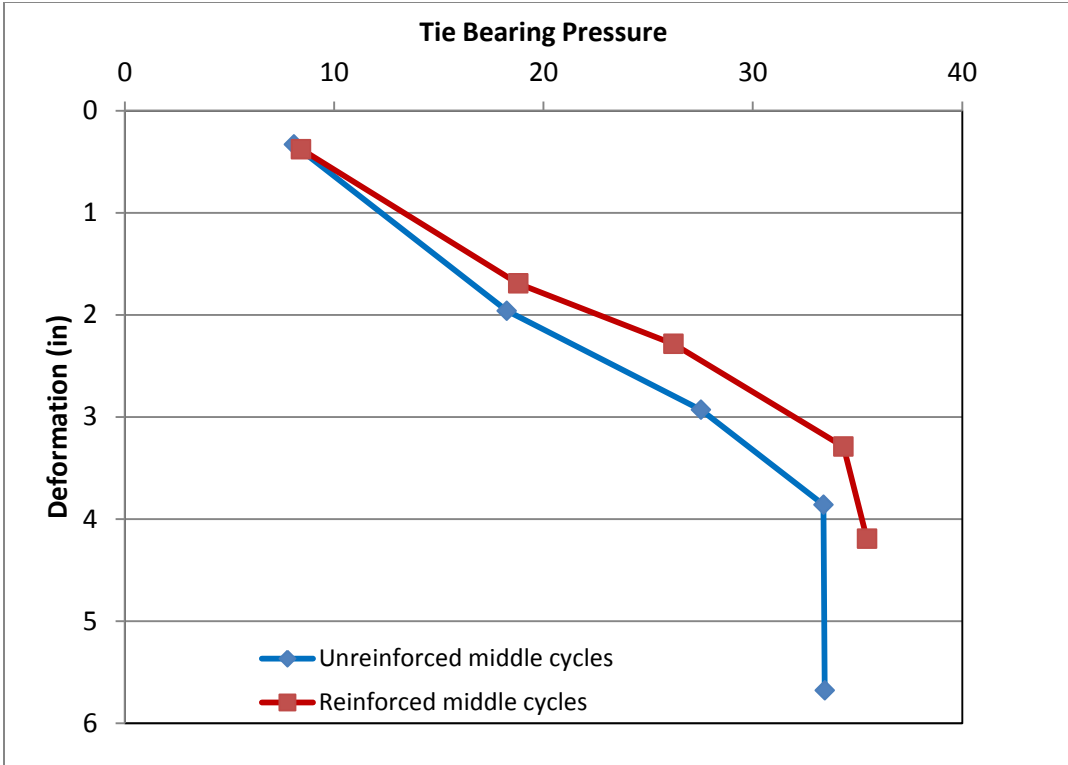


Figure 4.61 Deformation vs. actual tie bearing pressure at middle cycles (east)

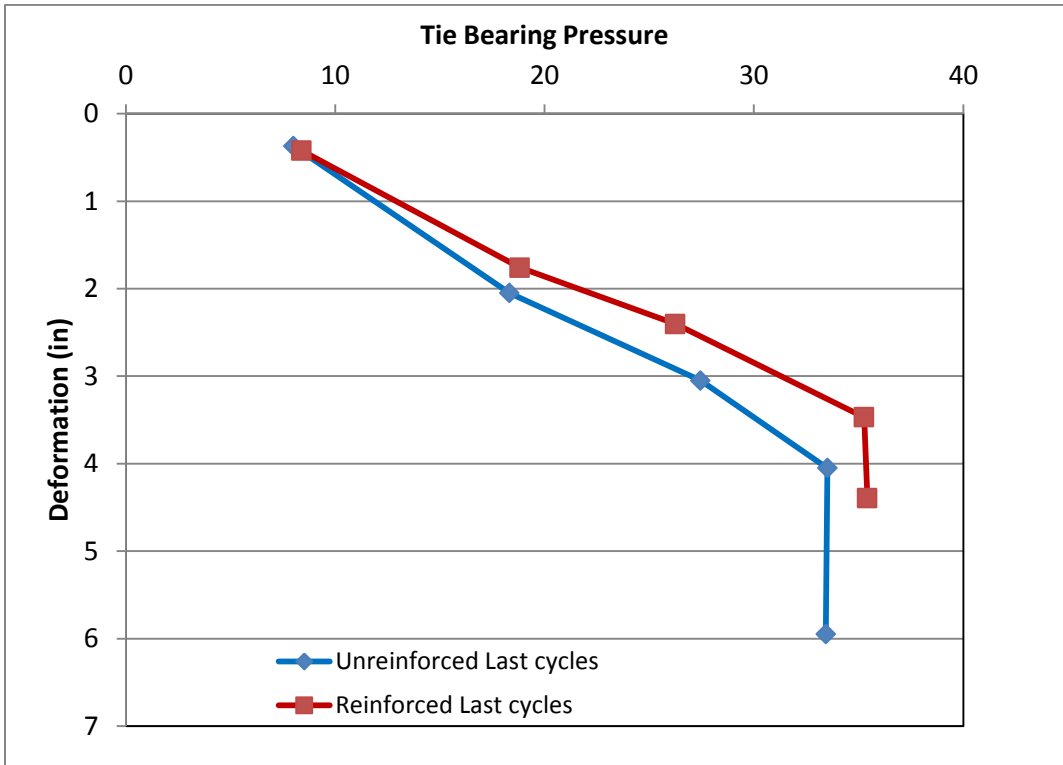


Figure 4.62 Deformation vs. actual tie bearing pressure at later cycles (east)

4.4 Additional Testing such as LWD, CBR, Sieve Analysis, and Tell-Tale Readings

4.4.1 LWD

The LWD was used before and after testing of both the reinforced and unreinforced test sections to find the modulus of elasticity of the subgrade section at six locations, as shown in figure 4.63. The average modulus results for the six locations are shown in table 4.11.

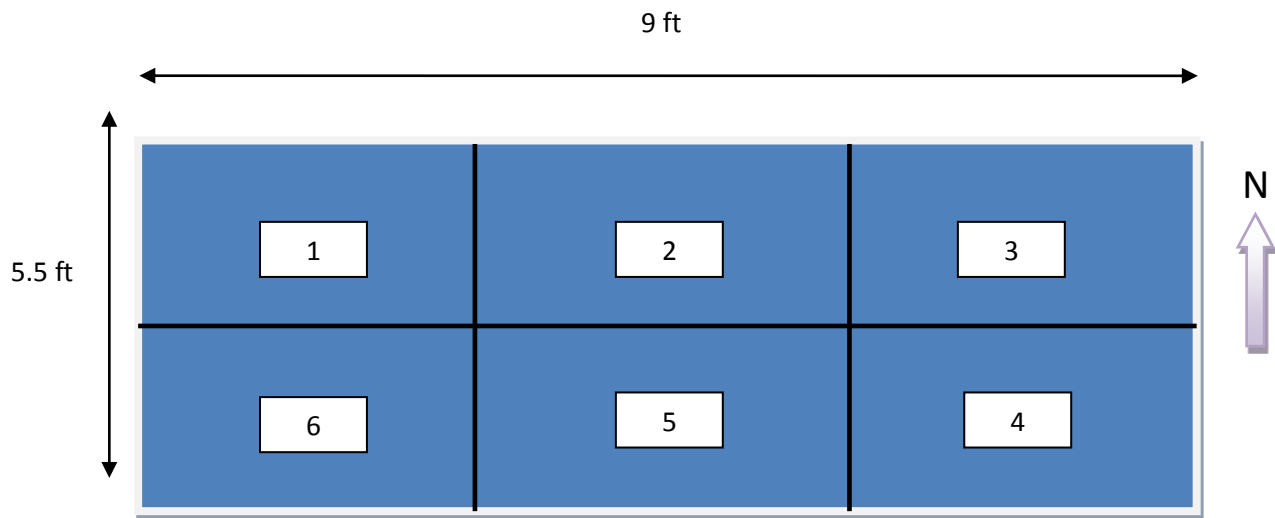


Figure 4.63 LWD reading locations

Table 4.11 LWD results

Subgrade	Plate Size (mm)	S_{avg} (mm)	s/v	E_{vd} MN/m ²
Before (unreinforced)	30	1.98	5.92	12.67
After (unreinforced)	30	1.78	6.53	12.98
Before (reinforced)	30	1.85	5.73	12.73
After (reinforced)	30	2.08	5.28	11.88

Note that in table 4.11 S_{avg} is the average settlement of the plate after 3 drops and s/v is Degree of Compactability, (if > 3.5, soil is further compactable and if <3.5, soil is not compactable).

4.4.2 CBR

CBR values were estimated from dynamic cone penetrometer data from six locations before, and after the unreinforced and reinforced tests. Average results from six locations are shown in figure 4.64. The average CBR value is approximately 2.0. It is slightly higher near the surface. Average CBR for the unreinforced test increased due to more compaction during the test. Also, the section was exposed for a longer period of time (seven days) in comparison to reinforced (three days) test before removing the ballast.

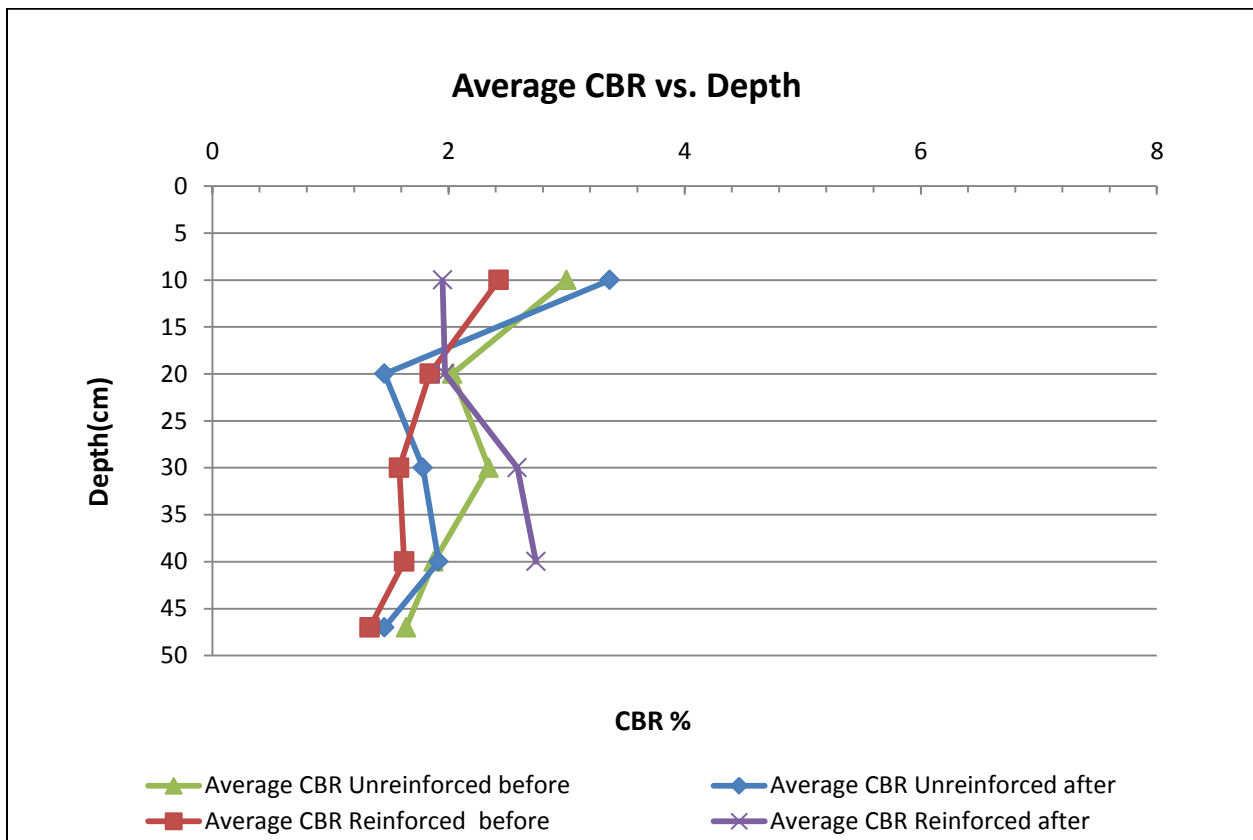


Figure 4.64 CBR vs. depth

4.4.3 Tell-Tales and Sources of Settlement

Four tell-tales were located as shown in figure 4.65. Two tell-tales were located at subgrade level (1 and 2) and two were located within the ballast (3 and 4). For both the unreinforced and reinforced cases these were located at 7 in. below the ties. Readings are reported for both the inner tube connected to the settlement plate and outer tube. Results are shown in table 4.12 Readings were taken before and after each test.

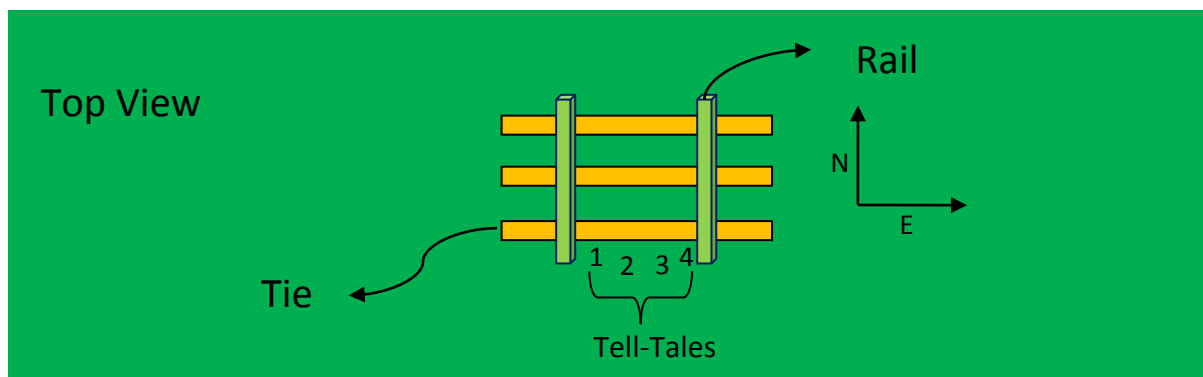


Figure 4.65 Tell-tale locations (not to scale)

Table 4.12 Tell-tale readings

Tell-Tales										
Unreinforced	Subgrade				Ballast				Average	
	1in	1out	2in	2out	3in	3out	4in	4out	Avg. In	Avg. Out
Before	7.5	6.30	8.5	6.9	17.5	16.25	17.5	13.9	12.8	10.8
After	4.5	3.25	5.5	3.25	13.5	12.5	13.25	10	9.2	7.3
Difference	3	3.05	3	3.65	4	3.75	4.25	3.9	3.6	3.6
Reinforced	Subgrade				Ballast				Average	
	1in	1out	2in	2out	3in	3out	4in	4out	Avg. In	Avg. Out
Before	10	8.5	8.5	7.25	10	9	11.5	10.5	10.0	8.8
After	7.5	6.75	6.25	5.5	6	6	8	8	6.9	6.6
Difference	2.5	1.75	2.25	1.75	4	3	3.5	2.5	3.1	2.3

When the information for the inner tell-tale tubes is combined with the overall settlement information, the settlement within the different layers can be calculated. The settlements for the

ballast above the geogrid depth, below the geogrid depth, and for the subgrade are shown in figure 4.66, along with the strain experienced by each layer. Values shown are averages for the east and west string pots and of the two tell-tales at each elevation. Given the large particle sizes involved and minor variation in placement, some natural variation in measurements is to be expected; the general trends, however, are clear. Settlement of the ballast between the base of the tie and the geogrid was 2.0 in., or 28% strain for the unreinforced section, which was 67% more than the strain in the reinforced section. This difference is more dramatic if only the east string pot is considered as the geogrid-level tell-tales were closer to the east side. For the east side the total settlements for the unreinforced and reinforced sections were 6.0 and 4.4 inches, respectively, and the settlements between the ties and geogrid were 1.8 and 0.6 inches, or 26 and 9 percent, respectively. For the lower portion of the section there was no observed benefit. Settlement of the subgrade was 0.6 in. less for the reinforced section. This may be due to random variation, or the geogrid may have contributed to this reduction in settlement by distributing the load more widely; however, the authors believe this possibility requires more testing for confirmation. The subgrade was observed to have less “waviness,” or differential movement, when the reinforced test was dismantled.

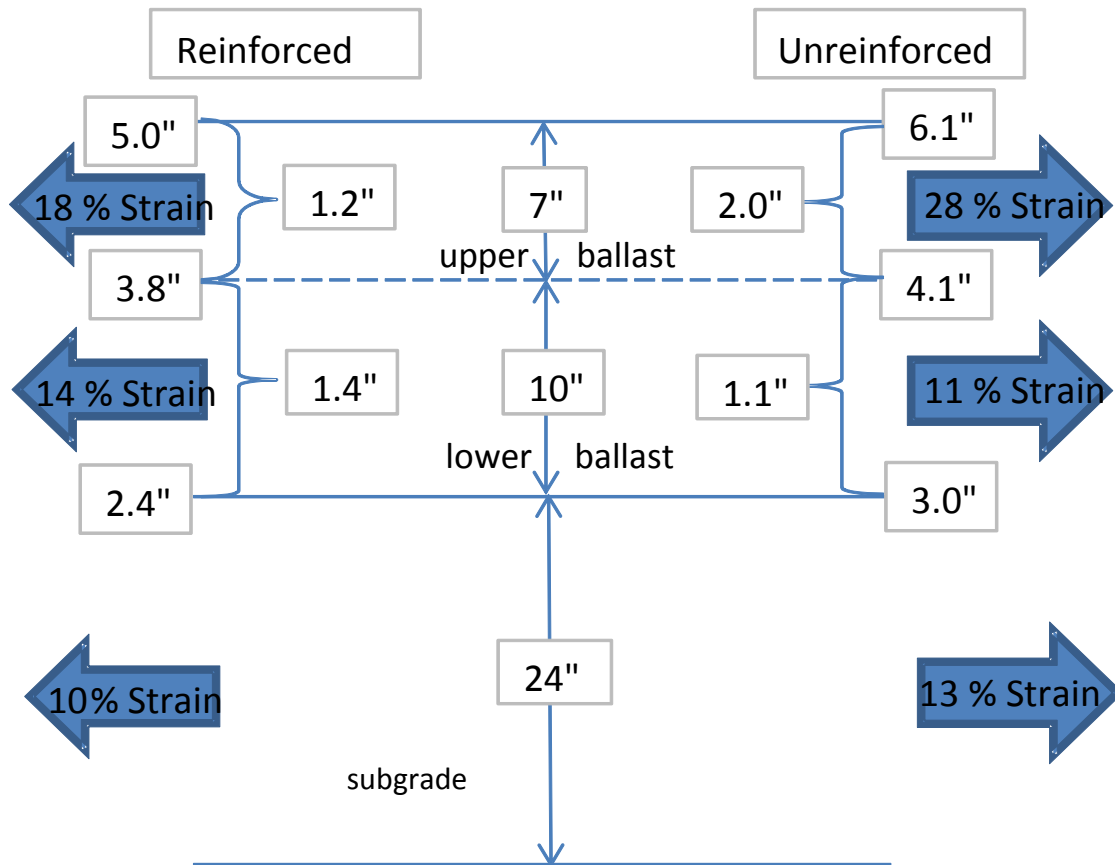


Figure 4.66 Settlements and strains within the sections

4.4.4 Generation of Fouling Material

Figures 4.67-4.70 show the condition of the ballast after the completion of the reinforced test and unreinforced test. Based on visual observation there was a concentration of rock dust at the bottom of the ballast after both tests. Given the open graded condition of the material it is likely that a significant portion of the dust was generated at a higher levels and filtered down to lower levels during the loading process or were washed down during the wetting process. It was also observed that more fines were present locally beneath the ties after the unreinforced test than after the reinforced test.



Figure 4.67 Condition of ballast after unreinforced test



Figure 4.68 Condition of ballast at top of subgrade after unreinforced test



Figure 4.69 Condition of ballast at top of geogrid after reinforced test

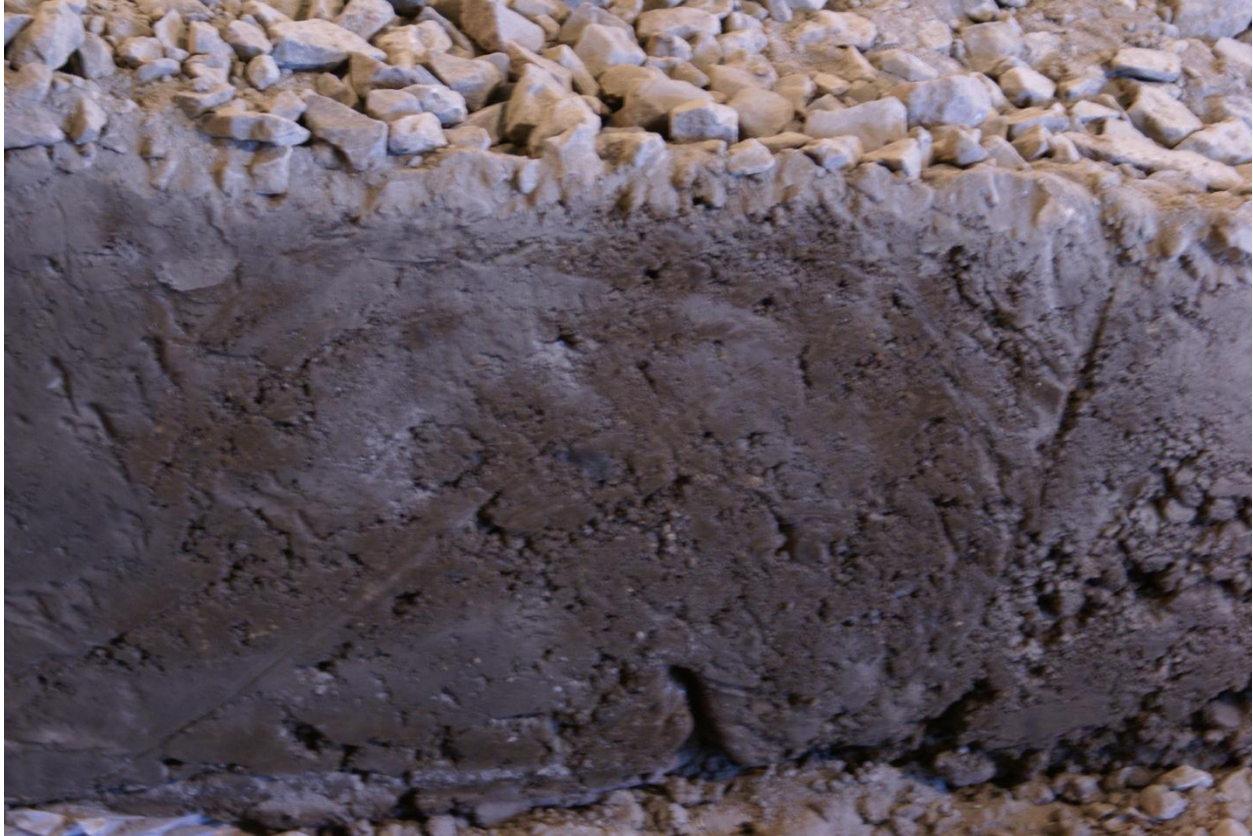


Figure 4.70 Condition of ballast at top of subgrade after reinforced test

A series of ballast samples was taken after each test from different locations in an attempt to determine if the presence of the geogrid reduced the breakdown of ballast. Effective sampling of the ballast material was challenging, as disturbance from the act of sampling caused some loss of fines to lower levels within the ballast. It is also possible that some segregation of material occurred during handling and placement of the ballast, particularly with respect to the ballast for the reinforced test, as there was additional handling of this material. These factors can be shown to have impacted the results, and therefore grain size distribution results (shown in fig. 4.71) should be viewed with caution. For example, the samples near the subgrade showed almost no small diameter material, which was not consistent with the visual observations. These distributions are not included.

These results do show, however, that of all samples, the sample taken below the tie for the unreinforced test had the highest percentage of material smaller than ½ inch in diameter. Additionally, the percentage of material smaller than ½ inch located below the tie for the reinforced test was among the lowest of all the samples, which is consistent with the visual observation. These results suggest that the presence of the geogrid helped to lock the ballast structure in place and limited crushing and grinding action from particle movement that would generate rock fines.

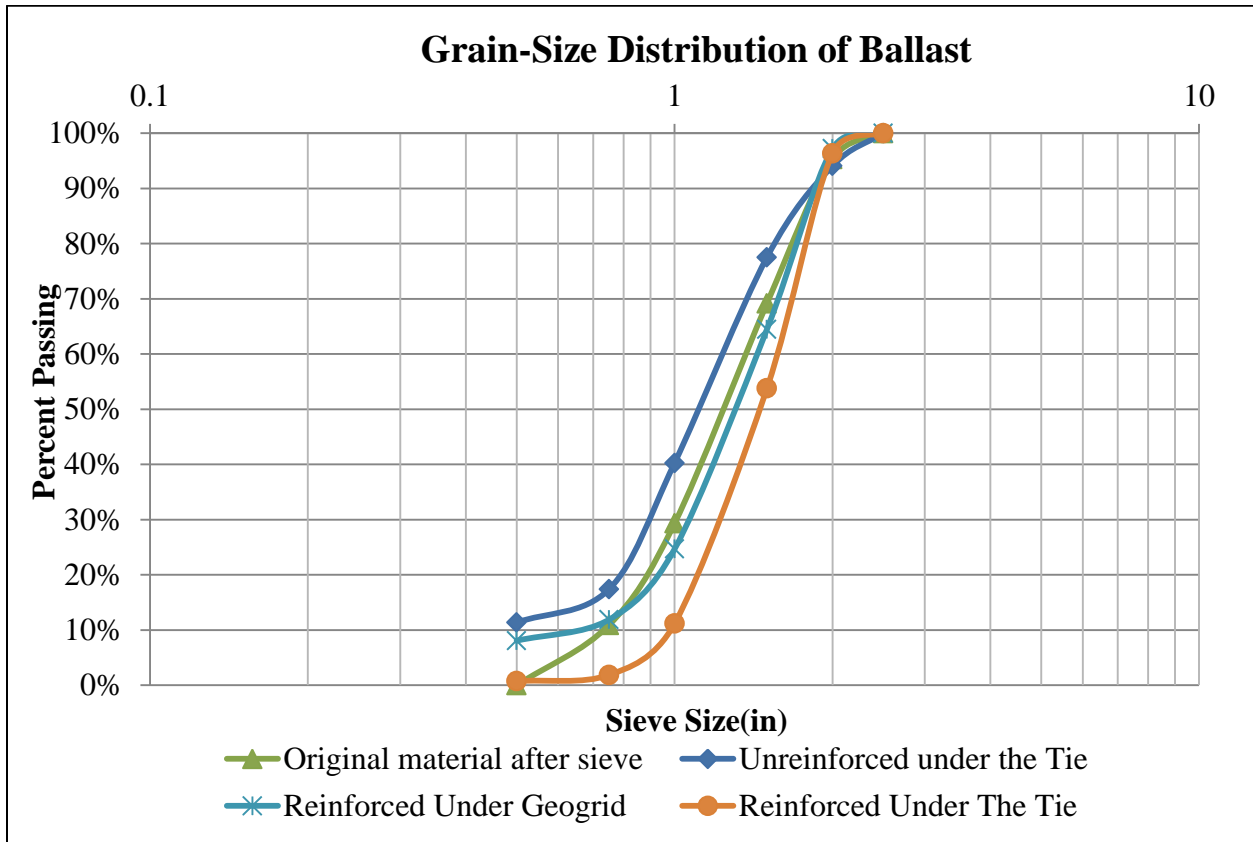


Figure 4.71 Grain size distribution of ballast

4.5 General Observations

1. Unevenness of the subgrade after both tests was observed, but, based on visual inspection, was greater after the unreinforced test.
2. After both tests, there was some damp ballast approximately 8 in. below the tie during excavation.
3. A higher percentage of small diameter material was observed beneath the ties after the unreinforced test than after the reinforced test.
4. The ballast penetrated the subgrade in both tests (approximately 1 in).
5. The amount of fines that accumulated close to the subgrade level was substantial.

Chapter 5 Conclusions and Recommendations

5.1 Conclusions

Full scale testing of railroad sections constructed with unreinforced recycled ballast and reinforced recycled ballast yielded the following observations:

- Settlement of the ballast between the ties and geogrid was 37 to 65 percent less than settlement of the equivalent portion of the unreinforced test section.
- More ballast breakdown resulting in the generation of small particles and dust was observed for the ballast beneath the ties in the unreinforced test than in the reinforced test.
- The reinforced test section supported more load prior to subgrade failure than the unreinforced test section.

Based on these observations it was concluded that ballast reinforcement provided benefits with regard to reduction of fines from the grinding and crushing of ballast, and some reduction in the settlement of the ballast.

5.2 Recommendations for Future Study

The experimental work in this study has demonstrated a benefit from using geogrid to reinforce railroad ballast. However, there is a need for additional research. Some areas where additional research would be beneficial include the following:

- This study has considered only one type of geogrid (TX190L) at one depth below the tie. Other studies are recommended with different geogrids (different stiffnesses) at different depths to pinpoint and optimize improvements. A geogrid could be destroyed during a maintenance action if it was placed at a depth in the ballast that was to be removed later by an undercutter. Therefore, evaluation of

geogrid benefits at depths below the level of potential undercutter activity is particularly recommended.

- A more thorough investigation of ballast breakdown and the potential benefits of breakdown prevention is warranted.
- Use of cyclic loading with a higher frequency to better simulate real world application is recommended.
- It is recommended this work be extended to other subgrade soils, and that testing be extended over a larger number of cycles.
- It is recommended that test sections with reinforcement be constructed on rail lines in service to provide field evaluation.

References

- Emersleben, A., and N. Meyer. 2005. "The use of geocells in road constructions over soft soil: vertical stress and falling weight deflectometer measurement." *Euro Geo4 Paper no. 132*. Retrieved from http://celltekdirect.com/pdf/paper_132.pdf
- Grabe, H. 2010. "Geosynthetics for Improving Poor Track Formations." Committee presentation for Transportation Research Board (TRB). Web. No longer posted.
- Indraratna, B., M. A. Shahin, C. Rujikiatkamjorn, and D. Christe. 2006. "Stabilization of Ballasted Rail Tracks and underlying soft formation soils with geosynthetic grids and drains." *Paper presented at Geo-Shanghai*, Shanghai, China.
- Indraratna, B., C. Rujikiatkamjorn, and S. Nimbalkar. 2011. "Use of Geosynthetics in railways including geocomposites and vertical drains." *Proceedings of the Geo-Frontiers Conference*, Dallas, Texas. Retrieved from ascelibrary.org
- Kea, J.K., P. J. Grabe, and J. S. Maree. 2007. "Geotechnical and field Measurements at Amandelbult." Test section Version 1.
- Kea, J.K. 2007. "Improving poor track formations using geosynthetics." Web. No longer posted.
- Koerner, R. M. *Designing with Geosynthetics*. Upper Saddle River, NJ: Prentice Hall.
- Menglet, M.J., T. B. Edil, and C. H. Benson. 2006. "Resilient modulus and plastic deformation of soil confined in a geocell." *Geosynthetics International*, 13, no 5: 195-205.
- Selig, E.T. and J. M. Waters. 1994. *Track Geotechnology and Substructure Management*. London: Thomas Telford.
- Tensar International. "Tensar Systems & Products." Last modified 2012. <http://www.tensarinternational.com/Systems-Products>.
- Tutumluer, E., W. Dombrow, and H. Huang. 2008. "Laboratory Characterization of Coal Dust Fouled Ballast Behavior." *Manuscript Draft Submitted for the AREMA 2008 Annual Conference and Exposition September 21-24, 2008*, Salt Lake City, UT.
- Webster, S.L. 1979a. "Investigation of beach sand trafficability enhancement using sand-grid confinement and membrane reinforcement concepts." *Report GL-79-20 (1)*. U.S. Army Engineer Waterways Experiment Station, Vicksburg, MS.

Zarembski, A. M. and J. F. Cikota, Jr. "Estimating maintenance costs for mixed high-speed passenger and freight rail corridors." *TR News*, 225, March-April 2008:29-31.